WT-1168

AEC Category: PHYSICS
Military Categories: 5-22 and 5-50

E-6

Operation TEAPOT

NEVADA TEST SITE

February – May 1955

Project 33.4

DISTRIBUTION AND DENSITY OF MISSILES FROM NUCLEAR EXPLOSIONS

Issuance Date: December 14, 1956

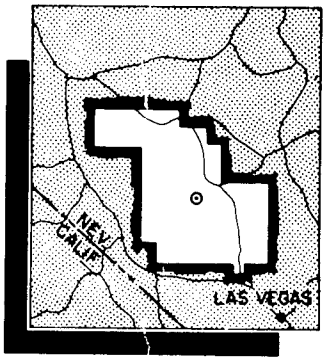

CIVIL EFFECTS TEST GROUP

NOTICE

This report is published in the interest of providing information which may prove of value to the reader in his study of effects data derived principally from nuclear weapons tests.

This document is based on information available at the time of preparation which may have subsequently been expanded and re-evaluated. Also, in preparing this report for publication, some classified material may have been removed. Users are cautioned to avoid interpretations and conclusions based on unknown or incomplete data.

Price $0.60. Available from the Office of
Technical Services, Department of Commerce,
Washington 25, D. C.

AEC, Oak Ridge, Tenn.

Report to the Test Director

DISTRIBUTION AND DENSITY OF MISSILES FROM NUCLEAR EXPLOSIONS

By

I. Gerald Bowen
Allen F. Strehler
Mead B. Wetherbe

Approved by: C. S. WHITE
Director, Program 33

Approved by: ROBERT L. CORSBIE
Director
Civil Effects Test Group

Lovelace Foundation for Medical Education and Research
Albuquerque, New Mexico

March 1956

ABSTRACT

A new experimental procedure was used in the open shot of Operation Teapot to study various properties of secondary missiles produced in houses, shelters, and open areas at distances of 1470 to 10,500 ft from a nuclear explosion with a yield approximately 50 per cent greater than nominal. The experimental technique involved trapping the missiles in an absorbing material consisting of Styrofoam 22. Laboratory calibrations of the Styrofoam made it possible to determine individual velocities for the trapped missiles. Velocities were calculated for 2611 missiles—95 per cent of which were window-glass fragments—obtained from 27 traps. Missile velocities, masses, and spatial distributions were analyzed statistically.

Computational procedures were proposed to predict the velocities of stone missiles in open areas from blast data and from assumed average aerodynamic constants for stones. The method was tested for the 5-psi overpressure region. The computed predicted velocities showed satisfactory correspondence with those empirically determined from data obtained from a missile trap placed in this region.

ACKNOWLEDGMENTS

The authors are indebted to the following individuals for technical advice and assistance in planning:

R. L. Corsbie, Atomic Energy Commission
C. S. White, Lovelace Foundation
J. C. Greene, Federal Civil Defense Administration
L. J. Vortman, Sandia Corporation
C. D. Broyles, Sandia Corporation

The authors also wish to express their appreciation to the following Foundation employees: M. A. Palmer and R. S. Harper for technical and documentary photography; R. A. Smith and Kay Harper for their assistance in preparation of the illustrations; Albert Dennis for his assistance in the analysis of the data; and Isabell Benton, Virginia Gilmore, Mary Louise LeNoir, and Gloria Tabacchi for stenographic aid.

CONTENTS

CONTENTS (Continued)

ILLUSTRATIONS

ILLUSTRATIONS (Continued)

ILLUSTRATIONS (Continued)

TABLES

CHAPTER 1

BACKGROUND

Although most of the recent work on wound ballistics has been concerned with missiles having velocities between 600 and 9000 ft/sec,[1–3] it is also a fact that relatively low-velocity missiles secondary to large-scale explosions have been a significant cause of casualties. In cases described in reports from Hiroshima and Nagasaki,[4] patients were lacerated by glass and other missiles at distances of 10,600 and 12,200 ft from Ground Zero, respectively, following atomic explosions over those cities. Similar documentation is given to the physical and biological damage caused by missiles in the disastrous 1947 explosions at Texas City, Tex. (See the engineering survey of Armistead[5] and the medical study of Blocker and Blocker.)[6] Also, attention is called to a recent study[7] which defines conditions just critical for penetration of a biological target in terms of missile impact area, mass, and velocity. It is significant that missiles with velocities well below 500 ft/sec—in some instances even less than 90 ft/sec—penetrated the abdominal wall of an experimental animal.

Thus it is clear that the wounding power of low-velocity missiles has been well established. Even so, no systematic study has been made to date of the nature and ballistic properties of the types of low-velocity missiles which would be found on the perimeter of a nuclear explosion and which may, indeed, be the primary cause of pathological damage in that area. Such an investigation is of obvious importance if one is to complete a survey of the biological and physical damage which could be expected to result from such missiles.

It was, therefore, the main purpose of the present study to examine systematically the ballistic properties of low-velocity missiles which are produced inside various types of houses following an actual nuclear explosion. Some attention was given to missile production in the vicinity of houses and in small home type shelters. Also, it has been possible to make brief mention of some of the biological implications of the physical data obtained in the field because of biological studies—a report of which will be made later—involving experimental animals and glass missiles which were undertaken in Albuquerque after the test series.

REFERENCES

1. A. N. Black, B. D. Burns, and S. Zuckerman, An Experimental Study of the Woudning Mechanisms of High Velocity Missiles, Brit. Med. J., 2: 872-874 (1941).
2. George R. Callender, Wound Ballistics—Mechanism of Production of Wounds by Small Arms, Bullets, and Shell Fragments, War Med., 3: 337-350 (1943).
3. E. Newton Harvey, The Mechanism of Wounding by High Velocity Missiles, Proc. Am. Phil. Soc., 92: 294-304 (1948).
4. Los Alamos Scientific Laboratory, "The Effects of Atomic Weapons," U. S. Government Printing Office, Washington, September 1950.
5. George Armistead, Jr., The Ship Explosions at Texas City, Texas, on April 16 and 17, 1947, and Their Results, Engineering Consultants Report to John G. Simonds and Company, Inc., Oil Insurance Underwriters, New York City; Washington, D. C., 1 June 1947.

6. Virginia Blocker and T. G. Blocker, The Texas City Disaster—A Survey of 3000 Casualties, Am. J. Surg., 78: 756-771 (1949).
7. I. Gerald Bowen, Julian P. Henry, Warren H. Lockyear, Merrill A. Palmer, Donald R. Richmond, and Clayton S. White, The Biophysics of Penetrating Missiles—Conditions Critical for Penetration, Report TID-5248, U. S. Atomic Energy Commission, 4 January 1955.

CHAPTER 2

OBJECTIVES

In order to carry out a systematic examination, such as is described in Chap. 1, of the ballistic properties of low-velocity missiles, produced by a nuclear explosion, the following information was needed:

1. The composition (e.g., glass, stone, wood) of the missiles.
2. Their respective shapes.
3. Their respective masses.
4. Their respective velocities.
5. Their trajectories (that is, their direction of travel).
6. Their density in space (that is, the number of them which pass through a unit area in a given vertical plane in space).

The above data were required for each of several typical locations, relative to Ground Zero and also relative to surrounding structures, in which human beings might find themselves in the presence of an actual explosion.

The means, both practical and theoretical, by which the types of data listed in points 1 to 6 were obtained are discussed in detail in the subsequent chapters.

CHAPTER 3

INSTRUMENTATION

3.1 STYROFOAM ABSORBER

Styrofoam 22 (made by Dow Chemical Co., Midland, Mich.) has most of the required properties of a good absorber of missiles for use in locations where the overpressure is not expected to exceed about 10 psi. Its relatively low shear properties and its nonfibrous structure result in localization of compressive deformations. This is very important for a trap which is expected to receive a number of missiles in random distribution. Styrofoam's resistance to deformation is low enough so that relatively slow missiles penetrate sufficiently to be measured accurately. One disadvantage of Styrofoam 22 as an absorber is its low heat resistance. Aluminum foil was used to protect the Styrofoam which was exposed to thermal radiation. The foil was so thin that it had little or no stopping effect on the missiles which passed through it.

With one exception, a cube of Styrofoam, 2 ft on each side, was used in each trap. The exception involved employment of one trap with half the volume of Styrofoam. To facilitate recovery of the missiles and evaluation of the data, the Styrofoam was placed in the traps in 1-in. layers parallel to the open side of the trap. These layers of absorber are referred to hereafter as cells.

3.2 CONSTRUCTION OF MISSILE-TRAP HOUSING

Figure 3.1 illustrates the construction of the missile-trap housing used in pressure areas of less than 10 psi. The housing for the trap for a higher pressure area was the same as that shown except that the absorber compartment was only 1 ft high.

The missile-trap housing was designed to produce rigidity at the open end. Two separated layers of $\frac{3}{4}$-in. plywood were used for the top in order to cushion the impact of falling debris. All joints were secured with glue and special cement-coated nails treated to resist removal. Dowel pins 1 in. in diameter and 12 in. in length were installed at the four corners of the top to increase rigidity. All traps were painted with a heat-resistant white paint.

3.3 ANCHORING FOR THE MISSILE TRAPS IN TEST AREAS

Traps placed in dwellings were oriented, where feasible, with their backs against walls or other solid objects. The traps were secured to the floor by means of chain anchored to the floor joist with lag screws and to concrete floors with Ramset fasteners (Ramset Fasteners, Inc., Cleveland 11, Ohio).

Securing traps in open areas presented special problems. A cube of concrete, measuring approximately 3 ft on each side and protruding 1 ft above ground level, was used to anchor each trap. Anchor bolts that were $\frac{1}{2}$ in. in diameter and embedded in the concrete were used to clamp two 3-in. channel irons against the top of the housing. To aid in preventing transla-

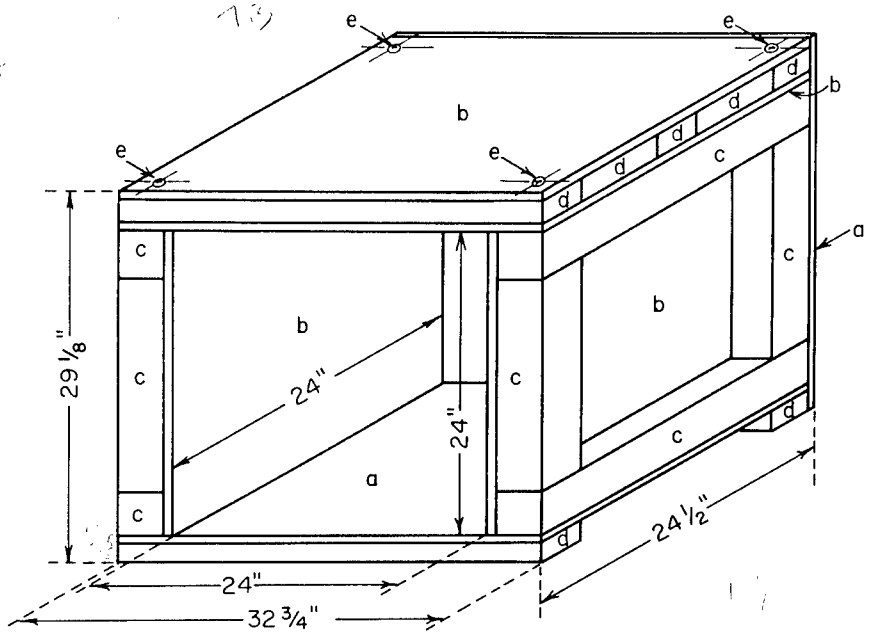

Fig. 3.1—Missile-trap housing. a, ½-in. plywood. b, ¾-in. plywood. c, 4 in. by 4 in. d, 2 in. by 4 in. e, dowel pins 1 in. by 12 in. (All joints were secured with glue and concrete-coated nails.)

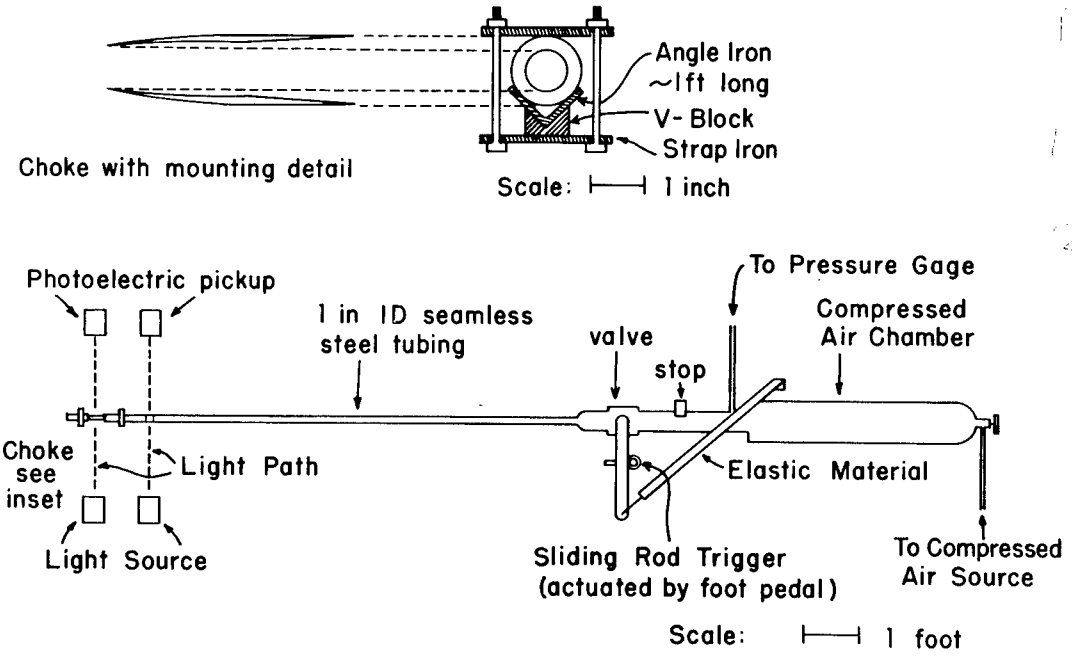

Fig. 3.2—Air gun used to calibrate Styrofoam absorber.

tional motion, a 2-in. angle iron was secured to the concrete with ½-in. anchor bolts at the rear of the missile-trap housing (see Figs. 4.19 to 4.21).

3.4 CALIBRATION OF STYROFOAM MISSILE ABSORBER

3.4.1 Experimental Methods

A diagram of the air gun used in the calibration of Styrofoam 22 is shown in Fig. 3.2. The gun was constructed by connecting a straight section of pipe to a standard compressed air cylinder by means of a fast-opening valve. The straight section of pipe was about 8 ft long and served as the gun barrel. The barrel was connected to the valve by means of pipe threads so that barrels of various sizes could be used. The barrels used in this experiment were made of 1- and 3-in.-I.D. seamless steel tubing.

A special mechanism was devised to produce uniform and rapid opening of the valve delivering compressed air to the barrel. The valve handle had a total travel of 90° and was spring loaded toward the open position. A triggering mechanism was installed to hold the valve in the closed position. The mechanism consisted of a steel rod made free to slide in a stationary section of pipe. The rod was connected to a foot pedal by means of a cable. Thus, when the pedal was depressed, the rod moved free of the valve handle, allowing the spring to open the valve.

Missile velocities were determined by measuring the time required for the missile to traverse a 1-ft interval near the end of the barrel. Figure 3.2 shows the positions of the 1-ft-apart parallel light beams which were interrupted in turn by the missile as it left the barrel. When the first beam was interrupted, the photocell pickup started a Hewlett-Packard 522B electronic timer. The timer was stopped by the second photocell when the second beam was interrupted. The electronic timer recorded the time to the nearest 10 μsec required by the missile to traverse the 1-ft interval.

It should be noted that the first light beam passed through a hole in the barrel 10.5 in. from the end. This means that the missile was accelerating over part of the distance in which the velocity was being determined, and this resulted in the measured velocities being lower than the actual terminal velocities. By means of velocity measurements made through analysis of high-speed pictures, it was shown that the following equation gave a satisfactory corrected velocity.

$$V = V_m \sqrt{\frac{S'}{S' - 0.375}} \tag{3.1}$$

where V = corrected velocity
V_m = electronically measured velocity
S' = distance of missile from end of barrel, in feet, before firing

A special sabot was used to shoot irregular missiles and spherical missiles whose diameter did not fill the gun barrel. The sabot for use with the 1-in. barrel consisted of a cylinder of Styrofoam 1 in. in length and 0.97 in. in diameter. The missile to be shot was embedded in the flat surface of the Styrofoam sabot. Since each sabot could be used only once, a jig was made to facilitate construction. This consisted of a short piece of 1-in.-I.D. steel tubing, one end of which was sharpened by turning in the lathe. The diameter of the cutting edge was then reduced to 0.97 in. by the process of spinning. Sabots were then cut by holding a sheet of 1-in. Styrofoam against the jig while it was being rotated by the lathe.

The choke shown in Fig. 3.2 was designed to slow or stop the sabot, separating it from the missile. The use of the choke was found unnecessary for the experiments reported here.

3.4.2 Results for Regular Missiles

Calibration data were obtained for the Styrofoam absorber by use of spherical missiles made of steel, glass, and cork, varying in size from 0.125 to 0.952 in. in diameter. See Table 3.1.

Table 3.1 — COMPUTATION OF THE RESISTIVE FORCE OF STYROFOAM 22 TO SPHERICAL MISSILES LESS THAN 1 IN. IN DIAMETER

Missile	Diameter, in.	Mass, g	Velocity, ft/sec	Energy, ft-lb	Penetration, in.	Resistive force, lb
Steel sphere	0.125	0.130	385	0.663	5.57	1.43
	0.125	0.130	280	0.351	3.33	1.27
	0.125	0.130	540	1.31	9.97	1.57
Glass sphere	0.217	0.250	322	0.892	2.81	3.82
	0.217	0.250	330	0.938	3.82	3.35
Steel sphere	0.250	1.06	251	2.30	5.08	5.43
	0.250	1.06	338	4.16	10.96	4.56
	0.250	1.06	449	7.37	18.33	4.83
	0.250	1.06	394	5.65	15.33	4.42
	0.375	3.80	232	7.04	8.94	9.46
	0.375	3.80	362	17.15	21.44	9.59
	0.375	3.80	291	11.08	13.44	9.89
	0.4375	5.60	199	7.64	7.74	11.8
	0.4375	5.60	149	4.28	4.24	12.1
	0.4375	5.60	303	17.7	17.11	12.4
	0.4375	5.60	320	19.7	19.24	12.3
	0.4375	5.60	120	2.78	2.86	11.7
Cork marble	0.732	0.50	521	4.67	1.735	32.3
	0.740	0.65	592	7.84	2.491	37.8
	0.744	0.65	657	9.67	3.620	32.1
Steel sphere	0.750	28.2	156	23.8	9.25	30.9
	0.750	28.2	98.7	9.46	3.50	32.4
	0.750	28.2	192	35.7	12.94	33.1
	0.750	28.2	226	49.4	18.62	31.9
Glass marble	0.917	17.0	155	14.2	3.39	50.1
	0.937	18.0	215	28.6	6.78	50.7
	0.952	18.9	256	42.6	10.04	50.9
	0.917	17.0	344	69.3	17.20	48.3

The cavity made by a sphere during penetration is cylindrical and has a hemispherical end where the missile stops. The volume of this cavity must be equated to the volume of a cylindrical cavity with a flat end in order to arrive at the true depth of penetration. This was done by measuring the depth of the cavity up to the nearest point on the sphere and adding to this measurement 0.833 times the diameter of the sphere.

Additional data were obtained for the Styrofoam absorber by use of cylindrical missiles that were 2.94 in. in diameter and made of redwood. The ends of the cylinders were the impact areas and were made flat, hemispherical, and conical with a 90° vertex angle. The depths of penetration were computed as the depth of a cylindrical cavity equivalent volumetrically to the actual cavity. The data from this study are presented in Table 3.2 and will be discussed later in this report.

3.4.3 Computations for Styrofoam Absorber Using Regular Missiles

It was observed from the data in Table 3.1 that, for a given spherical missile, the depth of penetration was directly proportional, within experimental error, to the impact kinetic energy of the missile. It can be concluded from this that the resistive force of Styrofoam for a given missile is constant over the entire stopping distance in the Styrofoam within the range of the

Table 3.2—COMPUTATION OF THE RESISTIVE FORCE AND PRESSURE OF STYROFOAM 22 TO CYLINDRICAL MISSILES OF FLAT, HEMISPHERICAL, AND CONICAL IMPACT SURFACES

	Impact surface							
	Flat			Hemispherical			Conical	
Diameter, in.	2.94	2.94	2.94	2.94	2.94	2.94	2.94	2.94
Effective area, in.^{2}	6.79	6.79	6.79	6.79	6.79	6.79	6.79	6.79
Mass, g	302	302	277	301	301	301	278	278
Velocity, ft/sec	72.3	207	129	204	136	85.2	143	88.5
Energy, ft-lb	54.4	446	159	432	192	75.2	196	75.0
Penetration, in. (cylindrical equivalent)	1.26	9.75	3.56	9.10	4.06	1.60	4.71	1.86
Resistive force, lb	518	549	536	570	568	563	499	484
Resistive pressure, psi	76.8	81.4	79.5	84.6	84.2	83.5	73.5	71.3

velocities investigated. If the force of resistance of Styrofoam is assumed to be constant for a given missile, the force can be computed by use of the energy relation

$$\frac{MV^2}{64} = F \times S \tag{3.2}$$

where M = missile mass, pounds
V = impact velocity, feet per second
F = resistive force of Styrofoam, pounds force
S = stopping distance, feet

The resistive force for each test missile is recorded in the last column of Table 3.1.

Assuming that the resistive forces are constant for a given size missile, it might be supposed that the force per unit impact area (resistive pressure) would be constant for all sizes of spherical missiles. However, this proved to be untrue if the impact area was taken as the cross-sectional area of the sphere. In fact, the pressures thus computed were roughly inversely proportional to missile diameter. This suggested that energy is absorbed not only by the Styrofoam directly in the missile path but also by a thin layer of Styrofoam surrounding the trajectory of the missile. If this layer is of constant thickness, its stopping effect on small missiles would be much greater than on large ones. This is exactly what was observed, in that the resistive pressure of the Styrofoam for small missiles was computed to be significantly higher than for large ones.

The next step in the analysis was to actually compute the thickness of this surrounding layer of influence where energy is absorbed. This was done by assuming that the actual resistive pressure of the Styrofoam is the same for all missiles up to 1 in. in diameter. The equation which states this is

$$\frac{F_1}{\frac{1}{4}\pi(D_1 + K)^2} = \frac{F_2}{\frac{1}{4}\pi(D_2 + K)^2} \tag{3.3}$$

where F_1 = resistive force for missile with diameter D_1
F_2 = resistive force for missile with diameter D_2
K = twice the thickness of absorbing layer of Styrofoam surrounding missile path

Solving Eq. 3.3 for K, we have

$$K = \frac{F_1^{0.5}D_2 - F_2^{0.5}D_1}{F_2^{0.5} - F_1^{0.5}} \tag{3.4}$$

Eight different diameters of missiles were used in this calibration (Table 3.1). K was solved for every combination of missile diameters. The average value of K was determined to be

Table 3.3—COMPUTATION OF THE AVERAGE DYNAMIC DEFORMATION PRESSURE, P_0, FOR STYROFOAM 22, ASSUMING AN EFFECTIVE DIAMETER OF IMPACT EQUAL TO THE MISSILE DIAMETER PLUS 0.041 IN.

	Missile type							
	Steel sphere	Glass sphere	Steel sphere	Steel sphere	Steel sphere	Cork marble	Steel sphere	Glass marble
Average force, lb	1.42	3.58	4.81	9.65	12.07	34.1	32.06	50.0
Missile diameter, in.	0.125	0.217	0.250	0.375	0.4375	0.739	0.750	0.931
Effective diameter (D + 0.041), in.	0.166	0.258	0.291	0.416	0.4785	0.780	0.791	0.972
Effective area, $in.^2$	0.0216	0.0523	0.0665	0.136	0.180	0.478	0.491	0.742
Pressure, psi	65.7	68.4	72.3	71.0	67.0	71.3	65.3	67.4

Average deformation pressure, P_0, = 68.6 psi

0.041 in. Using this value of K, effective areas of impact were computed for the eight different sizes of missiles (Table 3.3). Pressures were computed using this new concept of impact area. Within experimental error, the computed pressures were constant for the eight sizes of missiles. The average dynamic deformation pressure, P_0, was determined to be 68.6 psi.

Using the energy relation, Eq. 3.2, substituting pressure times area for force and converting certain units, we have

$$V = 361(D + 0.041)\ (s/m)^{0.5} \qquad (3.5)$$

where V = impact velocity, feet per second
D = diameter of the area of impact, D < 1 in.
s = stopping distance of the missile in Styrofoam 22, inches
m = missile mass, grams

It was realized at once that the diameter of impact, D, of Eq. 3.5 would be difficult to determine for irregularly shaped missiles. Therefore a test of the calibration equation, Eq. 3.5, was made by shooting eight irregular missiles into Styrofoam 22 at measured velocities. An attempt was made to determine the average diameter of impact from the holes left in the Styrofoam. This resulted in too small a value for D. The next trial was to determine an average diameter by averaging the longest dimension of the missile, the next longest one perpendicular to the first, and the longest dimension perpendicular to the first two. This procedure has some justification which it is assumed that irregular missiles probably experience some rotation during penetration. The latter technique was used to determine the average diameter of the eight irregular test missiles. The results of these tests are recorded in Table 3.4. The maximum error in velocity encountered in this study was 14 per cent.

Table 3.2 presents the data obtained by penetrating Styrofoam with 2.94-in.-diameter cylindrical missiles. The ends of the cylinders which were the impact areas were flat, hemispherical, and conical. The resistive pressure of the Styrofoam was computed for these missiles using the actual projected area of impact. Resistive pressure varied consistently with shape of impact surface and with depth of penetration. The conical surface penetrated with less pressure than the other two. This was, no doubt, due to a smaller accumulation of Styrofoam ahead of the missile than was the case with the flat and hemispherical impact surfaces. All three types of missiles showed an increase of pressure with depth of penetration. This indicates an increasing accumulation of compressed Styrofoam ahead of the

Table 3.4—IRREGULAR MISSILES SHOT FROM AIR GUN INTO STYROFOAM 22

		Brass rectangular slug	Steel nut	Stone	Wood chip	Glass chip	Sharp stone	Stone	Stone
Missile dimensions, in.	1.	0.850	0.926	0.724	0.928	0.717	0.788	0.952	1.103
	2.	0.850	0.926	0.709	0.445	0.559	0.536	0.582	0.602
	3.	0.693	0.315	0.559	0.750	0.205	0.670	0.425	0.476
		2.393	2.167	1.992	2.123	1.481	1.994	1.959	2.181
Equivalent diameter ($\overline{D}$), in.		0.798	0.722	0.664	0.708	0.494	0.665	0.653	0.727
K, in.		0.041	0.041	0.041	0.041	0.041	0.041	0.041	0.041
$\overline{D}$ + K, in.		0.839	0.763	0.705	0.749	0.535	0.706	0.694	0.768
Penetration, in.		13.25	8.87	6.62	6.50	5.75	7.50	8.75	3.00
$0.833\overline{D}$		0.66	0.60	0.55	0.59	0.41	0.55	0.54	0.61
s, in.		13.91	9.47	7.17	7.09	6.16	8.05	9.29	3.61
m, g		16.2	10.6	7.6	1.45	1.75	5.12	4.5	5.4
s/m		0.858	0.893	0.943	4.89	3.52	1.574	2.066	0.668
$(s/m)^{0.5}$		0.926	0.944	0.970	2.21	1.875	1.254	1.437	0.816
$V = 361(D + 0.041)(s/m)^{0.5}$, ft/sec		281	260	247	597	362	320	360	226
Measured velocity (V_m), ft/sec		246	247	271	524	418	323	346	204
$V - V_m$		+35	+13	−24	+73	−56	−3	+14	+22
Error, %		+14	+5	−9	+14	−13	−1	+4	+10

missile as penetration proceeds. It is not surprising that this effect was not noticed with missiles having impact diameters of less than 1 in. since, in this case, the missile dimension is small compared to the depth of penetration, resulting in the establishment of an equilibrium in the compressed Styrofoam ahead of the missile soon after impact.

3.4.4 Determination of Impact Velocities of Natural Missiles

Tests of Eq. 3.5 were made using irregular missiles shot into Styrofoam 22. The results, recorded in Table 3.4, show a maximum velocity error of 14 per cent for eight missiles whose equivalent diameters of impact were less than 1 in. The equivalent diameter of these missiles was computed, as described above, on the assumption of rotation during penetration. If actual missiles are found which obviously did not rotate, then the equivalent diameter of impact must be computed from the dimensions of the presenting cross section of the missile rather than by the method described above.

Natural missiles of equivalent impact diameters larger than 1 in. should be treated as special problems. A rough estimate of their impact velocities can be obtained using the data recorded in Table 3.2. To arrive at an estimate of their impact velocities, the missiles themselves should be shot from an air gun at measured velocities into a similar Styrofoam absorber.

3.5 CALIBRATION OF STYROFOAM ABSORBER FOR GLASS-FRAGMENT MISSILES

The use of Eq. 3.5 for evaluation of the velocity of irregular missiles has been described in Sec. 3.4.3. The most tedious procedure required in the use of this equation is the evaluation of an average diameter for each missile. Since 95 per cent of the missiles from the open shot were glass fragments, an attempt was made to develop, for this type of missile, a method for the evaluation of velocity which would not require the measurement of an average diameter.

3.5.1 Results

A total of 96 glass missiles—typical of those encountered in the field (see Fig. 6.1)—ranging in mass from 0.0164 to 4.99 g were shot into Styrofoam at measured velocities ranging from 142 to 344 ft/sec (see Table 3.5). The air gun used for this purpose is described in Sec. 3.4.1.

3.5.2 Analysis of the Data

Equation 3.5 was rearranged as follows:

$$k = (V/361)\ (m/s) \tag{3.6}$$

where k is the effective diameter, measured in inches, corresponding to (D + 0.041) in Eq. 3.5.

Equation 3.6 was used to compute k for each of the 96 test missiles. Figure 3.3 shows a logarithmic plot of the computed k values as a function of missile mass. A regression analysis of these data indicated that the mathematical relation between effective diameter and missile mass was

$$\log m = 1.240 + 3.285 \log k \tag{3.7}$$

where m is the mass of glass-fragment missiles in grams and k is the effective diameter in inches. The standard error of estimate was found to be 10.5 per cent. Equation 3.7 is plotted as the solid line in Fig. 3.3.

The dashed curve in Fig. 3.3 was plotted from

$$k = (6m/\pi d)^{1/3} + 0.041 \tag{3.8}$$

where d is the density of glass in grams per cubic inch. The first term, $(6m/\pi d)^{1/3}$, represents the diameter of a glass sphere of mass m. The second term, 0.041, is the diameter-correction

Table 3.5—DATA USED FOR THE CALIBRATION OF STYROFOAM 22 FOR GLASS-FRAGMENT MISSILES

m = missile mass, grams
V = measured impact velocity, feet per second
s = depth of penetration in Styrofoam, inches

m	V	s	m	V	s	m	V	s
1.760	180	2.650	0.451	184	0.830	0.068	204	0.428
0.215	244	1.212	1.200	158	0.970	0.096	174	0.607
0.215	243	1.322	1.220	245	2.910	0.104	195	0.807
0.215	245	1.105	1.220	168	2.910	0.101	173	0.710
0.0821	249	1.182	1.620	184	1.950	0.0292	172	0.385
0.0840	189	0.682	1.270	190	1.435	0.0164	250	0.460
0.110	188	0.432	1.730	174	1.925	0.0387	253	0.650
0.110	192	0.802	1.780	178	2.565	0.0805	194	0.628
0.110	251	1.065	1.350	180	1.865	0.0386	236	0.485
0.110	244	0.970	0.792	216	1.465	0.0400	242	0.550
0.445	237	1.717	1.500	175	1.730	0.438	178	0.904
0.446	186	1.215	1.180	201	1.490	0.718	194	1.730
0.445	205	1.437	1.200	192	1.705	0.298	295	2.450
0.818	152	0.645	1.550	216	2.240	0.613	221	1.405
0.818	201	1.777	0.438	294	1.950	1.230	189	1.695
1.150	142	1.117	0.719	276	2.270	0.422	178	1.040
1.140	196	1.950	0.298	294	2.550	0.756	151	1.005
1.910	203	4.100	0.613	275	2.520	0.944	123	0.923
2.070	245	4.455	1.230	240	2.390	0.550	148	0.804
4.990	220	7.230	0.422	299	2.405	0.393	153	0.700
0.111	272	1.262	0.756	268	2.455	0.456	232	2.385
0.111	244	1.272	0.944	244	2.380	0.059	195	0.447
0.111	174	0.812	0.550	270	2.910	0.448	186	1.035
0.451	328	2.752	0.393	294	2.390	0.121	192	0.750
0.295	340	2.395	0.210	248	1.515	0.366	180	1.035
0.240	344	2.385	0.181	252	1.545	0.466	183	1.320
0.362	288	2.000	0.498	181	1.050	0.448	326	2.940
0.0746	309	1.020	0.385	186	1.130	0.449	322	2.905
0.484	275	2.120	0.494	181	0.975	1.210	195	1.995
0.378	243	1.655	0.438	178	1.070	1.510	190	2.500
0.318	239	1.425	0.400	184	1.185	0.769	210	1.645
0.230	245	1.715	0.328	181	0.915	1.440	183	1.745

term which was determined in the calibration of Styrofoam using spherical missiles. An examination of Fig. 3.3 indicates that this curve fits the experimental data almost as well as the regression curve, Eq. 3.7. This somewhat surprising relation indicates that, on the average, a glass fragment—at least for the size and weight dealt with here—acts upon impact with Styrofoam as if it were a glass sphere of the same mass.

Thus two expressions were at hand relating the effective diameter of a glass-fragment missile to its mass. Chiefly because of its mathematical simplicity, it was decided to use Eq. 3.7 to arrive at a new calibration equation for glass-fragment missiles absorbed in Styrofoam. This was done by combining Eqs. 3.6 and 3.7, eliminating the parameter k. The resulting equation was

$$V = 151 m^{-0.1955} s^{0.500} \qquad (3.9)$$

where V = velocity of the glass fragment at impact, feet per second
m = mass of the glass fragment missile, grams
s = depth of penetration in Styrofoam, inches

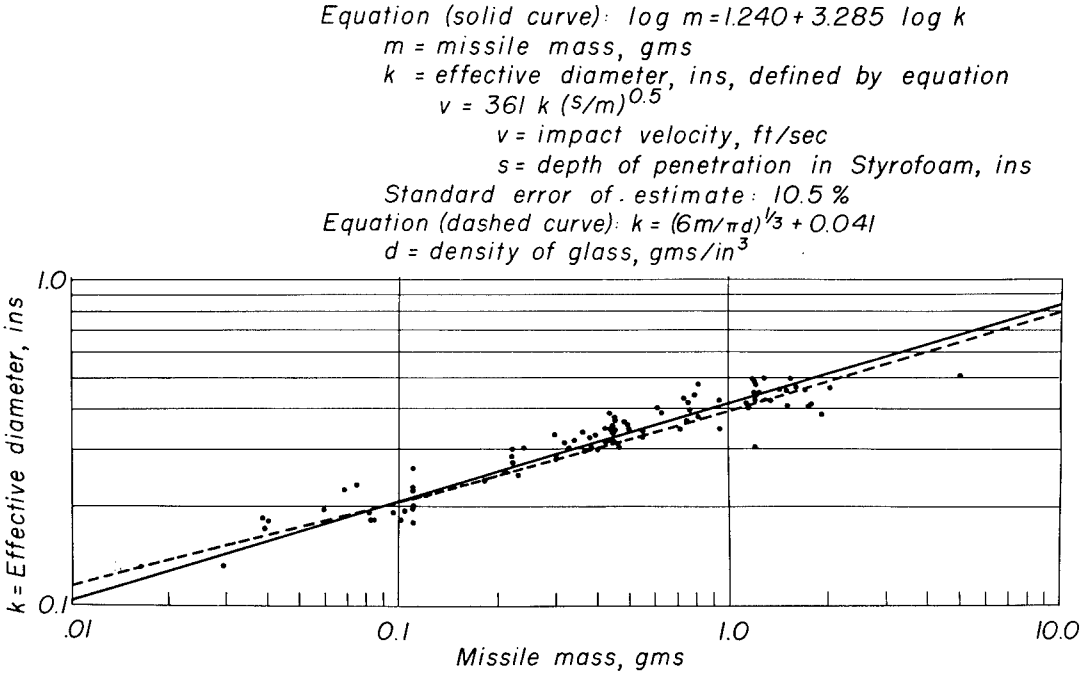

Fig. 3.3—Effective diameter of glass-fragment missiles as a function of missile mass for penetration into Styrofoam 22.

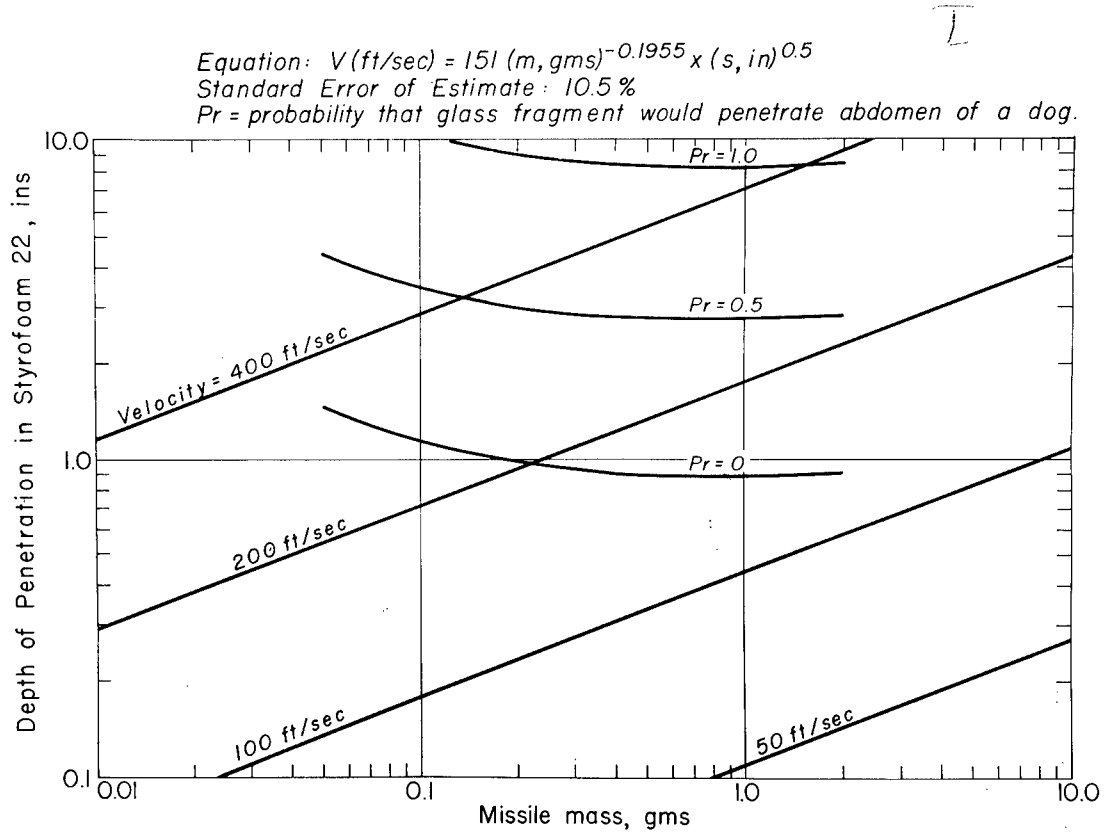

Fig. 3.4—Velocity of glass-fragment missiles at impact as a function of mass and depth of penetration into Styrofoam 22.

Figure 3.4 is a graphical expression of this relation.* The logarithm of the depth of penetration is plotted against the logarithm of missile mass for constant velocities of 50, 100, 200, and 400 ft/sec. These velocity values form a geometric progression, but when plotted as in Fig. 3.4 they form a family of equidistant and parallel straight lines. This permitted the evaluation of velocity values between the constant velocity lines by means of a suitable logarithmic scale.

*A parenthetical explanation of the probability curves in Fig. 3.4 is necessary. An additional biophysical study (to be presented in a separate report) was made to determine the probability of penetration of glass missiles into the abdomens of dogs. The probability of penetration of a given glass missile was found to depend on missile mass and impact velocity. Since these parameters appear in Fig. 3.4, it was possible to plot probability lines, thus relating probability of penetration in the abdomen of a dog to missile mass and depth of penetration in Styrofoam.

CHAPTER 4

MISSILE-TRAP INSTALLATIONS AND THE GROSS EFFECTS OF THE DETONATION

Table 4.1 indicates the location of the 27 traps used in the operation. The yield of the open shot was approximately 50 per cent greater than nominal (a nominal atomic bomb has an energy release equivalent to 20 kt of TNT).

Figure 4.1 is a map of the test area showing the location of the houses where missile traps were installed. The locations of the six traps placed behind houses are also shown.

Figures 4.2 to 4.8 are floor plans of the various houses indicating the locations of the missile traps. Particular attention was given to the description of windows and the location of furniture.

Figures 4.9 to 4.29 are photographs of 14 representative missile-trap installations. These photographs illustrate the anchoring techniques which were discussed in Sec. 3.3 and some of the gross effects of the detonation.

Figure 4.9 is an "after" picture of the half-size missile trap placed in the open basement exit shelter at a distance of 1470 ft from Ground Zero. The effect of the blast was to compress the Styrofoam. Evidently, several sheets of Styrofoam were then pulled out of the housing by the negative pressure phase. The remainder of the traps, located at distances of 4700 to 10,500 ft from Ground Zero, were found to be in good condition and securely anchored after the detonation.

Figure 4.10 is a picture of trap 2A taken before the detonation. Figure 4.11 shows the remains of the brick house where this trap was located. Trap 2A can be seen still anchored to the partition wall on the second floor. The debris which is seen attached to the front surface of the trap is the remains of a metal venetian blind. It is of interest to note that 250 glass missiles were recovered from this trap. This means that at least some of the glass fragments must have arrived at the trap before the venetian blind. However, that the venetian blind provided some shielding for the trap is evidenced by Fig. 5.24, and the reader is referred to Sec. 5.3 for additional information.

Figure 4.12 shows the loaction of trap 2C between the living room and dining room of the rambler house at a range of 4700 ft. This trap was held in place with three chains secured to the concrete floor with $\frac{3}{8}$-in. Ramset fasteners. Angle iron was secured to the floor against the rear of the trap to prevent translational motion. Figure 4.13 shows the same trap after the detonation. Only one of the three chains remained in place. The living room of this house was completely demolished.

Figure 4.14 shows the location of traps $2D_1$ and $2D_2$ in the center front bedroom of the same house. Figure 4.15 is a picture of these traps after the detonation. The face of trap $2D_2$ was almost completely covered by the twisted and mangled metal venetian blind. In spite of this covering, 231 glass missiles were retrieved from trap $2D_2$ as compared to 246 from $2D_1$.

Figure 4.16 is a picture of traps $2E_1$ and $2E_2$, which were placed in the front bedroom of the reinforced concrete house at a range of 4700 ft. The tower at Ground Zero can be seen in the right window. This window was later covered by curtains. Figure 4.17 shows the same traps after the detonation. The breakage of windows was practically the only damage done to

Table 4.1 — LOCATIONS OF MISSILE TRAPS IN THE OPEN SHOT

Missile trap No.	Structure No.	Distance from Ground Zero, ft	Remarks
1A	34.1 d-2	1,470	Half-size trap, basement exit shelter with open door
2A	31.1 a-1	4,700	Second floor, brick house, bedroom No. 2. on 36-in. stand facing window toward Ground Zero
2B	31.1 c-1	4,700	Second floor, brick house, bedroom No. 3, on 24.25-in. stand facing window away from Ground Zero
2C	31.1 c-1	4,700	Between living room and dining room, rambler house, on floor facing large window toward Ground Zero
$2D_1$, $2D_2$	31.1 c-1	4,700	Rambler house, center front bedroom, $2D_2$ stacked on $2D_1$, facing window toward Ground Zero
$2E_1$, $2E_2$	31.1 e-1	4,700	Precast concrete house, front bedroom, $2E_2$ stacked on $2E_1$, facing window toward Ground Zero
2F	31.1 a-1	4,742	30 ft behind center of brick house
2G	31.1 c-1	4,733	20 ft behind center of dining-room window, rambler house
2H	31.1 c-1	4,800	100 ft behind center of rambler house
3A, 3B	31.1 b-1	5,500	Half-size traps in lean-to shelter, basement of two-story frame house; 3A facing opening of shelter toward WSW; 3B facing opening of shelter toward ENE
$3C_1$, $3C_2$	31.1 b-1	5,500	Second floor, frame house, bedroom No. 2, $3C_2$ stacked on $3C_1$, facing window toward Ground Zero
$4A_1$, $4A_2$	31.1 e-2	10,500	Precast concrete house, back bedroom, $4A_2$ stacked on $4A_1$, facing large window away from Ground Zero
$4B_1$, $4B_2$, $4B_3$, $4B_4$	31.1 e-2	10,500	Living room of precast concrete house facing large window toward Ground Zero; $4B_2$ stacked on $4B_1$, WSW of $4B_4$ stacked on $4B_3$
4C	31.1 c-2	10,500	On 18-in. stand in living room, rambler house, against WSW wall, facing 90° away from blast line
4D	31.1 c-2	10,500	Between living room and dining room, rambler house, on floor facing large window toward Ground Zero
4E	31.1 c-2	10,500	On 36-in. stand, back corner bedroom, rambler house, against wall, facing window on ENE side of house
4F	31.1 f-2	10,600	100 ft behind center of concrete block house
4G	31.1 c-2	10,533	20 ft behind center of dining-room window, rambler house
4H	31.1 c-2	10,600	100 ft behind center of rambler house

this house. Two hundred and forty-one missiles were recovered from trap $2E_1$ and 726 from $2E_2$. Note the glass debris on the bed and floor and the damage to the wall behind the trap which was caused by flying glass.

Figure 4.18 shows trap 2F placed 30 ft behind the brick house at a range of 4700 ft. A hydraulic press and an electric motor can be seen between the trap and the house. Figure 4.19, a picture of the same trap after the detonation, indicates that part of the roof and pieces of brick and other miscellaneous debris fell in the vicinity of the trap. The trap, however, caught only six missiles, all of which were fragments of glass.

Figure 4.20 is a picture of trap 2G taken after the detonation. This trap, located 20 ft behind the rambler house on the 4700-ft line, was not damaged in spite of the fact that a large portion of the house roof fell directly on it. Only six glass missiles satisfactory for analysis were obtained from this trap. Many other missiles, not traveling fast enough to be embedded, made dents in the surface of the Styrofoam.

Figure 4.21 shows trap 2H, 100 ft behind the rambler house at a range of 4700 ft, after the detonation. The black marks to be seen on the surface of the wood housing were caused by thermal radiation. The Styrofoam, however, was protected by aluminum foil and showed no signs of thermal damage. Part of the aluminum foil was evidently blown away by the blast. This trap caught 100 missiles, 86 of which were small stones.

Figure 4.22 shows trap 3A after the explosion. It was located in the lean-to shelter in the basement of the two-story frame house at a range of 5500 ft. No missiles were caught by this trap. Figure 4.23 is a picture of traps $3C_1$ and $3C_2$ which were placed in a second-floor bedroom of the same house. Figure 4.24 shows these traps after the detonation. In spite of the debris which was thrown against the face of the traps, $3C_1$ caught 61 missiles and $3C_2$, 259 missiles.

Figure 4.25 is a picture of traps $4A_1$ and $4A_2$ taken after the detonation. These traps were placed in the back bedroom of the reinforced concrete house on the 10,500-ft line facing 180° away from the blast. Although no missiles were caught by these traps, fragments of glass can be seen on the floor around the traps. Experience has shown that missiles traveling less than about 50 ft/sec do not embed themselves in the Styrofoam.

Figure 4.26 shows the bank of traps placed in the front room of the reinforced concrete house at a range of 10,500 ft. The results of the blast are shown in Fig. 4.27. A total of 22 missiles were caught by these four traps.

Missile traps 4C and 4D are shown in Fig. 4.28 placed in the living-room and dining-room area of the rambler house on the 10,500-ft line. Trap 4D was facing the blast in a position corresponding to trap 2C on the 4700-ft line. Trap 4C was facing 90° away from the blast and caught no missiles. Figure 4.29, depicting 4D after the detonation, indicates that many fragments of glass must have been in motion during the blast, although only 15 missiles were found embedded in the Styrofoam.

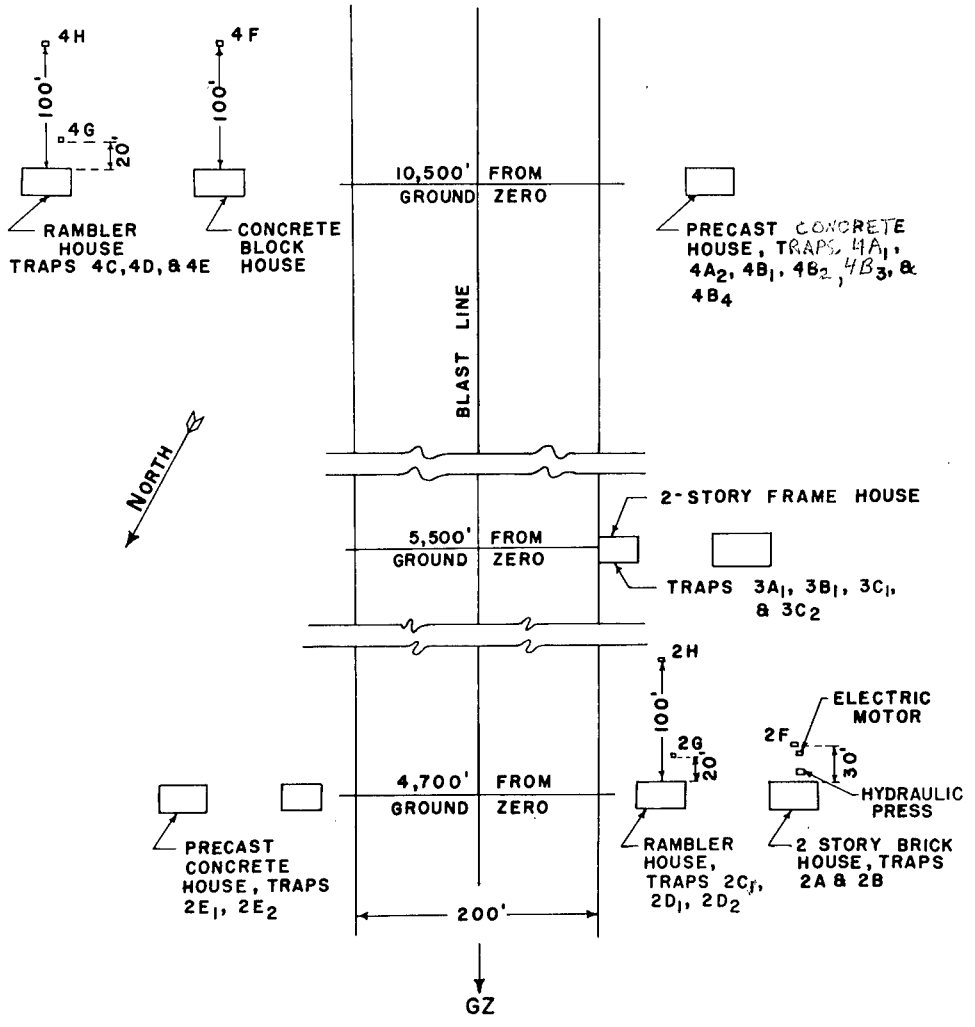

Fig. 4.1 — Location of missile traps in the open shot, Operation Teapot.

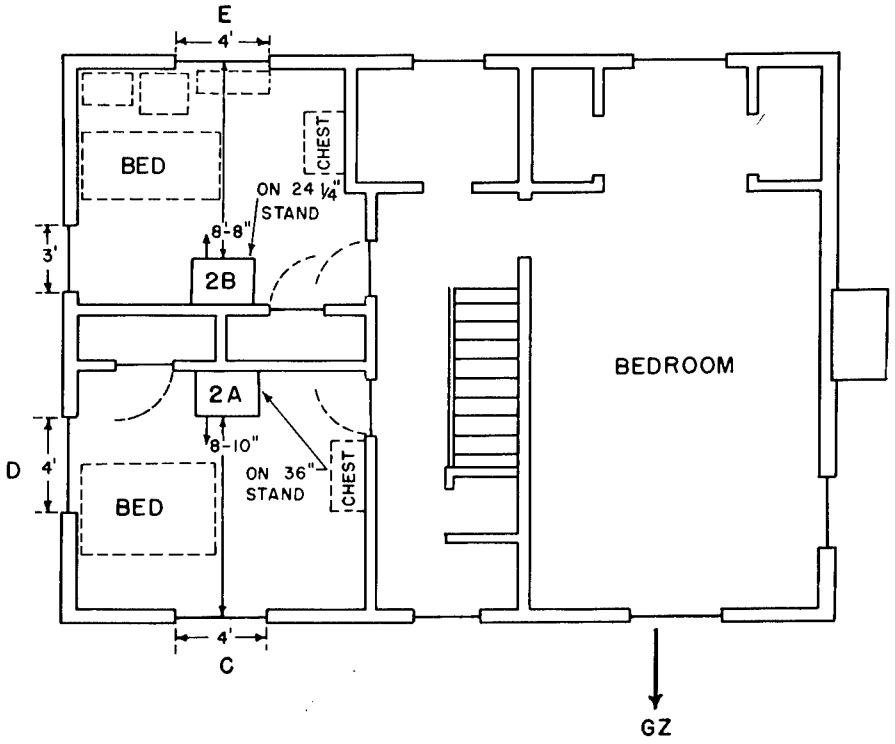

Fig. 4.2—Second-floor plan of FCDA two-story brick house, showing location of missile traps 2A and 2B, 4700 ft from Ground Zero. Windows C, D, and E: covered with venetian blinds, 33½ in. from the floor, 49½ in. high, 16 panes (12 in. by 12 in.), and wooden frames.

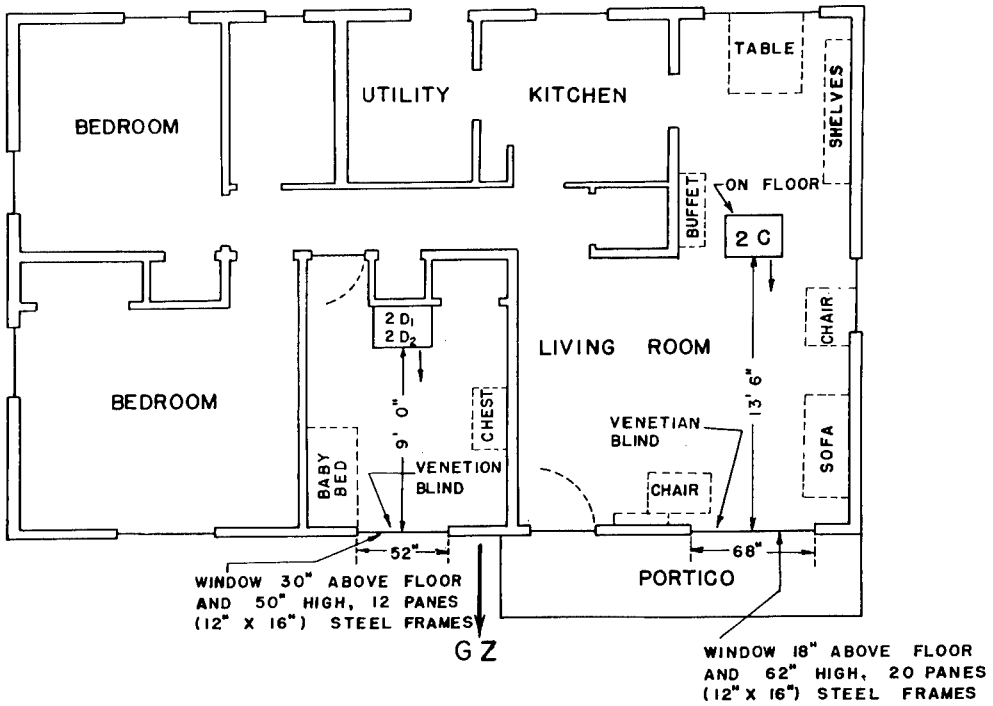

Fig. 4.3—FCDA frame rambler house, showing location of missile traps 2C, $2D_1$, and $2D_2$ ($2D_2$ stacked on $2D_1$), 4700 ft from Ground Zero.

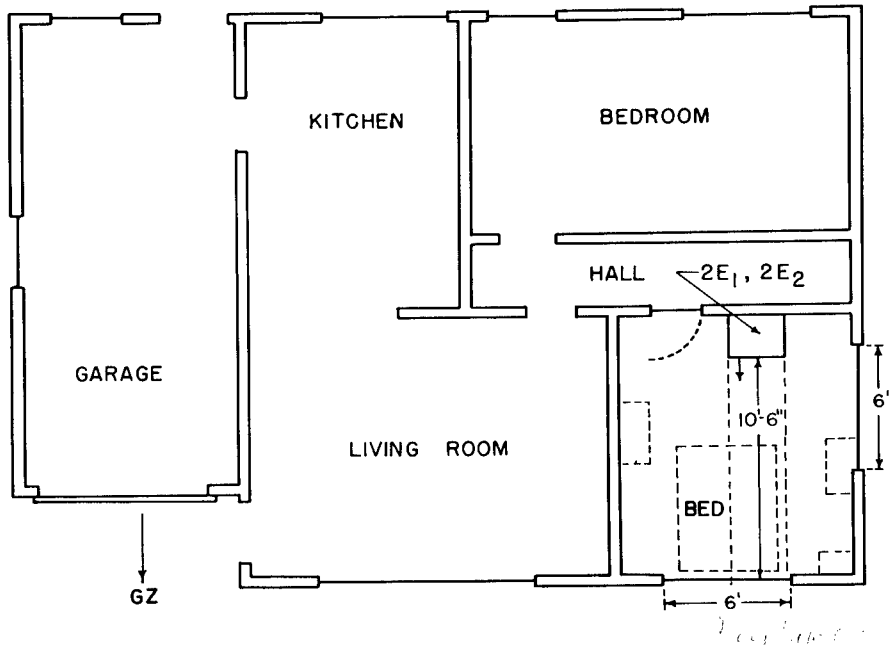

Fig. 4.4—Plan view of precast concrete house, showing location of missile traps $2E_1$ and $2E_2$ ($2E_2$ stacked on $2E_1$), 4700 ft from Ground Zero. Windows: covered with curtains, steel frames, 42 in. above the floor, $37\frac{1}{2}$ in. high, nine panes (12 in. by $23\frac{1}{2}$ in.).

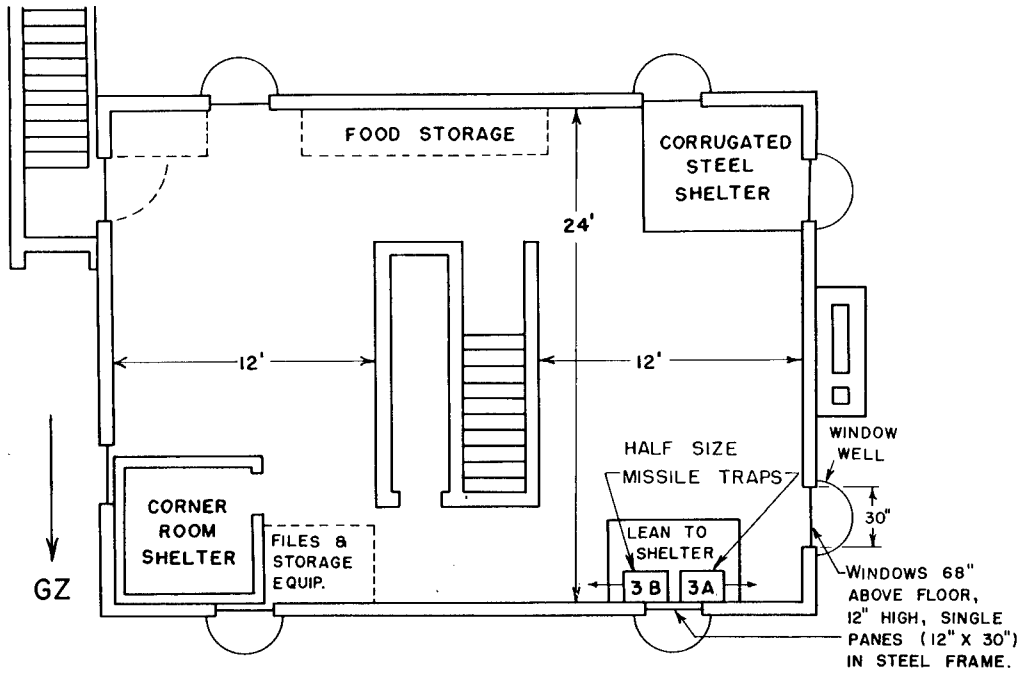

Fig. 4.5—Basement plan of FCDA redesigned two-story frame house, showing location of missile traps 3A and 3B, 5500 ft from Ground Zero.

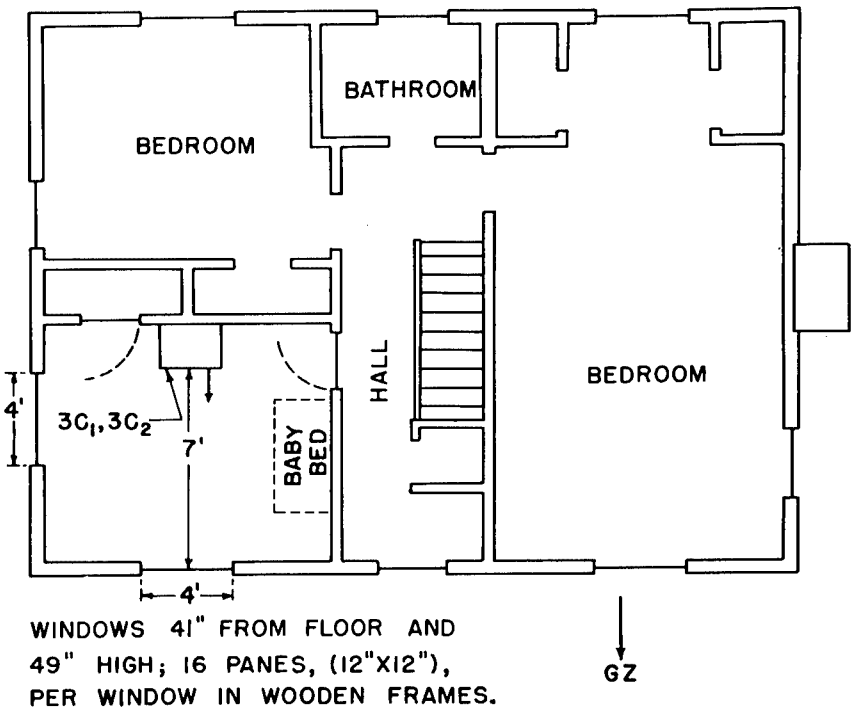

Fig. 4.6—Second-floor plan of FCDA redesigned two-story frame house, showing location of missile traps $3C_1$ and $3C_2$ ($3C_2$ stacked on $3C_1$), 5500 ft from Ground Zero. Windows were partly covered by drapes.

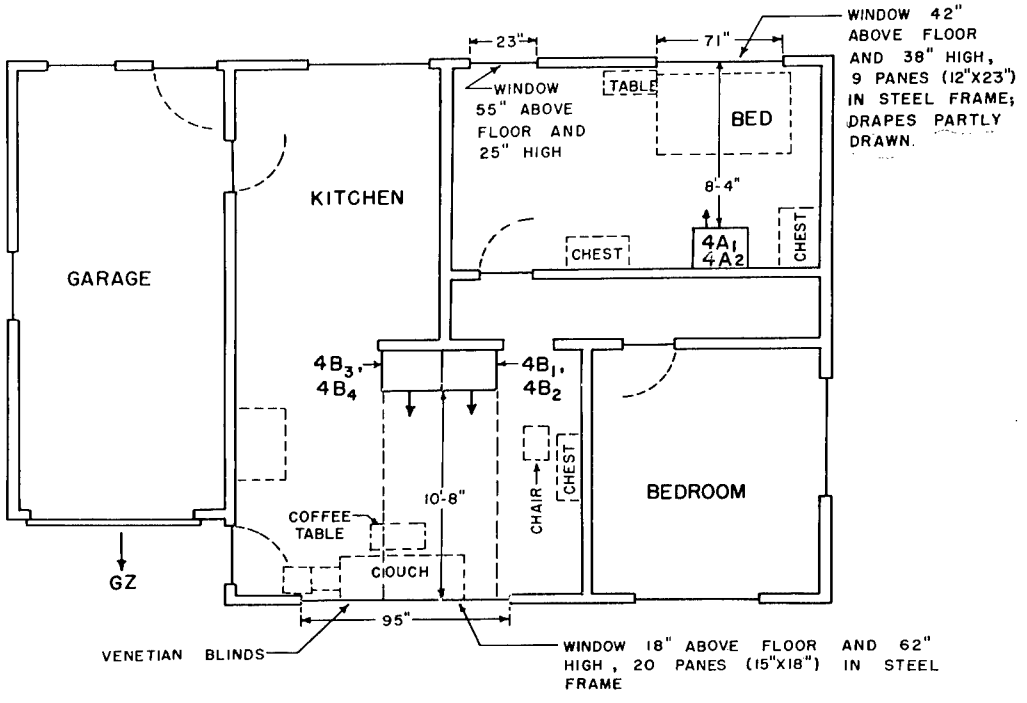

Fig. 4.7—Floor plan of precast concrete house, showing location of missile traps $4A_2$ stacked on $4A_1$, $4B_2$ stacked on $4B_1$, and $4B_4$ stacked on $4B_3$, 10,500 ft from Ground Zero.

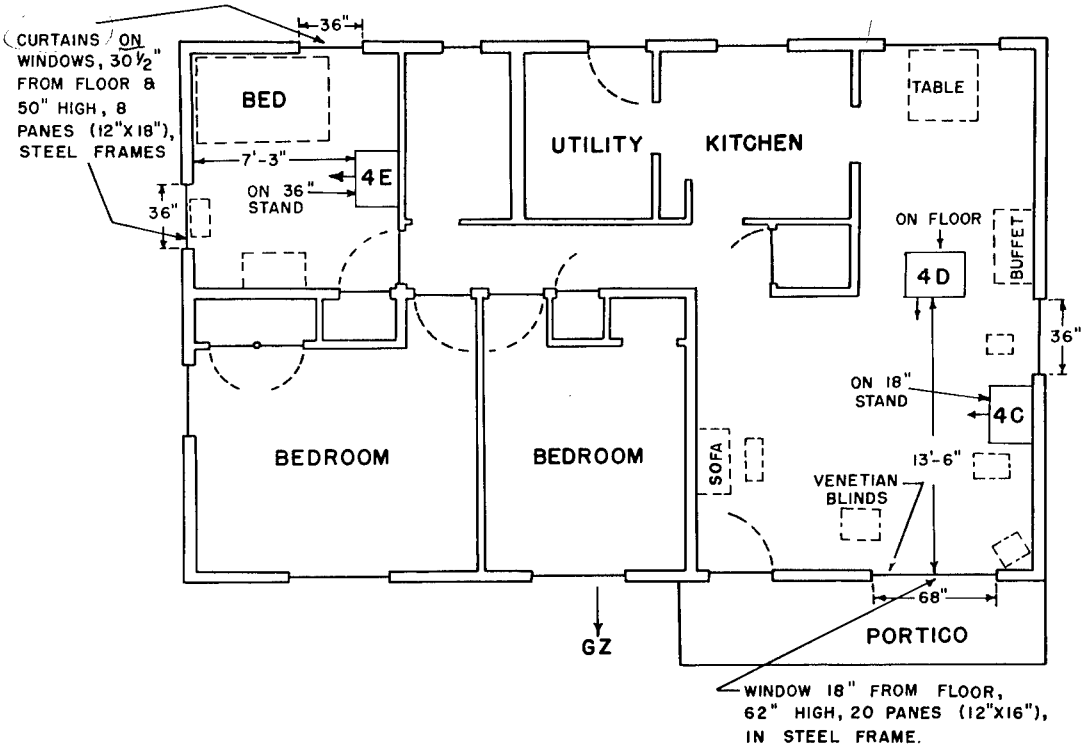

Fig. 4.8—FCDA frame rambler house, showing location of missile traps 4C, 4D, and 4E, 10,500 ft from Ground Zero.

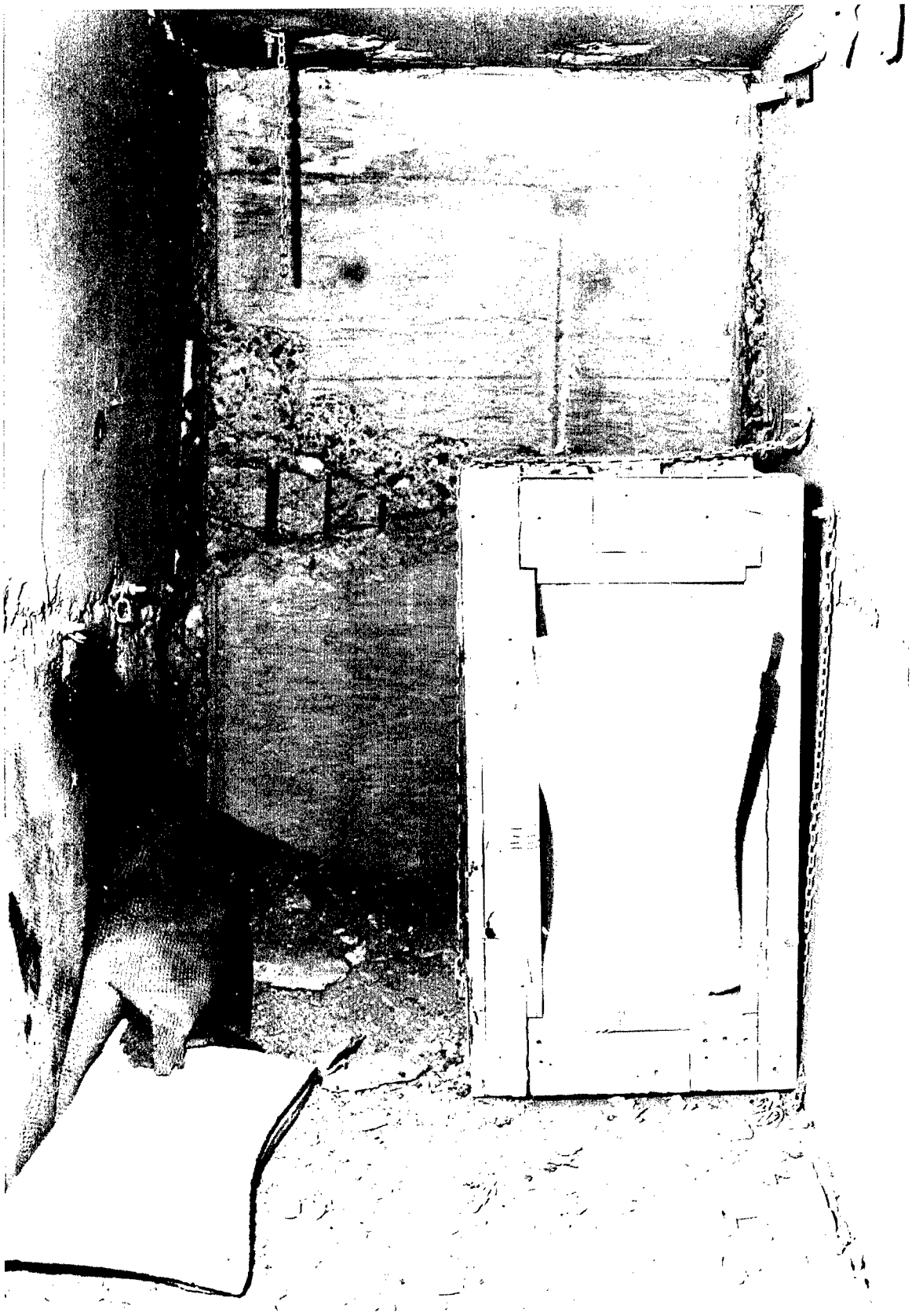

Fig. 4.9 — Trap 1A, postshot, half-size trap in basement exit shelter (34.1 d-2) with open door, 1470 ft from Ground Zero.

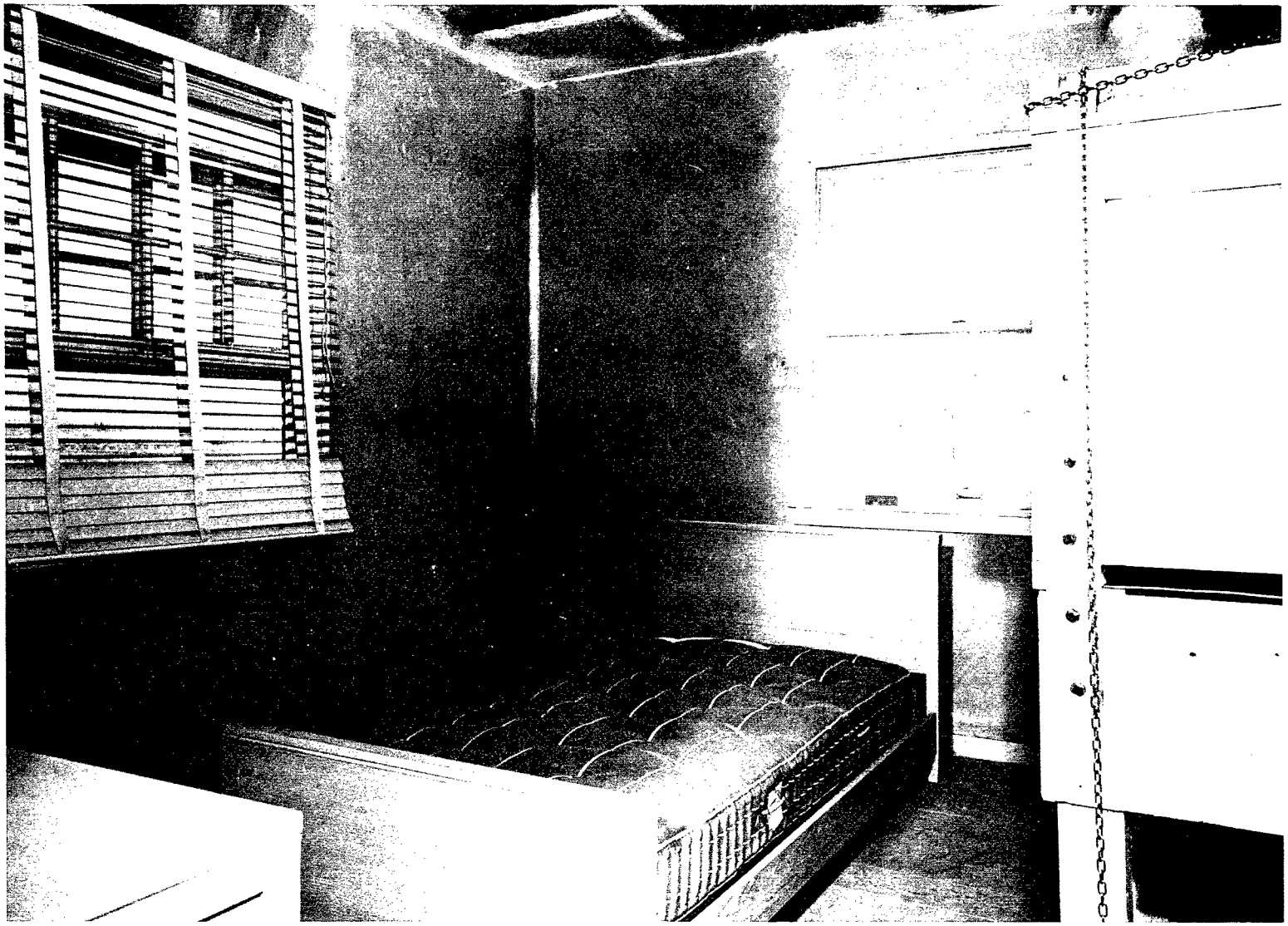

Fig. 4.10 — Trap 2A, preshot, second-floor bedroom of brick house (31.1 a-1) on 36-in. stand facing window toward Ground Zero, 4700 ft from Ground Zero.

Fig. 4.11—Trap 2A after the detonation. See Fig. 4.10.

Fig. 4.12—Trap 2C, preshot, between living room and dining room of rambler house (31.1 c-1), facing large window toward Ground Zero, 4700 ft from Ground Zero.

Fig. 4.13—Trap 2C after the detonation. See Fig. 4.12.

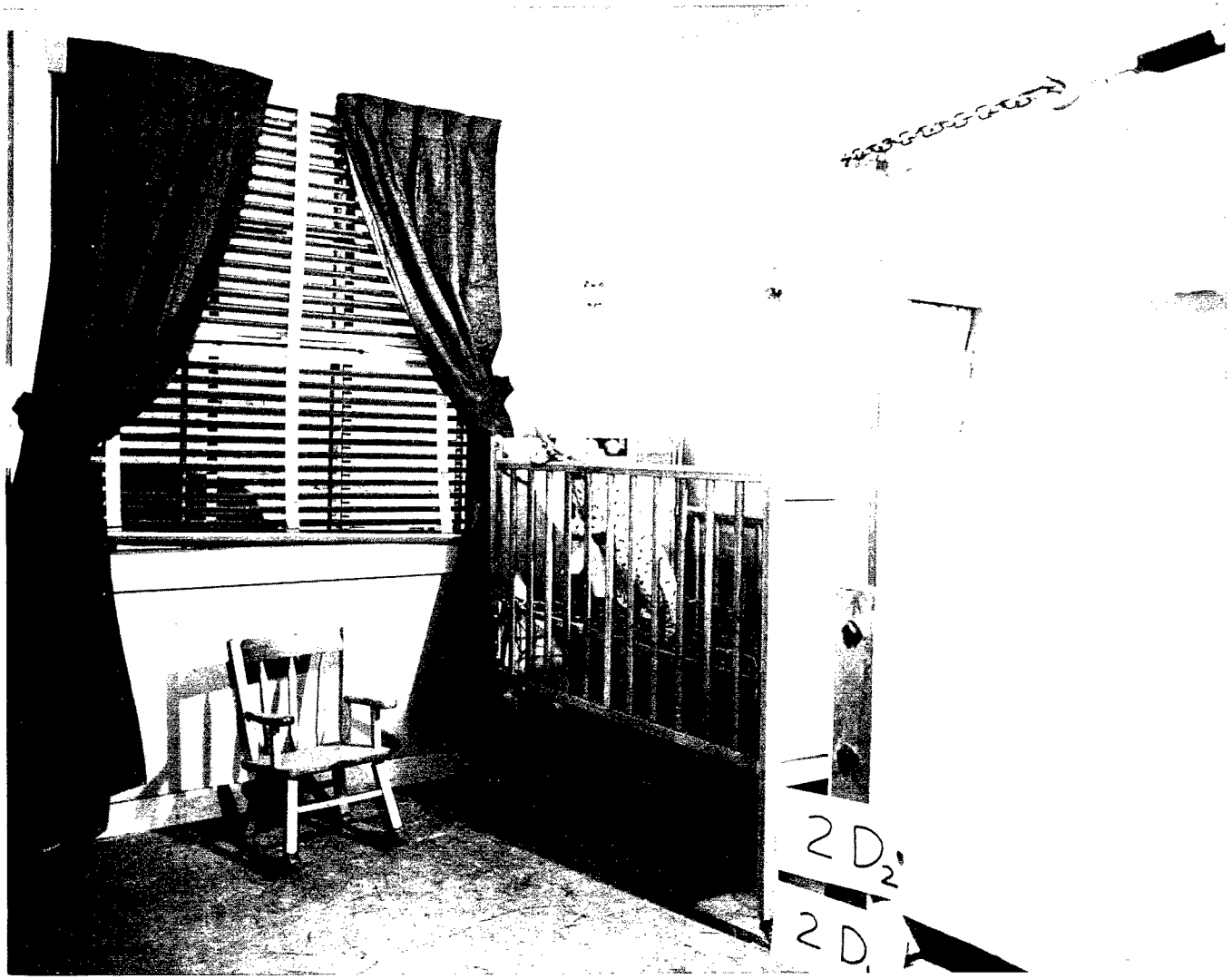

Fig. 4.14—Traps $2D_1$ and $2D_2$, preshot, center front bedroom of rambler house (31.1 c-1), facing window toward Ground Zero, 4700 ft from Ground Zero.

Fig. 4.15—Traps $2D_1$ and $2D_2$ after the detonation. See Fig. 4.14.

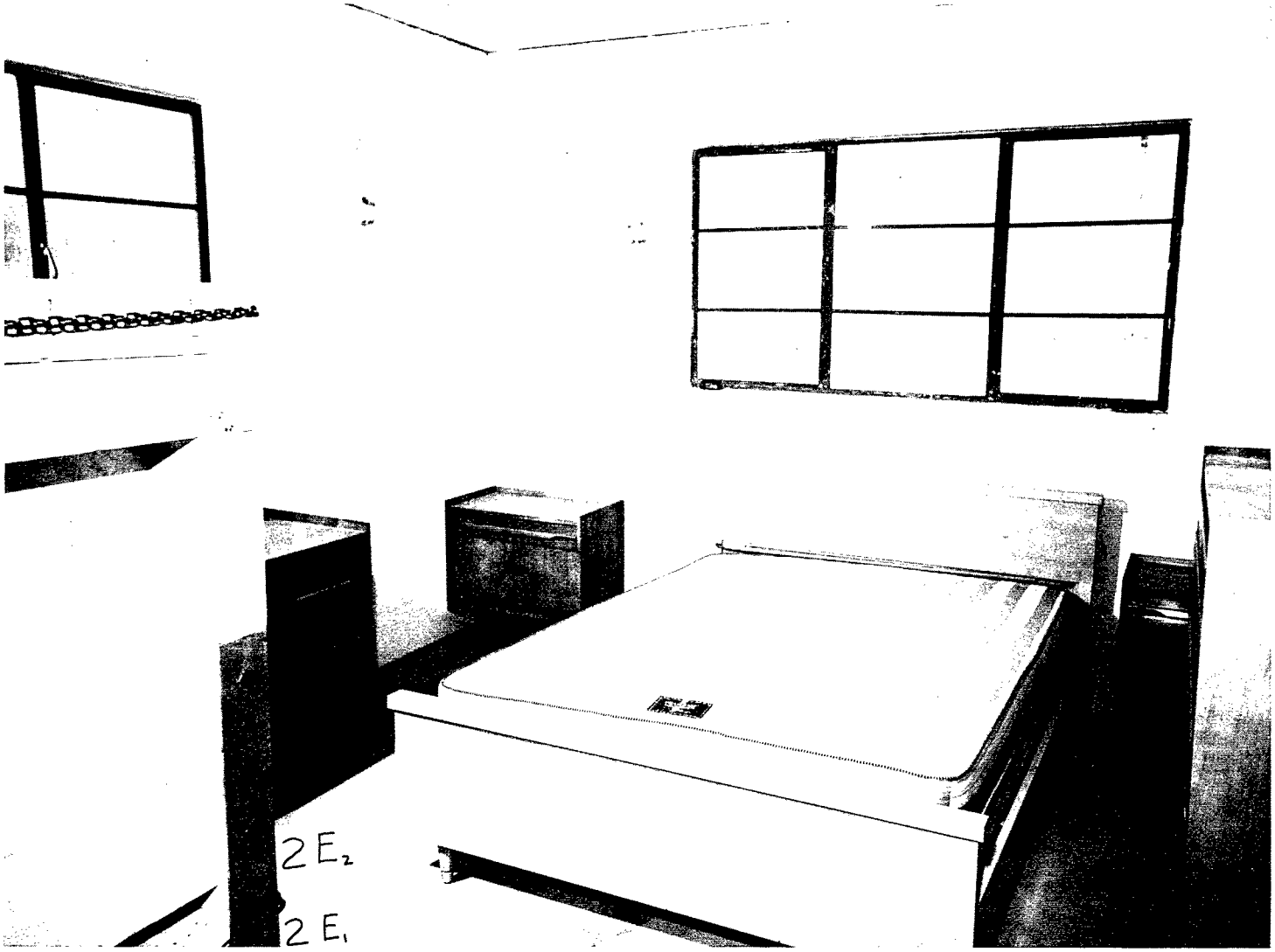

Fig. 4.16—Traps $2E_1$ and $2E_2$, preshot, facing window toward Ground Zero in precast concrete house (31.1 e-1), 4700 ft from Ground Zero. (Curtains were added after picture was taken.)

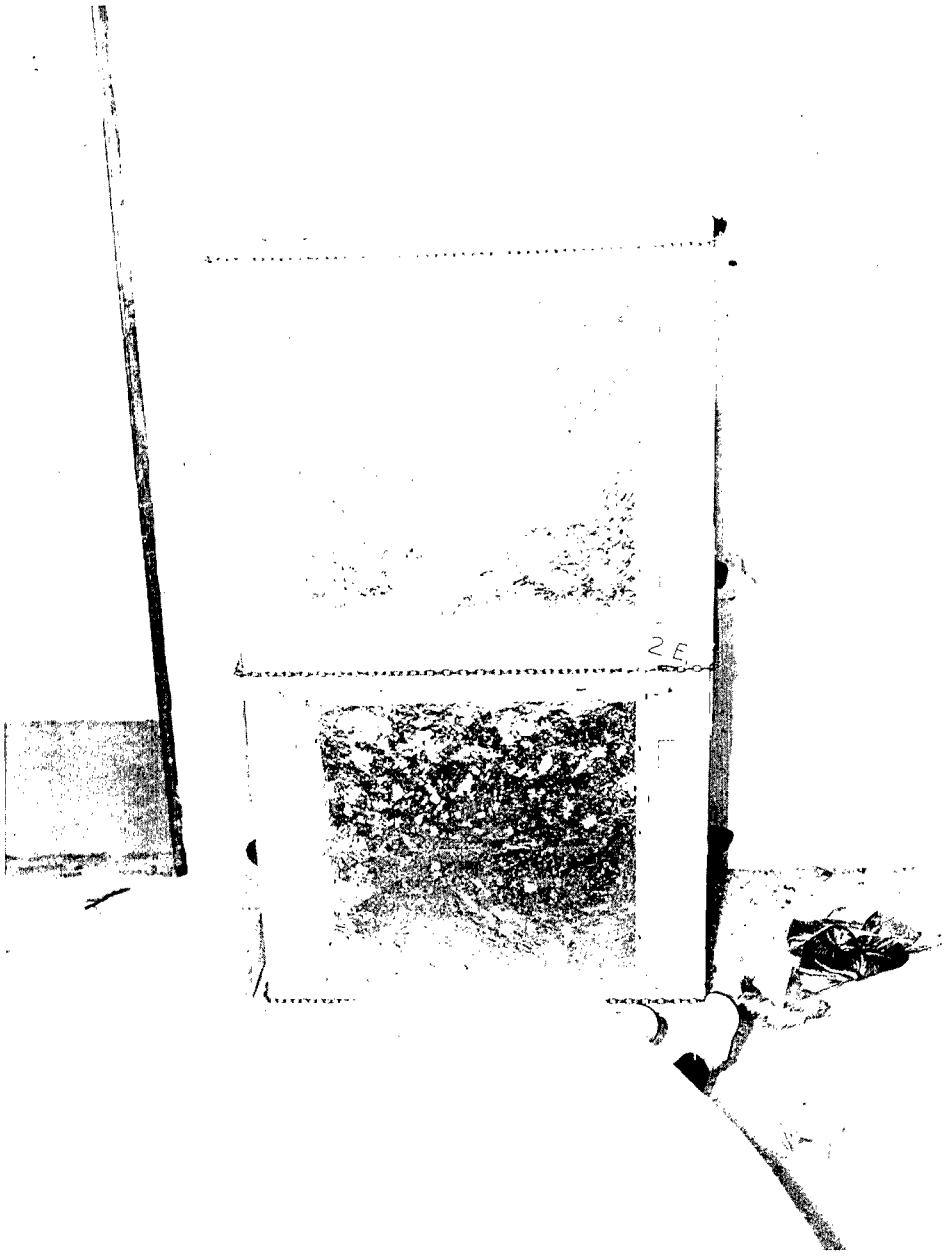

Fig. 4.17 — Traps $2E_1$ and $2E_2$, postshot. See Fig. 4.16.

Fig. 4.18—Trap 2F, preshot, 30 ft behind center of brick house (31.1 a-1), 4742 ft from Ground Zero.

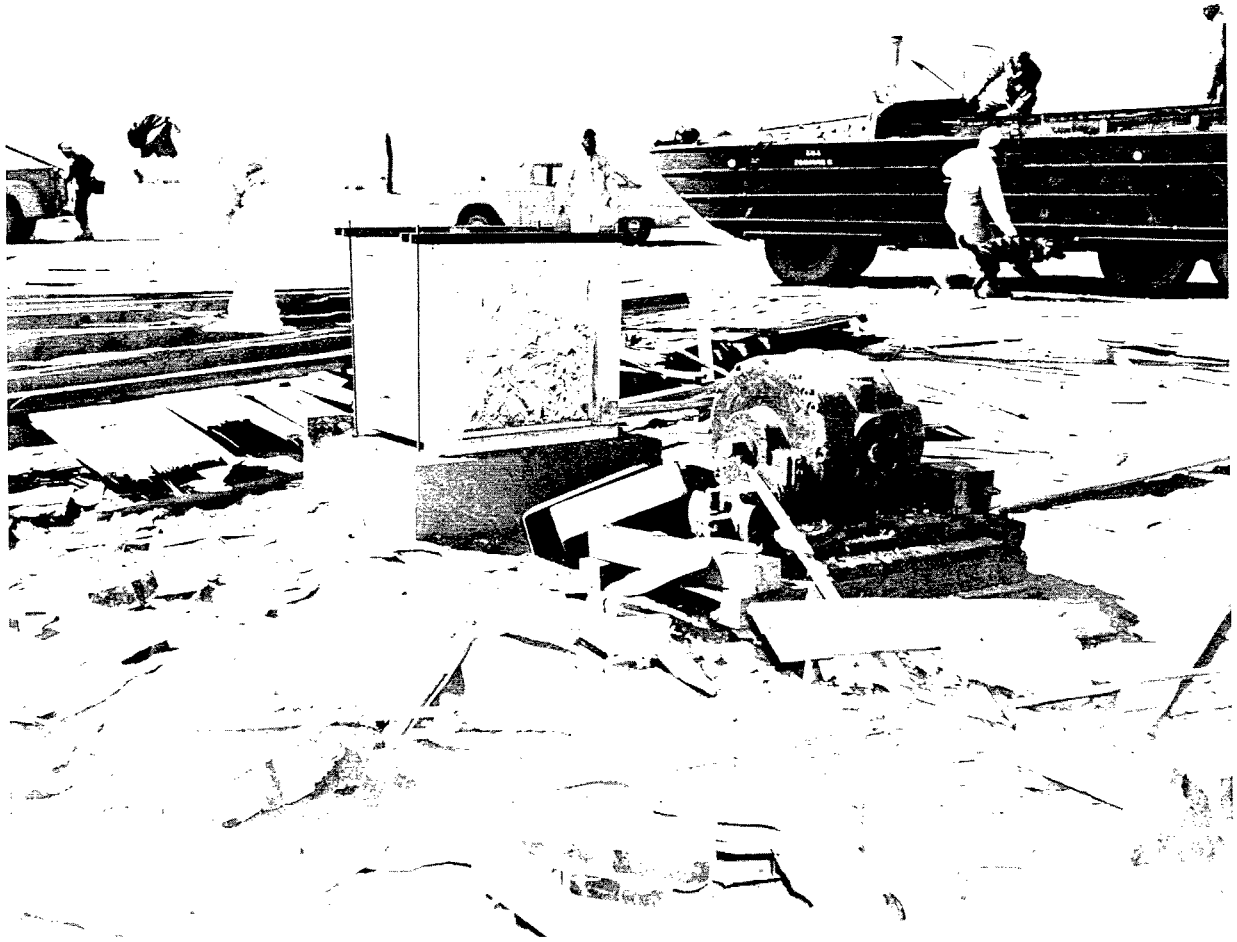

Fig. 4.19—Trap 2F after the detonation. See Figs. 4.18 and 4.11.

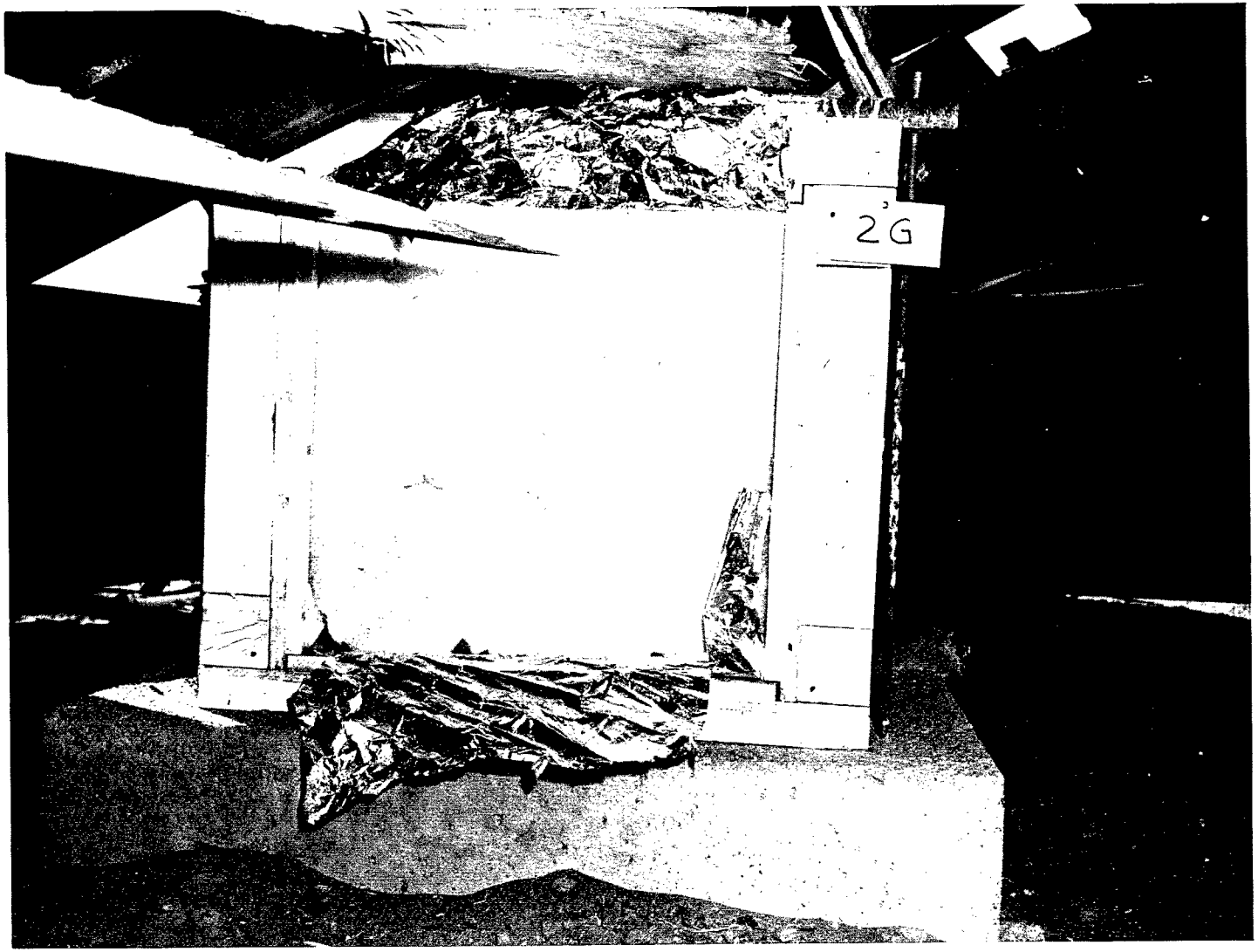

Fig. 4.20—Trap 2G, postshot, in open area 20 ft behind center of dining-room window of rambler house (31.1 c-1), 4733 ft from Ground Zero. A segment of the roof of the rambler house fell on the trap.

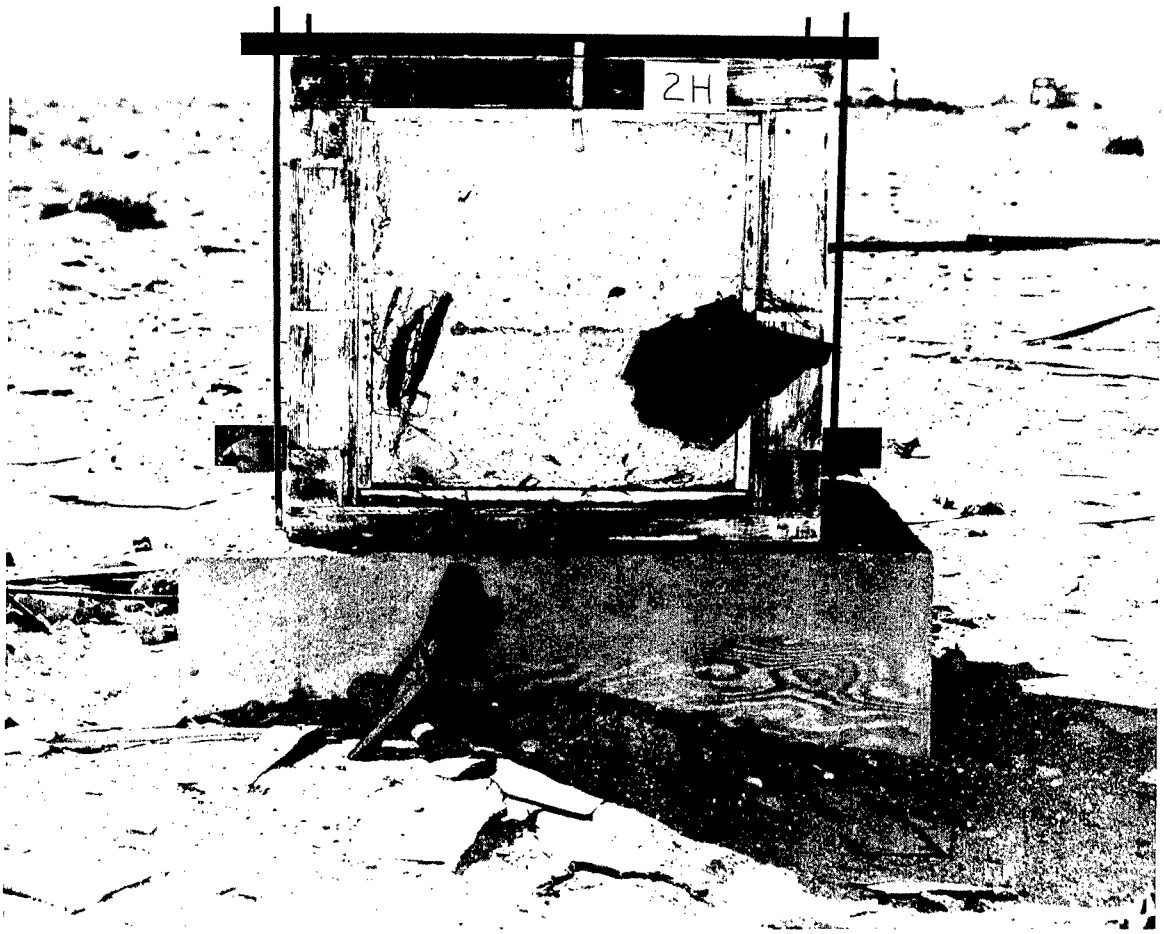

Fig. 4.21—Trap 2H, postshot, 100 ft behind center of rambler house (31.1 c-1), 4800 ft from Ground Zero.

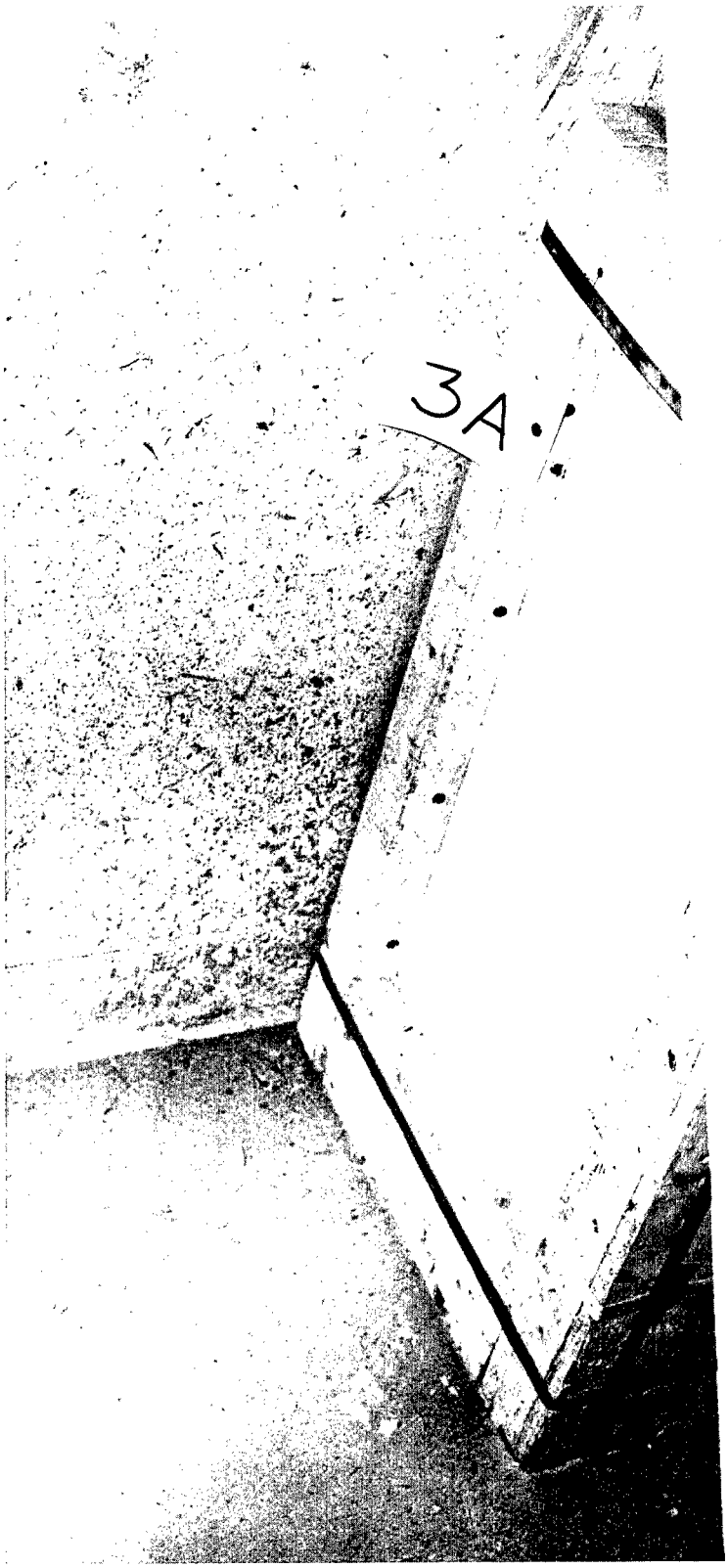

Fig. 4.22—Trap 3A, postshot, half-size trap in lean-to shelter, basement of two-story frame house, (31.1 b-1), 5500 ft from Ground Zero.

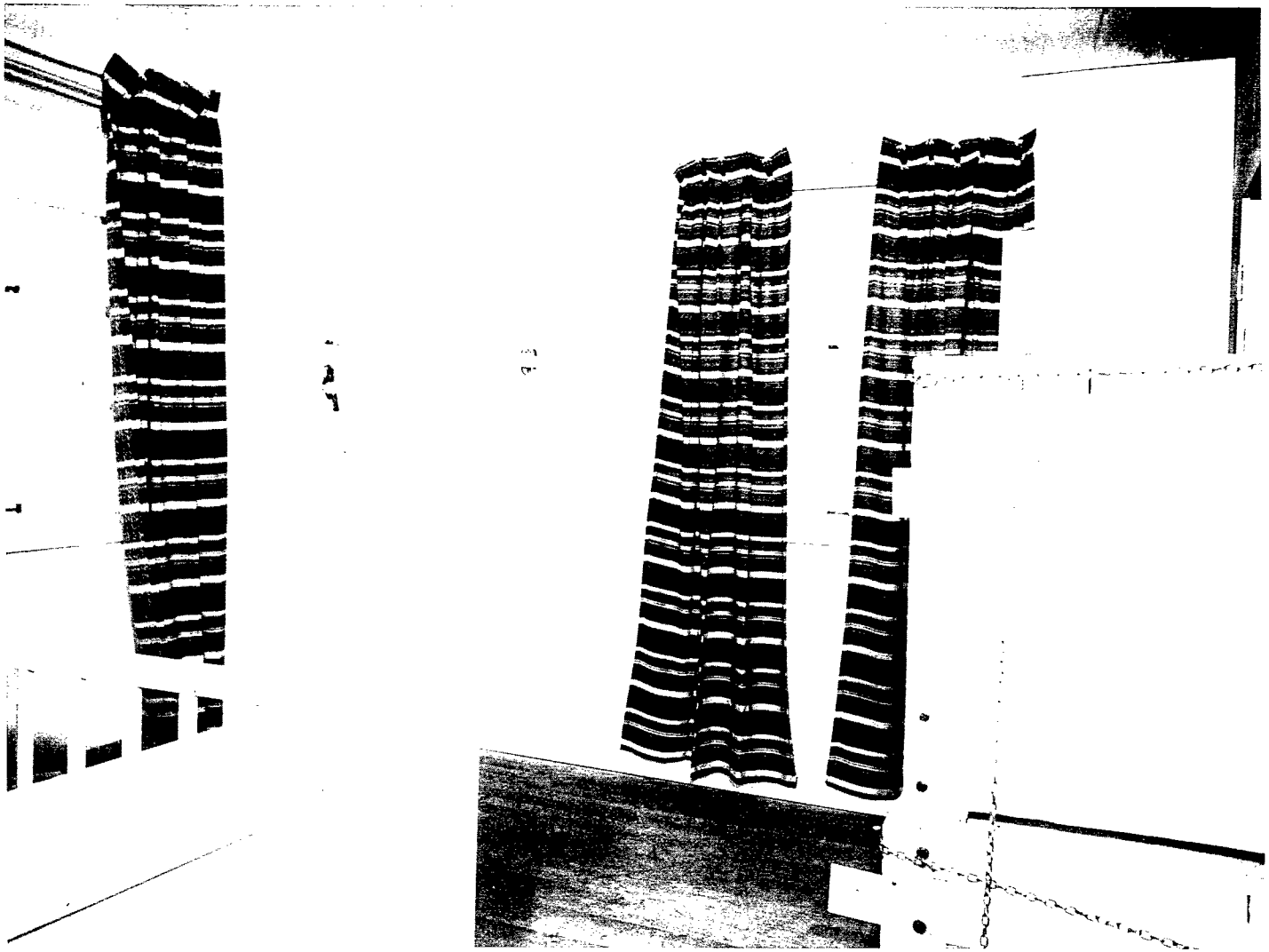

Fig. 4.23—Traps $3C_1$ and $3C_2$, preshot, second-floor bedroom of frame house (31.1 b-1), facing window toward Ground Zero, 5500 ft from Ground Zero.

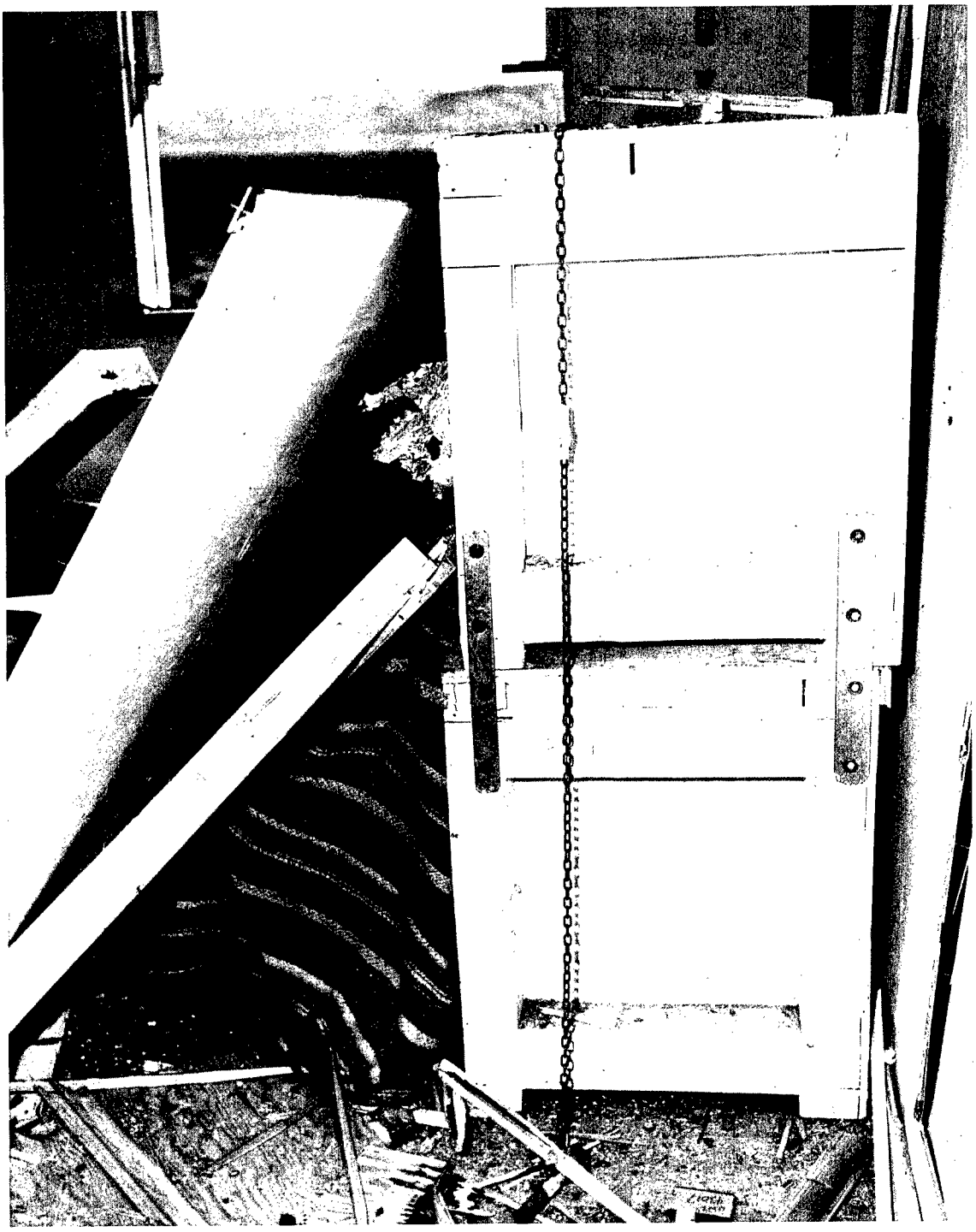

Fig. 4.24—Traps $3C_1$ and $3C_2$, postshot. See Fig. 4.23.

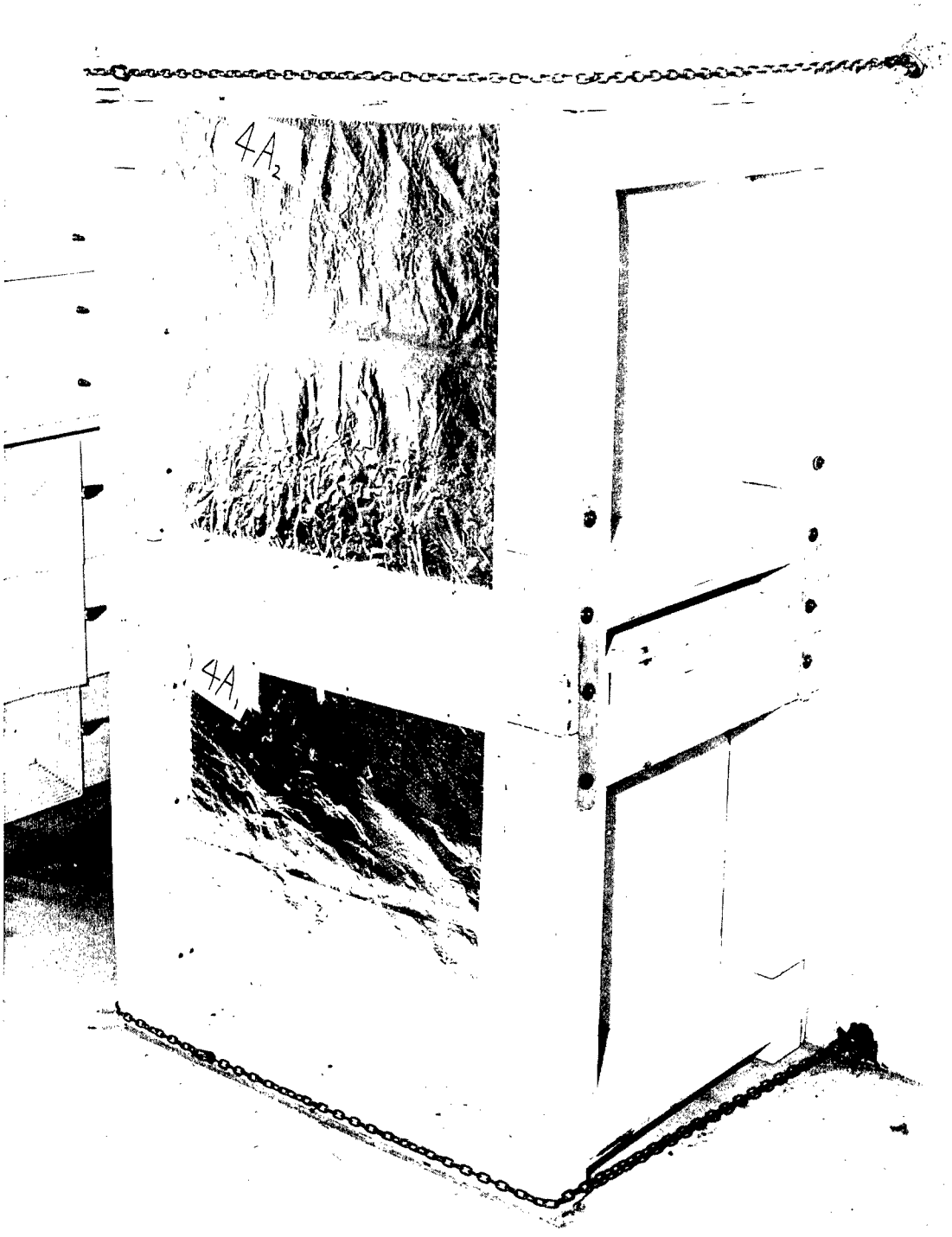

Fig. 4.25 — Traps $4A_1$ and $4A_2$, postshot, back bedroom of precast concrete house (31.1 e-2), facing large window away from Ground Zero, 10,500 ft from Ground Zero.

Fig. 4.26 — Traps $4B_1$, $4B_2$, $4B_3$, and $4B_4$, preshot, living room of precast concrete house (31.1 e-2), facing large window toward Ground Zero, 10,500 ft from Ground Zero.

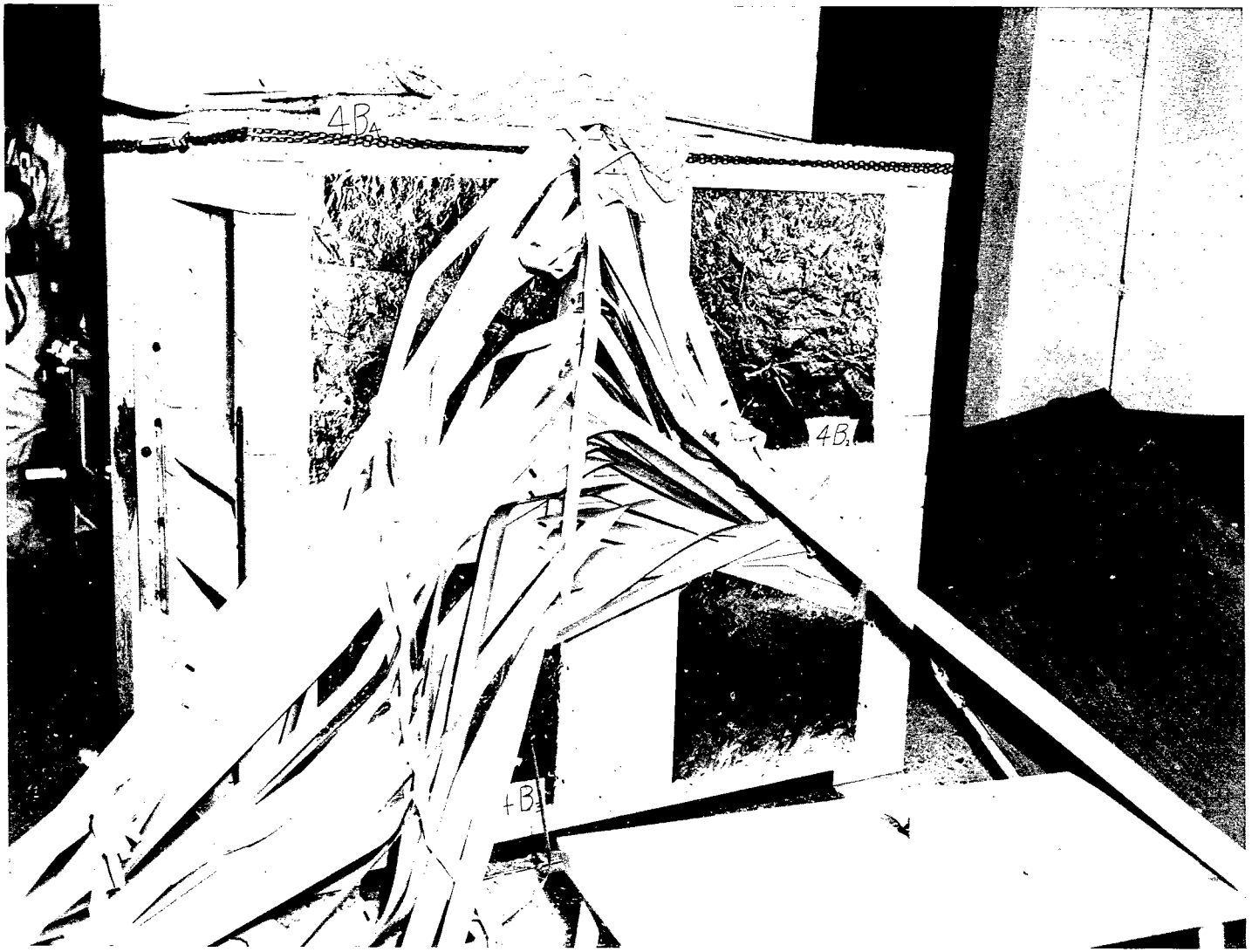

Fig. 4.27—Traps $4B_1$, $4B_2$, $4B_3$, and $4B_4$, postshot. See Fig. 4.26.

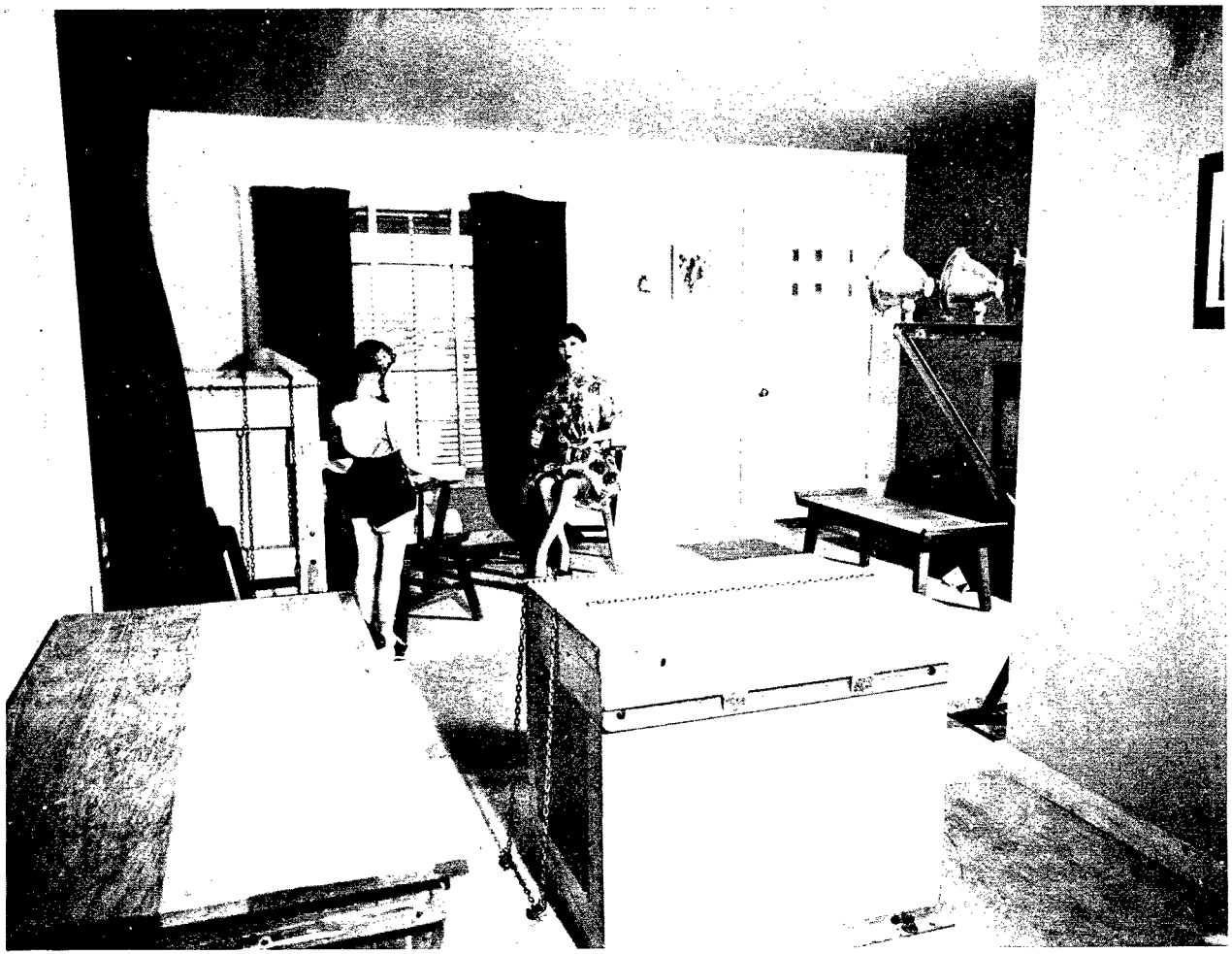

Fig. 4.28—Traps 4C and 4D, preshot, living room and dining room of rambler house (31.1 c-2); 4C on 18-in. stand, facing 90° away from blast line, and 4D on floor, facing large window toward Ground Zero; 10,500 ft from Ground Zero.

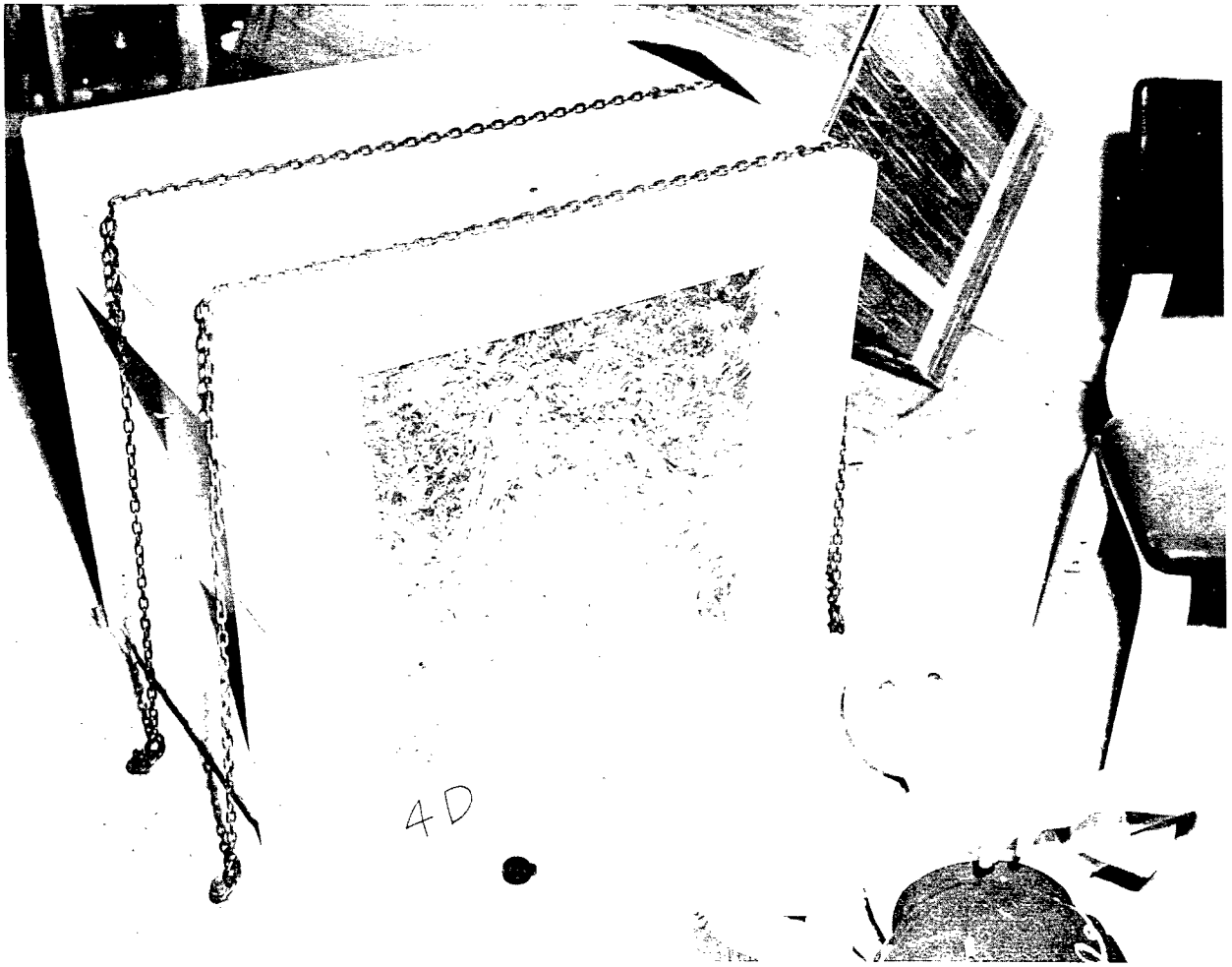

Fig. 4.29 — Trap 4D, postshot. See Fig. 4.28.

CHAPTER 5

RESULTS (ANALYSIS OF DATA)

5.1 GENERAL

The missiles were removed individually from the various traps and placed in small envelopes. The following data were recorded on each envelope:

1. Trap number.
2. Location of missile in trap; x and y coordinates.
3. Type of missile; glass, stone, etc.
4. Missile mass.
5. Depth of penetration.
6. For missiles other than glass, three dimensions used to compute an average diameter.

These data were tabulated for each trap, and velocities were computed for each missile by the methods described in Secs. 3.4 and 3.5. A total of 2611 missiles from the traps in the open shot were processed in this fashion.

For illustrative purposes, the data obtained from a typical trap, 2A—located facing Ground Zero on the second floor of the brick house at a range of 4700 ft (see Figs. 4.10 and 4.11)—are tabulated in Table 5.1. Less cumbersome and more meaningful statistical methods for presenting these data for the various traps are developed in the next two sections. However, the data for those traps which caught too few missiles for statistical treatment are given in Table 5.2.

5.2 STATISTICAL TREATMENT OF MISSILE MASS AND VELOCITY DATA

Figures 5.1 and 5.2 show the distribution of the 254 missiles from trap 2A according to mass and velocity, respectively.* Even a cursory examination of these distributions reveals that they are not normal; e.g., they demonstrate a definite asymmetry, or "skewness."

The data for trap 2A presented in Table 5.1 were arranged according to increasing missile mass. Since there were 254 missiles in this trap, the median mass has a value between that

---

*An additional postfield biophysical study to be reported subsequently (see footnote, page 26) was made to determine the probability of penetration of glass missiles having various velocities and masses. The abdomens of anesthetized dogs were used as targets. Thus, from the biological point of view, it was possible to calculate the expected number of penetrations for any group of glass missiles whose velocities and masses are known. For trap 2A it was found that 10.6 penetrations could be expected with a probability of 1.0. The shaded areas of Figs. 5.1 and 5.2 represent the distribution of these 10.6 expected penetrations according to missile mass and velocity, respectively. It is well to state quite clearly that the meaning of these data in terms of the human target is not known with any degree of certainty.

for missiles 127 and 128 (0.146 g). The difference between this value and the average missile mass (0.226 g) is a measure of the asymmetry present in this distribution.

An "average" missile mass was determined from the logarithms of the masses, rather than from the masses, and it was found that the antilogarithm of the average "log mass" was 0.140 g. This is in good agreement with the median mass of the distribution (0.146 g), suggesting that for analytical purposes the distribution could be made symmetrical, and perhaps normal, if the distribution of the 254 missiles were determined according to the logarithm of the masses rather than the actual masses.

A probability chart was used to make further tests for normalcy. The logarithmic mass-frequency summation curves for missiles from traps 2A (Figs. 4.10 and 4.11) and 2C (located facing Ground Zero in the ramber house at a range of 4700 ft—see Figs. 4.12 and 4.13) are shown in Fig. 5.3. The fact that the data for trap 2A plotted on this chart approximate a straight line indicates that the distribution of missiles according to the logarithm of the missile masses is approximately normal. The data for trap 2C, however, deviate somewhat from the normal distribution above 90 per cent and to a lesser degree below 10 per cent. A further interpretation of these deviations is that there were "too few" missiles larger than 0.5 g and "too many" smaller than 0.04 g.

The logarithm of the standard geometric deviation is the standard deviation of the log-mass distribution. The mean log mass plus and minus one standard deviation includes, by definition, 68.26 per cent of the total missiles. A more convenient expression for these limits is that 68.26 per cent of all missiles have masses between $M_{50} \times \sigma_{gm}$ and M_{50}/σ_{gm}, where M_{50} is the geometric mean mass and σ_{gm} is the standard geometric deviation. The value of M_{50} was determined directly from the logarithmic probability chart as the mass corresponding to the 50 per cent value. This mass value is also, by definition, the median mass. The standard geometric deviation was computed from data obtained from the same chart using the relation

$$\sigma_{gm} = (M_{84.13}/M_{15.87})^{1/2} \tag{5.1}$$

where $M_{84.13}$ and $M_{15.87}$ are the masses corresponding to the 84.13 per cent and 15.87 per cent values, respectively. Since the 84.13 per cent mass value is $M_{50} \times \sigma_{gm}$ and the 15.87 per cent value is M_{50}/σ_{gm}, these two parameters (M_{50} and σ_{gm}) completely define the distribution, providing there is no deviation from normalcy. An advantage of using the geometric mean rather than an average as a means of comparison between traps is that the geometric mean is affected less by large missiles than is the average.

The velocity distributions for the various traps were found to have a pattern similar to the mass distributions, with standard geometric deviations about half that for the mass distributions. The velocity distributions for traps 2A and 2C are shown in Fig. 5.4. The data for trap 2A form a straight line over almost the whole range of velocites. The data for trap 2C, however, deviate from a normal log-velocity distribution in that there were too few missile velocities above 190 ft/sec (90 per cent level) and below 100 ft/sec (3 per cent level).

The velocity and mass distributions for the remainder of the traps catching as many as 100 missiles are shown in Figs. 5.5 to 5.12. In general, the agreement of the data with the normal logarithmic distribution is good except in the low- and high-percentage regions. One instance of disagreement of particular interest is shown in Fig. 5.9. These data are for a trap (2H) placed in an open area which caught mostly natural stone missiles. As will be shown in Chap. 6, the ability of a given wind field to accelerate a stone missile diminishes as missile mass increases. Thus it is not surprising that "too few" heavy missiles were caught by trap 2H, assuming, of course, that the distribution of available natural stones according to the logarithms of their masses is normal.

Figures 5.13 and 5.14 show, respectively, the logarithmic mass-frequency and velocity-frequency summation curves for traps placed at three ranges from Ground Zero. At the 4700-ft range "too few" heavy missiles were caught. At the 5500- and 10,500-ft ranges "too few" light missiles and "too many" heavy missiles were caught. It should be pointed out that light missiles in general require a higher threshold velocity than heavy ones in order to accomplish penetration into Styrofoam. Figure 5.14 shows that the distribution of the 4700-ft-range missiles according to log velocity is practically normal over the entire range of velocites. At

the 5500-ft range fewer missiles were caught, and the data show that "too few" of these had low velocities. A similar trend is indicated for traps at the 10,500-ft range. These latter observations may reflect an inefficiency of the traps in catching low-velocity missiles.

Table 5.3 is a collection of the various statistical parameters for all the traps catching missiles and for traps grouped according to range from Ground Zero. Also indicated in the table are the dimensions of the window panes supplying the glass missiles and the average window glass thickness.

In order to better visualize these data, a few of the more important parameters were plotted in Figs. 5.15 to 5.17. Values for the standard error of the mean shown on these charts were computed according to the regular procedure from the standard geometric deviation and the sample size (number of missiles). In the three cases of stacked traps ($2D_2$ on $2D_1$, $2E_2$ on $2E_1$, and $3C_2$ on $3C_1$—for location, see Table 4.1), it is of interest to note that, for the top trap compared to the bottom one, the geometric mean mass is lower and the geometric mean velocity is higher in every instance. See Figs. 5.15 and 5.16, respectively. The geometric mean mass for trap 2H, placed in an open area, is significantly lower than that for traps placed in houses at the same range.

It is somewhat incongruous that the geometric mean velocities for inside traps $3C_1$ and $3C_2$, at the 5500-ft range (see Fig. 5.16), are not significantly lower than those for the inside traps at the 4700-ft range. No firm explanation for these findings can be offered at the present time. However, a few remarks will be made in the general discussion presented in Chap. 7.

Figure 5.17 depicts geometric mean missile mass for glass as a function of maximum overpressure. Points X, Y, and Z represent the missile mass data from traps at ranges of 4700, 5500, and 10,500 ft, respectively. Only data from traps catching principally glass missiles were included in these computations. The relatively large standard error of the mean for point Z may very well be due to the small sample of only 48 missiles.

5.3 SPATIAL DISTRIBUTION OF MISSILES

Figures 5.18 to 5.21 are pictures of the front and back sides of the first four Styrofoam cells (1 in. thick) of trap 2A. An x-y coordinate system was placed over each cell when the pictures were taken. Since this trap was struck by a venetian blind (see Fig. 4.11), there was considerable gross deformation of the Styrofoam. This made it impossible to evaluate velocities for a considerable number of the slower glass missiles which struck the trap.

Figures 5.22 to 5.29 are pictures of the front sides of the first cell for other traps placed at the 4700- and 5500-ft ranges, as well as the back side of the last cell in which missiles were found. Figure 5.24, trap $2D_2$, shows the deformation caused by the impact of a venetian blind (see Fig. 4.15). Around the edges of this deformation can be seen the holes made by glass missiles. It is evident that the venetian blind afforded considerable, though not complete, shielding of the trap from glass missiles. Note Fig. 5.31 for the spatial missile density which was found for the area beneath the venetian blind.

The first cell of trap $2E_2$, located inside the concrete house at a range of 4700 ft, shown in Fig. 5.26, was in fairly good condition in spite of the fact that 732 missiles were later retrieved from this trap. Figure 5.27 shows two pieces of roofing material stuck in the first cell of trap 2H. These pieces of roofing material evidently came from the rambler house 100 ft in front of the trap.

The x and y coordinate values determined for each missile (see Table 5.1) were used to determine the spatial distribution of missiles for traps catching 100 or more missiles. The presenting area of each trap was divided into 6- or 8-in. squares, and the average missile density in number per square foot was determined for each square. Figures 5.30 to 5.34 show these average spatial densities plotted in the center of their respective squares. The lines shown on these charts connect points of equal spatial densities.

The interpretation of the spatial distribution of missiles was made difficult by large objects obstructing the path of the glass missiles. Traps $2E_1$ and $2E_2$, placed inside the concrete house at a range of 4700 ft, were exceptions to this circumstance. Figure 5.32 shows that the missile density for these traps ($2E_2$ stacked on $2E_1$) increases with height above floor level. An increase in missile density from right to left is also indicated. Two circumstances

may have caused the latter missile density gradient. Figure 4.4 shows that these traps were not centered behind the window toward Ground Zero. They were placed off center in such a way as to produce the missile density gradient which was observed. The other condition which may have contributed to this missile density gradient was the presence of a side window, also shown in Fig. 4.4. Air arriving in the room from this window may have deflected the missile trajectories in such a way as to produce the observed density gradient.

Figure 5.33 indicates that a maximum missile density occurred in the center of trap 2H located in the open at 4800 ft from Ground Zero. Since this trap was placed 100 ft behind the rambler house at 4700 ft, it is reasonable to assume that wind streaming around the trap may have carried some of the missiles with it. However, it is difficult to visualize the actual wind flow which existed, and little else can be said relevant to the spatial distribution for trap 2H without further study.

Average missile densities in number per square foot are presented in the last column of Table 5.3 for every trap catching missiles. These figures are based on the missiles whose velocities were computed. Judging from the appearance of the front of the first cells of several traps, it was estimated that about 60 per cent of the missiles striking a trap arrived in such a way that their velocities could not be computed. Missiles striking the trap at low velocities failed to embed themselves in the Styrofoam. Other missiles entered holes already made by previous missiles, and some missiles were lost because their trajectories stopped at the boundary between cells. It has already been pointed out that the impact of large objects made gross deformations in the Styrofoam, making it impossible to evaluate the velocites for smaller glass missiles which were already present.

An estimate of the total number of glass missiles originating from a particular window can be computed if it is assumed that the masses of these missiles have an average value equal to that of the missiles caught by a trap or traps placed behind the window. Such an estimate was computed for the steel-frame window, 72 in. wide and 37.5 in. high, in front of traps $2E_1$ and $2E_2$ in the concrete house at the 4700-ft range (see Fig. 4.4). Using 0.284 g as the average missile mass (computed from the data for both traps), it was estimated that a total of 46,900 glass missiles originated from the window described above. The spatial density of these missiles was computed to be 2,500 per square foot.

The results obtained from traps $2E_1$ and $2E_2$ include data for only 974 missiles with a maximum spatial density (see Fig. 5.32) of 388 per square foot. Consideration should be given to the fact that these traps were estimated to have an efficiency of about 40 per cent in catching missiles. However, it seems reasonable to postulate that the principal reasons for the low spatial missile densities measured was a dispersion of the missiles in the 10.5-ft interval between the window and the traps. Evidence of scattering of missiles during flight is to be found in the results from trap $2E_1$ (Fig. 5.32) which was entirely below the window level (Fig. 4.4).

Table 5.1—DATA OBTAINED FROM TRAP 2A
(All missiles were glass except numbers 12, 18, 28, and 249, which were putty.)

Parameters: n = missile number
x and y = location of missile in trap (see Figs. 5.18 to 5.21)
s = depth of penetration, inches
m = missile mass, grams
V = measured impact velocity of missile, feet per second

n	x	y	s	m	V
1	7.2	15.6	0.535	0.0096	274
2	14.9	18.4	0.250	0.0122	179
3	7.5	15.2	0.240	0.0136	172
4	7.6	14.1	0.250	0.0166	168
5	7.0	13.6	0.215	0.0168	156
6	12.6	3.4	0.400	0.0182	210
7	7.3	18.7	0.320	0.0207	183
8	15.7	16.2	0.100	0.0214	102
9	12.8	20.3	0.485	0.0217	222
10	8.1	17.4	0.315	0.0242	176
11	5.7	1.0	0.300	0.0234	173
12	19.5	1.6	0.230	0.0240	177
13	23.5	18.9	0.125	0.0250	110
14	0.5	3.1	0.190	0.0253	135
15	16.6	13.0	0.210	0.0260	142
16	1.8	18.5	0.175	0.0279	127
17	1.2	7.6	0.295	0.0294	163
18	10.2	22.8	0.320	0.0296	196
19	1.1	15.5	0.215	0.0318	138
20	9.1	14.6	0.355	0.0320	177
21	18.0	14.0	0.330	0.0324	170
22	1.2	18.6	0.140	0.0346	109
23	16.0	16.4	0.325	0.0352	166
24	5.7	12.9	1.195	0.0371	315
25	13.2	16.4	0.245	0.0372	142
26	17.0	12.5	0.575	0.0373	218
27	8.5	8.2	0.315	0.0377	161
28	20.2	23.0	0.505	0.0401	230
29	22.6	0.9	0.340	0.0402	165
30	1.7	22.7	0.245	0.0403	140
31	15.4	3.9	0.240	0.0409	138
32	13.0	12.4	0.280	0.0413	149
33	16.3	16.7	0.150	0.0416	109
34	2.0	1.0	0.640	0.0436	223
35	7.1	0.6	0.450	0.0443	186
36	1.5	7.0	0.240	0.0448	136
37	10.8	21.6	0.245	0.0459	137
38	1.5	4.3	0.300	0.0467	151
39	5.5	13.2	1.625	0.0470	350
40	23.2	5.0	0.175	0.0476	115
41	8.3	17.8	0.715	0.0482	231
42	13.6	16.4	0.355	0.0489	163
43	20.8	23.5	0.650	0.0514	218
44	1.7	21.5	0.365	0.0516	163
45	0.7	12.4	0.550	0.0532	199

Table 5.1 — (Continued)

n	x	y	s	m	V
46	0.6	19.2	0.570	0.0533	202
47	1.1	19.9	0.640	0.0566	212
48	18.1	13.4	0.205	0.0577	120
49	4.0	9.8	0.415	0.0579	170
50	10.6	21.4	0.150	0.0580	102
51	11.0	22.4	0.190	0.0582	115
52	11.8	9.2	0.550	0.0583	195
53	6.2	0.9	0.270	0.0602	136
54	8.3	14.7	0.435	0.0621	172
55	1.0	17.5	0.590	0.0624	200
56	4.9	8.9	0.315	0.0628	146
57	1.6	18.4	0.270	0.0629	135
58	16.5	14.2	0.550	0.0631	192
59	14.0	22.5	0.275	0.0632	136
60	17.0	8.1	0.315	0.0633	146
61	11.4	22.5	0.200	0.0656	115
62	13.9	16.0	0.250	0.0659	129
63	7.4	15.2	0.360	0.0658	155
64	11.5	16.3	0.475	0.0668	177
65	2.5	22.7	1.000	0.0676	256
66	12.5	2.8	0.465	0.0677	175
67	5.6	6.5	0.675	0.0679	210
68	11.9	21.6	0.250	0.0715	127
69	10.1	16.0	0.350	0.0717	150
70	1.5	22.5	0.305	0.0717	140
71	10.7	22.0	0.320	0.0718	143
72	8.4	8.6	0.510	0.0723	180
73	11.7	21.7	0.340	0.0740	147
74	4.8	1.0	0.560	0.0756	187
75	5.5	9.5	0.510	0.0759	178
76	12.9	9.6	0.405	0.0759	159
77	20.0	14.0	0.355	0.0760	149
78	10.8	15.5	0.320	0.0782	141
79	22.8	6.7	0.190	0.0799	108
80	16.5	6.7	0.200	0.0806	111
81	15.4	0.9	1.310	0.0821	281
82	12.8	1.5	1.520	0.0825	303
83	12.8	16.1	0.460	0.0848	166
84	18.0	13.9	0.370	0.0851	149
85	17.5	6.1	0.640	0.0878	195
86	15.0	19.9	0.715	0.0879	206
87	16.0	7.8	0.745	0.0887	210
88	0.6	2.6	0.485	0.0897	169
89	4.9	8.8	0.210	0.0908	111
90	14.8	19.7	0.235	0.0932	117
91	18.6	12.8	0.850	0.0939	221
92	17.0	6.8	0.300	0.0942	131
93	15.4	16.0	0.300	0.0955	131
94	6.6	6.7	0.355	0.0962	142
95	22.7	8.8	0.500	0.0977	169
96	8.4	13.9	0.505	0.0987	169
97	3.5	16.2	1.360	0.0991	276
98	0.9	5.5	0.375	0.1015	145

Table 5.1 — (Continued)

n	x	y	s	m	V
99	23.1	7.0	1.350	0.1032	273
100	10.3	15.5	0.305	0.1033	130
101	18.5	13.1	0.390	0.1040	147
102	18.5	13.0	1.225	0.1050	260
103	5.2	8.8	0.285	0.1054	125
104	1.1	19.0	0.325	0.1064	133
105	15.6	6.5	0.360	0.1115	139
106	2.0	22.0	0.590	0.1127	177
107	11.2	10.0	0.360	0.1143	138
108	11.3	14.0	1.465	0.1146	279
109	16.5	13.4	0.265	0.1176	118
110	1.5	21.0	0.220	0.1186	107
111	3.9	9.5	0.765	0.1194	200
112	10.8	0.5	0.375	0.1213	140
113	12.7	6.9	0.495	0.1236	160
114	1.6	1.0	0.725	0.1243	193
115	6.5	1.0	0.425	0.1245	148
116	8.8	16.2	0.460	0.1254	153
117	0.9	20.4	0.515	0.1278	162
118	13.8	7.3	0.685	0.1313	186
119	11.9	16.5	0.575	0.1321	170
120	7.6	9.2	0.645	0.1356	180
121	1.2	7.6	0.540	0.1358	165
122	2.1	21.6	0.510	0.1359	160
123	17.8	7.1	0.550	0.1374	165
124	16.4	12.6	0.590	0.1374	171
125	4.3	8.7	1.180	0.1384	241
126	23.4	2.1	0.250	0.1434	110
127	1.0	19.6	1.260	0.1447	248
128	5.5	8.6	0.350	0.1472	130
129	22.8	9.1	1.1640	0.1496	236
130	16.3	7.8	0.580	0.1506	166
131	17.5	13.5	0.340	0.1508	127
132	0.9	17.9	0.345	0.1522	128
133	16.3	6.5	0.800	0.1528	195
134	6.4	9.0	0.520	0.1540	157
135	1.4	20.5	1.260	0.1557	243
136	14.5	7.4	0.360	0.1574	130
137	18.1	13.6	0.310	0.1574	120
138	0.8	13.0	0.725	0.1620	183
139	17.3	17.5	1.260	0.1656	241
140	20.8	1.0	0.420	0.1657	139
141	1.5	17.4	2.900	0.1672	365
142	3.9	9.2	0.605	0.1683	166
143	14.0	10.0	1.175	0.1696	231
144	11.4	13.3	1.595	0.1721	269
145	16.4	23.0	0.645	0.1736	171
146	16.1	16.5	1.290	0.1737	241
147	3.8	1.1	0.660	0.1770	172
148	1.1	0.9	0.450	0.1775	142
149	1.5	16.7	0.825	0.1786	192
150	18.2	5.3	0.475	0.1798	145

Table 5.1 — (Continued)

n	x	y	s	m	V
151	16.5	14.1	0.825	0.1800	192
152	17.1	3.9	1.105	0.1808	221
153	14.0	7.6	0.400	0.1816	133
154	0.8	19.3	1.390	0.1826	248
155	11.7	0.5	0.760	0.1828	183
156	2.3	0.5	0.480	0.1837	145
157	14.0	1.0	0.535	0.1840	153
158	1.4	18.3	0.565	0.1884	157
159	12.7	0.8	0.365	0.1943	126
160	15.2	0.8	0.445	0.1960	138
161	2.0	17.3	0.800	0.1967	186
162	14.2	3.5	1.160	0.1996	223
163	22.9	5.0	0.640	0.2020	165
164	7.7	9.4	1.425	0.2078	242
165	11.2	3.0	0.575	0.2106	155
166	7.1	6.7	0.530	0.2117	148
167	4.7	6.6	0.670	0.2218	166
168	3.2	1.8	0.385	0.2238	125
169	14.4	1.0	0.385	0.2266	125
170	12.0	10.1	1.320	0.2327	230
171	8.0	14.5	0.850	0.2366	185
172	13.0	1.2	0.485	0.2373	139
173	4.4	8.9	0.595	0.2382	154
174	17.6	7.0	0.590	0.2426	153
175	2.4	23.5	1.000	0.2434	198
176	18.5	13.7	0.900	0.2435	189
177	23.1	9.2	1.530	0.2456	246
178	18.5	13.0	0.610	0.2467	155
179	13.9	3.7	0.635	0.2496	158
180	19.5	20.3	1.475	0.2498	240
181	8.6	14.4	0.660	0.2521	160
182	7.6	3.7	0.665	0.2550	161
183	2.6	1.7	0.680	0.2568	162
184	11.0	17.0	0.500	0.2577	139
185	3.1	1.1	0.640	0.2586	157
186	23.1	20.5	0.480	0.2594	136
187	8.5	19.0	0.600	0.2597	152
188	15.0	23.0	0.580	0.2616	149
189	15.7	4.0	0.425	0.2674	127
190	14.1	8.5	0.525	0.2770	141
191	8.9	9.4	1.345	0.2805	224
192	23.0	7.1	0.480	0.2808	134
193	7.3	1.3	1.000	0.2887	193
194	6.0	12.1	2.000	0.2900	272
195	16.0	13.4	1.000	0.2918	192
196	11.1	13.3	1.660	0.2934	247
197	15.6	7.8	0.685	0.2972	158
198	5.0	8.4	1.100	0.2998	200
199	0.7	2.0	0.645	0.3083	152
200	12.1	9.7	0.890	0.3146	179
201	2.0	22.1	1.265	0.3176	212
202	18.6	16.3	1.420	0.3200	225
203	13.1	9.5	1.405	0.3201	223
204	6.0	8.0	0.645	0.3207	151
205	16.0	6.6	0.945	0.3257	183

Table 5.1 — (Continued)

n	x	y	s	m	V
206	15.9	16.5	0.820	0.3328	169
207	13.2	17.9	1.545	0.3381	231
208	6.2	13.0	1.515	0.3466	228
209	5.2	9.2	0.940	0.3566	179
210	12.1	9.6	1.230	0.3600	206
211	13.0	21.7	0.620	0.3658	144
212	1.0	21.4	1.455	0.3660	221
213	11.5	21.8	0.580	0.3673	140
214	1.2	20.5	0.810	0.3775	164
215	23.3	9.0	1.470	0.3790	221
216	1.4	2.1	2.400	0.3802	283
217	9.1	14.7	0.875	0.3802	171
218	11.3	13.3	1.570	0.3892	227
219	4.1	15.7	1.210	0.3893	200
220	13.0	14.1	1.965	0.3983	253
221	21.5	11.5	1.425	0.3984	216
222	1.0	18.3	0.780	0.4195	158
223	1.5	20.5	1.000	0.4357	178
224	11.7	21.5	0.755	0.4382	154
225	6.0	8.8	0.380	0.4448	109
226	14.0	17.5	0.750	0.4470	153
227	20.4	14.3	0.890	0.4626	165
228	15.9	22.5	1.450	0.4820	210
229	8.8	8.4	0.790	0.5000	154
230	2.4	22.7	0.995	0.5046	172
231	8.5	13.5	1.895	0.5354	235
232	8.5	9.5	0.730	0.5401	145
233	11.0	15.9	1.570	0.5558	212
234	6.6	9.0	1.340	0.5581	196
235	9.0	16.2	1.435	0.5621	203
236	14.3	14.4	2.800	0.5641	283
237	8.2	9.2	0.845	0.5798	154
238	8.4	16.2	1.505	0.5873	206
239	14.4	5.9	0.935	0.6504	159
240	12.9	15.8	1.795	0.7472	214
241	3.5	1.0	2.030	0.8000	225
242	17.9	16.9	1.490	0.8140	192
243	10.0	13.0	0.800	0.8160	141
244	1.0	17.0	1.000	0.8301	157
245	16.0	23.1	1.660	0.8336	202
246	14.4	22.9	0.940	0.8758	150
247	9.5	13.6	1.000	0.9048	154
248	13.2	14.0	1.225	0.9238	170
249	6.5	8.5	0.830	1.0112	177
250	18.0	4.4	0.910	1.0772	142
251	17.0	14.0	0.640	1.1213	118
252	23.0	10.7	0.835	1.4538	128
253	15.5	16.4	2.015	1.7410	192
254	22.7	6.0	1.850	1.779	184

Table 5.2—DATA OBTAINED FROM MISSILE TRAPS 2B, 2F, 2G, $4B_1$, $4B_2$, $4B_3$, $4B_4$, 4D, 4E, AND 4G
(All missiles were glass.)

Parameters: n = missile number
x and y = location of missile in trap (see Figs. 5.18 to 5.21)
s = depth of penetration, inches
m = missile mass, grams
V = measured missile velocity, feet per second

Trap	n	x	y	s	m	V
2B	1	8.0	18.3	0.320	0.160	122
	2	20.2	18.6	0.490	0.229	141
2F	1	6.5	17.9	0.400	0.340	78
	2	12.6	3.0	0.250	0.500	76
	3	18.2	8.5	0.600	0.850	93
	4	16.2	10.0	0.400	1.000	52
	5	3.7	18.5	0.550	1.090	157
	6	19.1	12.7	1.150	3.240	70
2G	1	4.9	1.6	0.455	0.077	168
	2	22.3	19.9	0.300	0.116	126
	3	17.0	22.0	0.490	0.130	141
	4	6.4	17.6	0.445	0.138	148
	5	2.6	22.4	0.570	0.157	164
	6	10.0	11.9	0.315	0.255	111
$4B_1$	1	6.7	23.0	0.725	2.125	111
$4B_2$	1	3.0	10.9	0.430	0.376	120
	2	16.8	11.0	0.420	0.553	110
	3	4.2	5.7	0.140	0.804	59
	4	19.2	7.5	0.530	0.966	111
	5	7.5	3.8	0.485	1.192	102
	6	8.6	21.2	0.550	1.391	105
	7	18.1	16.5	0.395	1.537	88
	8	4.6	4.1	0.155	1.629	54
	9	18.6	13.2	0.840	2.018	120
	10	18.5	17.5	0.625	3.812	92
	11	21.0	16.9	1.015	4.169	115
$4B_3$	1	9.0	22.0	0.350	0.977	90
	2	13.7	17.5	0.365	1.357	86
	3	18.5	20.0	0.475	1.397	98
	4	11.0	19.0	0.610	2.016	103
	5	11.0	17.0	0.940	2.775	120
$4B_4$	1	19.0	22.5	0.800	2.071	133
	2	17.7	15.5	1.000	2.907	123
	3	18.0	3.5	1.010	4.759	112
	4	7.0	20.5	0.580	5.032	84
	5	17.0	20.5	0.980	11.533	93
4D	1	20.1	22.4	0.275	0.051	142
	2	15.9	15.9	0.230	0.065	124
	3	19.3	5.7	0.300	0.200	113
	4	6.0	20.5	0.730	0.290	164
	5	14.5	21.7	0.300	0.400	99
	6	20.5	5.5	0.700	0.780	133
	7	15.4	5.5	0.355	0.860	92
	8	10.4	5.0	0.800	0.890	138
	9	14.8	17.2	0.350	0.960	90
	10	16.8	22.8	0.400	1.040	95

Table 5.2—(Continued)

Trap	n	x	y	s	m	V
	11	2.5	19.7	0.400	1.270	92
	12	11.0	17.5	0.800	1.300	128
	13	13.8	20.5	0.350	3.090	72
	14	6.0	22.8	0.900	4.130	109
	15	20.8	21.0	0.400	4.350	72
4E	1	21.5	16.6	0.230	0.029	145
	2	14.4	21.5	0.485	0.188	146
	3	7.2	18.9	0.440	0.330	125
	4	0.7	20.5	0.535	0.468	128
	5	8.0	22.0	1.055	0.497	178
	6	4.3	20.1	0.320	0.538	97
	7	9.0	21.0	0.570	0.632	125
	8	13.0	15.4	0.625	0.782	125
	9	21.0	15.5	0.535	4.434	83
4G	1	16.0	14.0	0.450	1.697	92
	2	14.5	13.0	0.280	6.398	56

Table 5.3—STATISTICAL PARAMETERS FOR MISSILES FROM VARIOUS TRAPS

N = total missiles
N_g = glass missiles
$\overline{V}$ = average velocity, feet per second
V_{50} = geometric mean velocity, feet per second
σ_{gv} = standard geometric deviation in velocity
$\sigma_{g\overline{v}}$ = standard error of geometric mean velocity
$\overline{M}$ = average mass, grams
M_{50} = geometric mean mass, grams
σ_{gm} = standard geometric deviation in mass
$\sigma_{g\overline{m}}$ = standard error of geometric mean mass
t = average thickness of window panes, inches
d = dimensions of each window pane, inches
N_s = number of missiles per square foot passing through the front surface of trap (see Sec. 5.3)
X = combined data from traps 2A, 2C, 2D, $2D_1$, $2D_2$, $2E_1$, and $2E_2$
Y = combined data from $3C_1$ and $3C_2$
Z = combined data from $4B_1$ through 4G

Trap	N	N_g	$\overline{V}$	V_{50}	σ_{gv}	$\sigma_{g\overline{v}}$	$\overline{M}$	M_{50}	σ_{gm}	$\sigma_{g\overline{m}}$	t	d	N_s
2A	254	250	176	171	1.29	1.02	0.226	0.140	2.75	1.06	0.092	12 × 12	72.1
2B	2	2	132				0.194				0.093	12 × 12	0.6
2C	423	417	151	146	1.23	1.01	0.282	0.140	2.75	1.05	0.096	12 × 16	120.1
$2D_1$	247	246	180	176	1.27	1.01	0.307	0.113	3.63	1.09	0.094	12 × 16	70.1
$2D_2$	231	231	184	180	1.25	1.02	0.140	0.095	2.57	1.06	0.089	12 × 16	65.6
$2E_1$	242	241	170	166	1.24	1.01	0.415	0.153	3.97	1.09	0.124	12 × 23½	68.7
$2E_2$	732	726	186	178	1.22	1.01	0.241	0.142	2.83	1.04	0.122	12 × 23½	207.9
2F	6	6	88				1.170						1.7
2G	6	6	143				0.146						1.7
2H	100	6	140	137	1.24	1.02	0.158	0.050	2.94	1.11			28.4
X	2129	2111	175	170	1.27	1.005	0.264	0.133	3.01	1.02	0.107		
$3C_1$	61	61	148	146	1.27	1.03	1.275	0.810	3.71	1.18	0.120	12 × 12	17.3
$3C_2$	259	232	179	175	1.23	1.01	0.993	0.540	3.81	1.09	0.118	12 × 12	73.6
Y	320	293	173	168	1.25	1.013	1.047	0.580	3.47	1.07	0.118		
$4B_1$	1	1	111				2.125				0.124	15 × 18	0.3
$4B_2$	11	11	98				1.677				0.123	15 × 18	3.1
$4B_3$	5	5	99				1.704				0.124	15 × 18	1.4
$4B_4$	5	5	109				5.260				0.124	15 × 18	1.4
4D	15	15	111				1.312				0.088	12 × 16	4.3
4E	9	9	128				0.878				0.085	12 × 18	2.6
4G	2	2	74				4.047						0.6
Z	48	48	108	108	1.25	1.037	1.897	1.450	3.35	1.22	0.104		

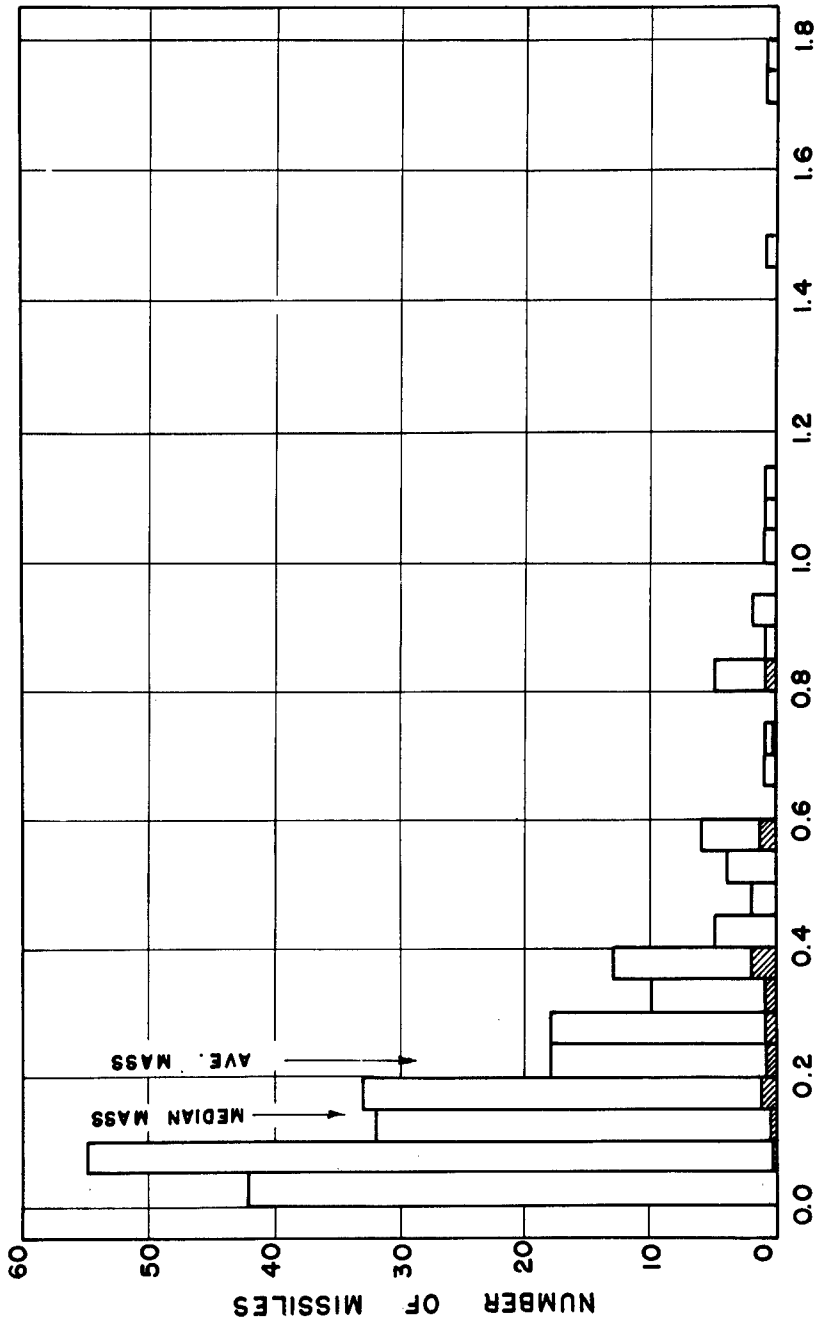

Fig. 5.1 — Distribution of 254 missiles from trap 2A according to mass. Shaded area: expected number of penetrations into the abdomen of a dog. Total expectation: 10.6 penetrations (see text).

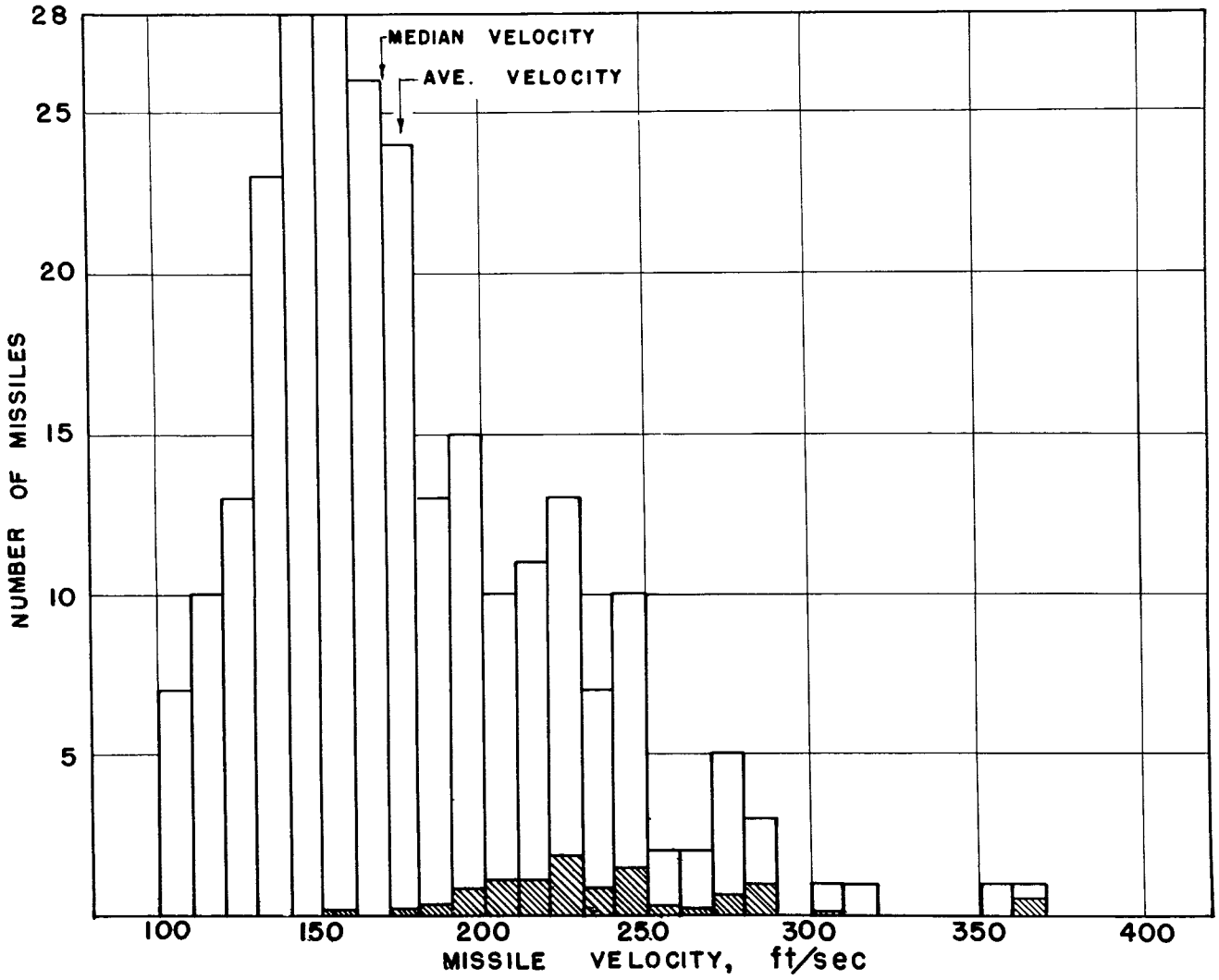

Fig. 5.2—Distribution of 254 missiles from trap 2A according to velocity. Shaded area: expected number of penetrations into the abdomen of a dog. Total expectation: 10.6 penetrations (see text).

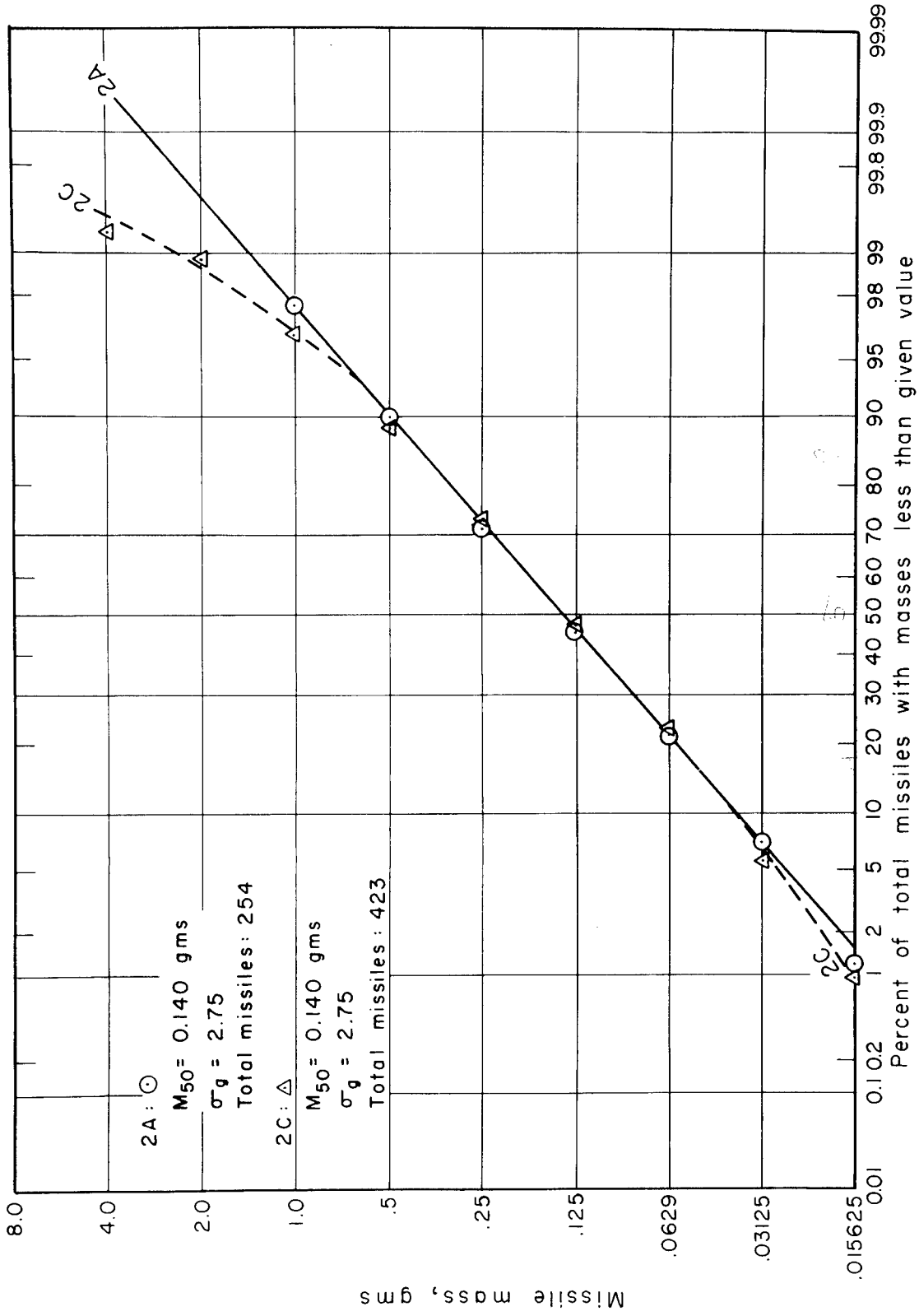

Fig. 5.3—Logarithmic mass-frequency summation curves for missiles from traps 2A and 2C.

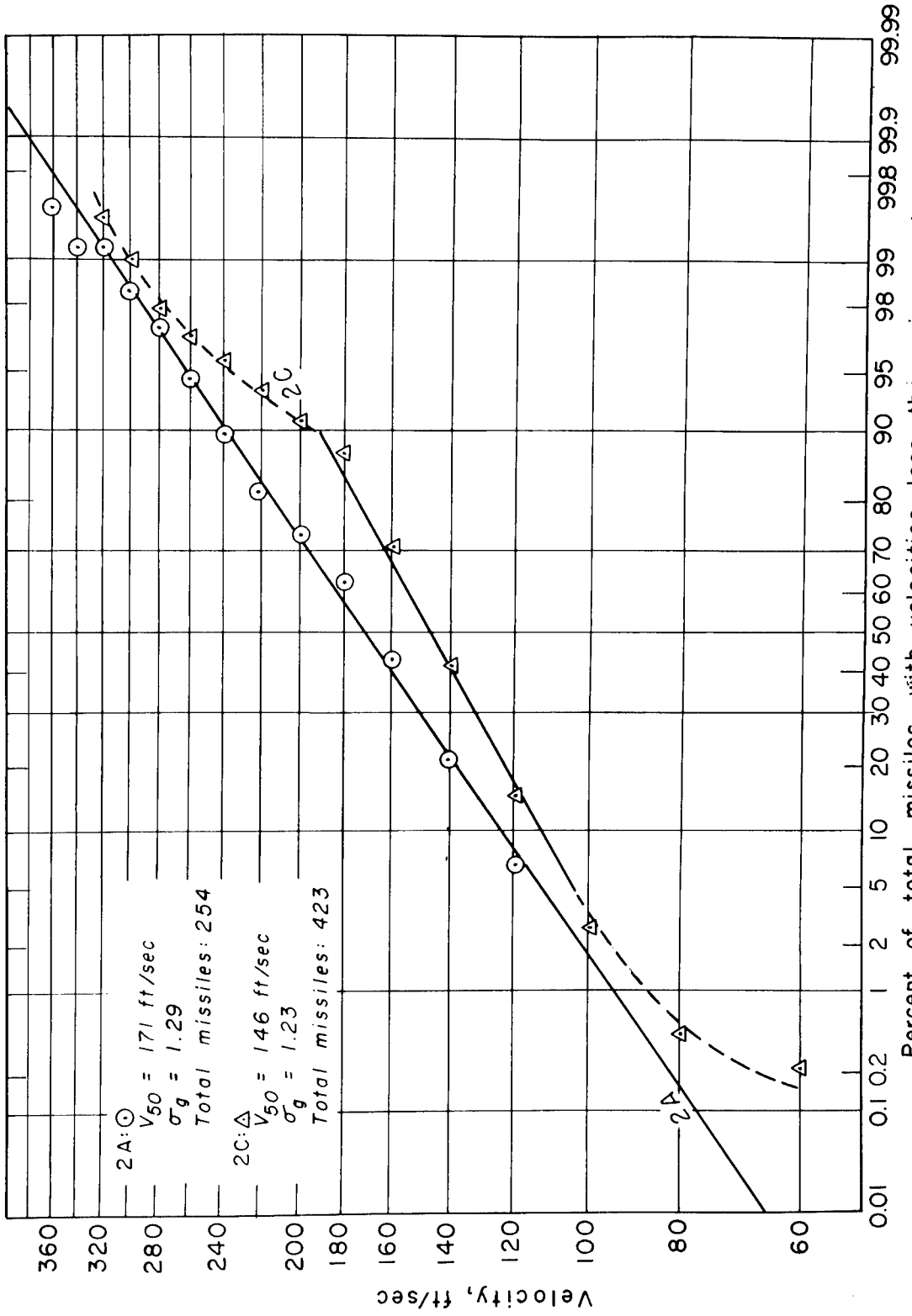

Fig. 5.4—Logarithmic velocity-frequency summation curves for missiles from traps 2A and 2C.

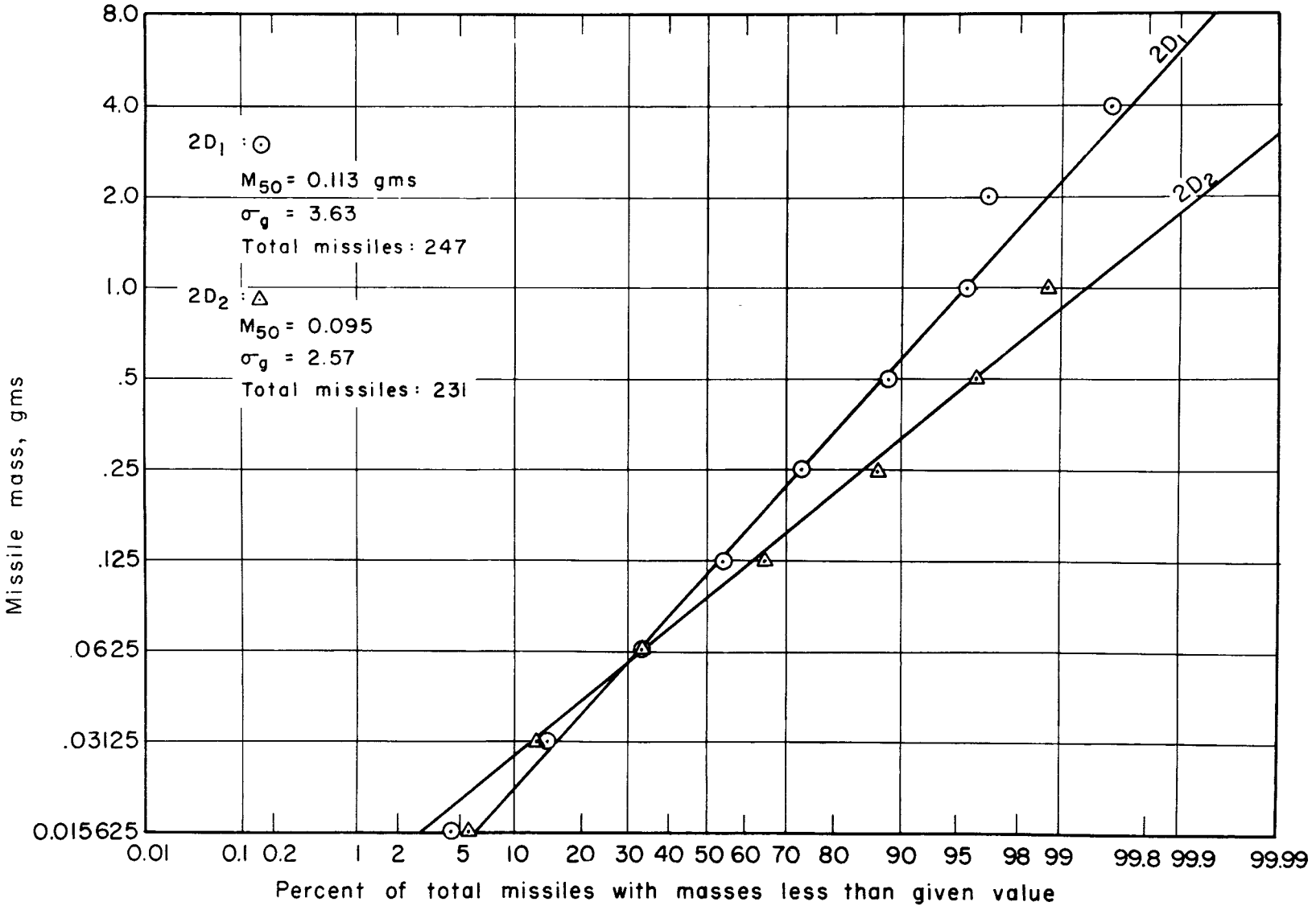

Fig. 5.5—Logarithmic mass-frequency summation curves for missiles from traps $2D_1$ and $2D_2$.

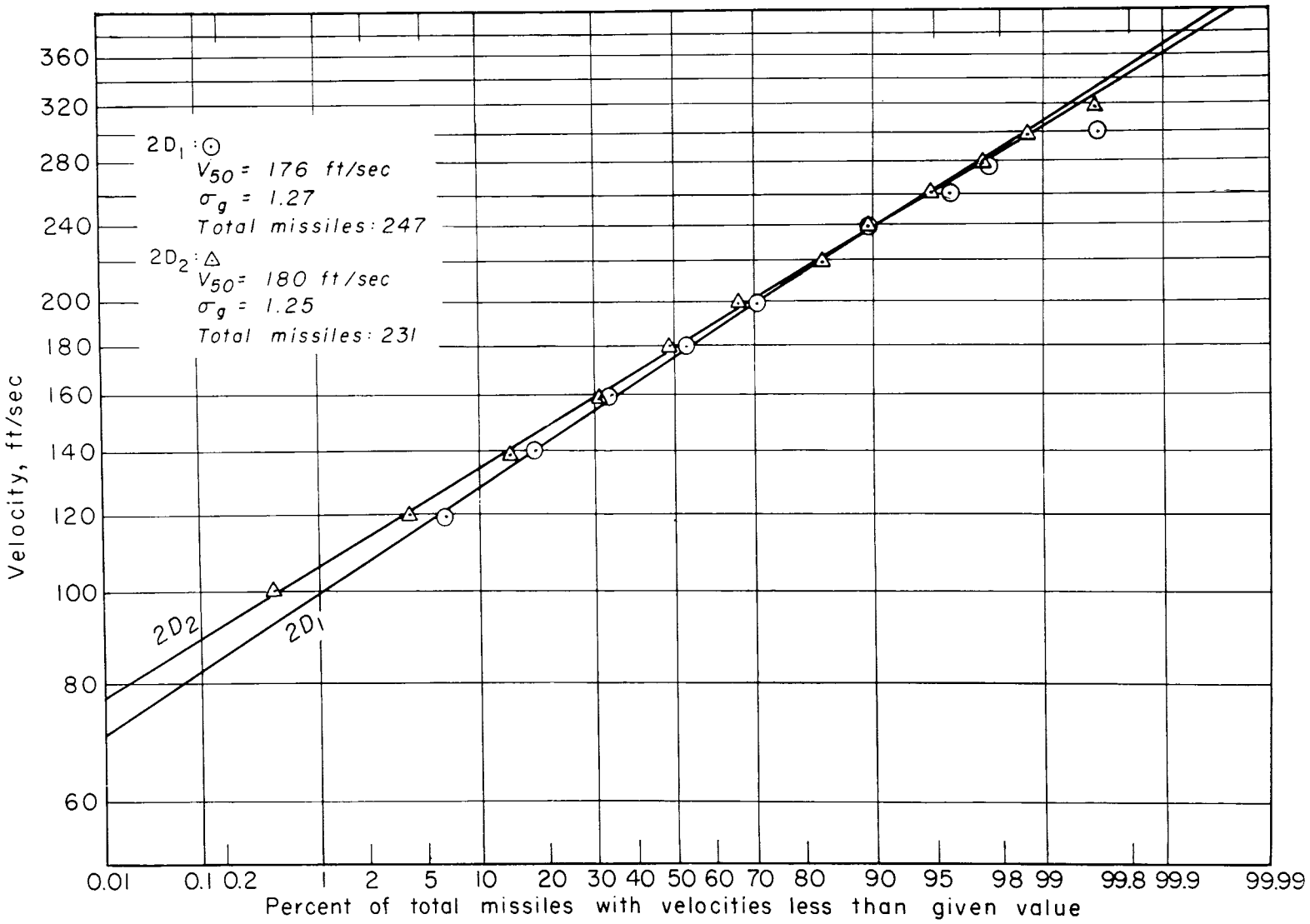

Fig. 5.6—Logarithmic velocity-frequency summation curves for missiles from traps $2D_1$ and $2D_2$.

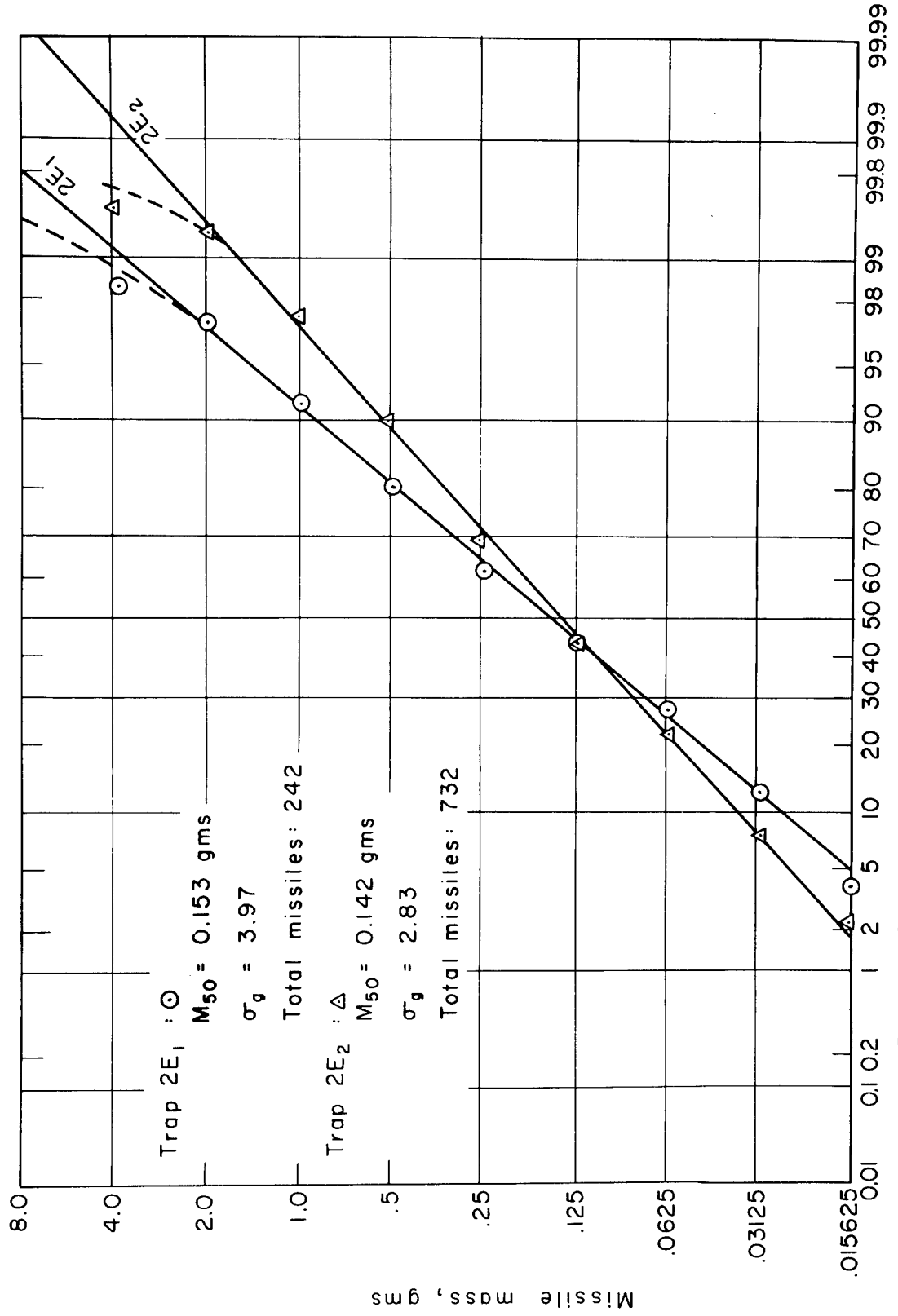

Fig. 5.7—Logarithmic mass-frequency summation curves for missiles from traps $2E_1$ and $2E_2$.

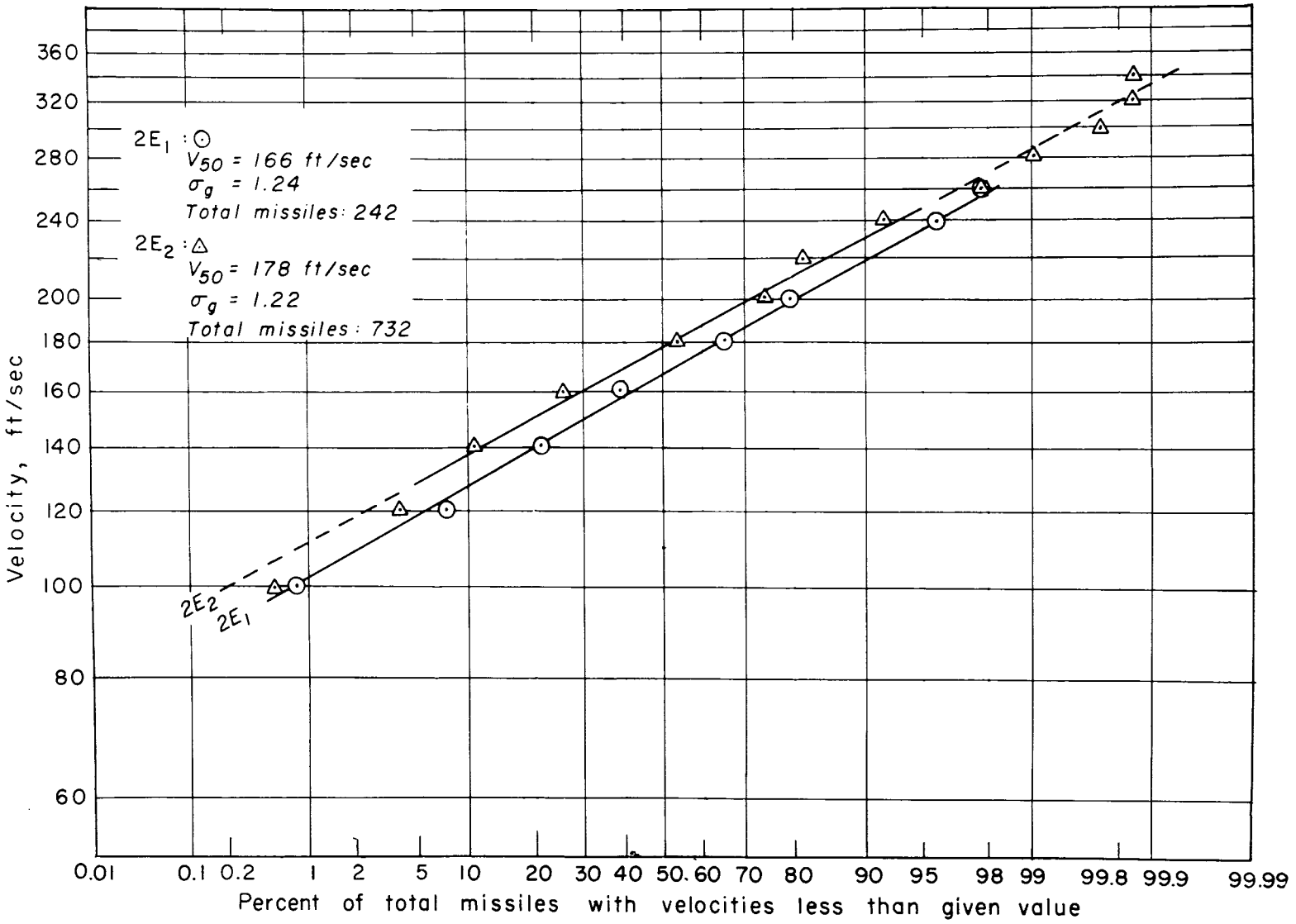

Fig. 5.8—Logarithmic velocity-frequency summation curves for missiles from traps $2E_1$ and $2E_2$.

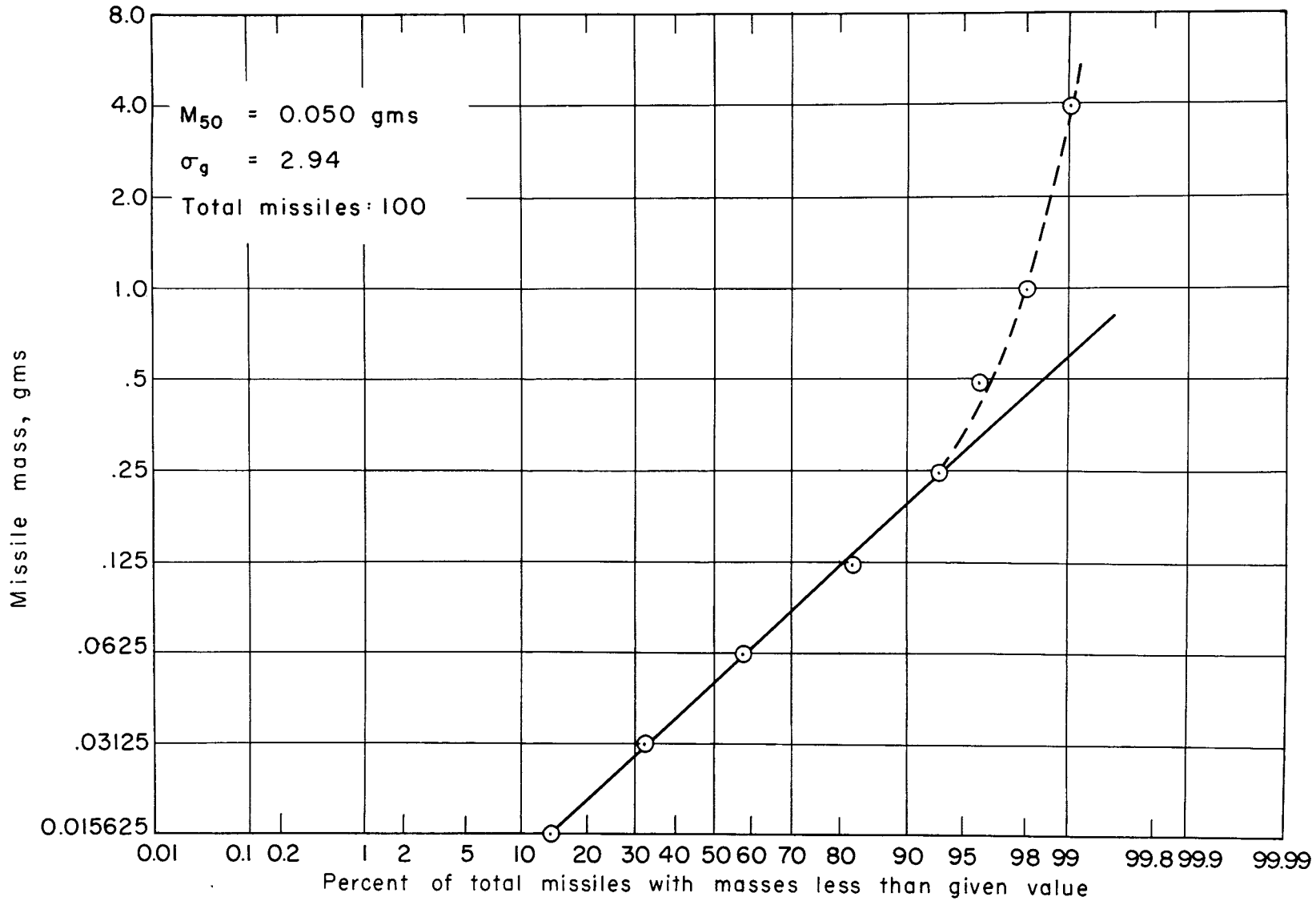

Fig. 5.9—Logarithmic mass-frequency summation curve for missiles from trap 2H.

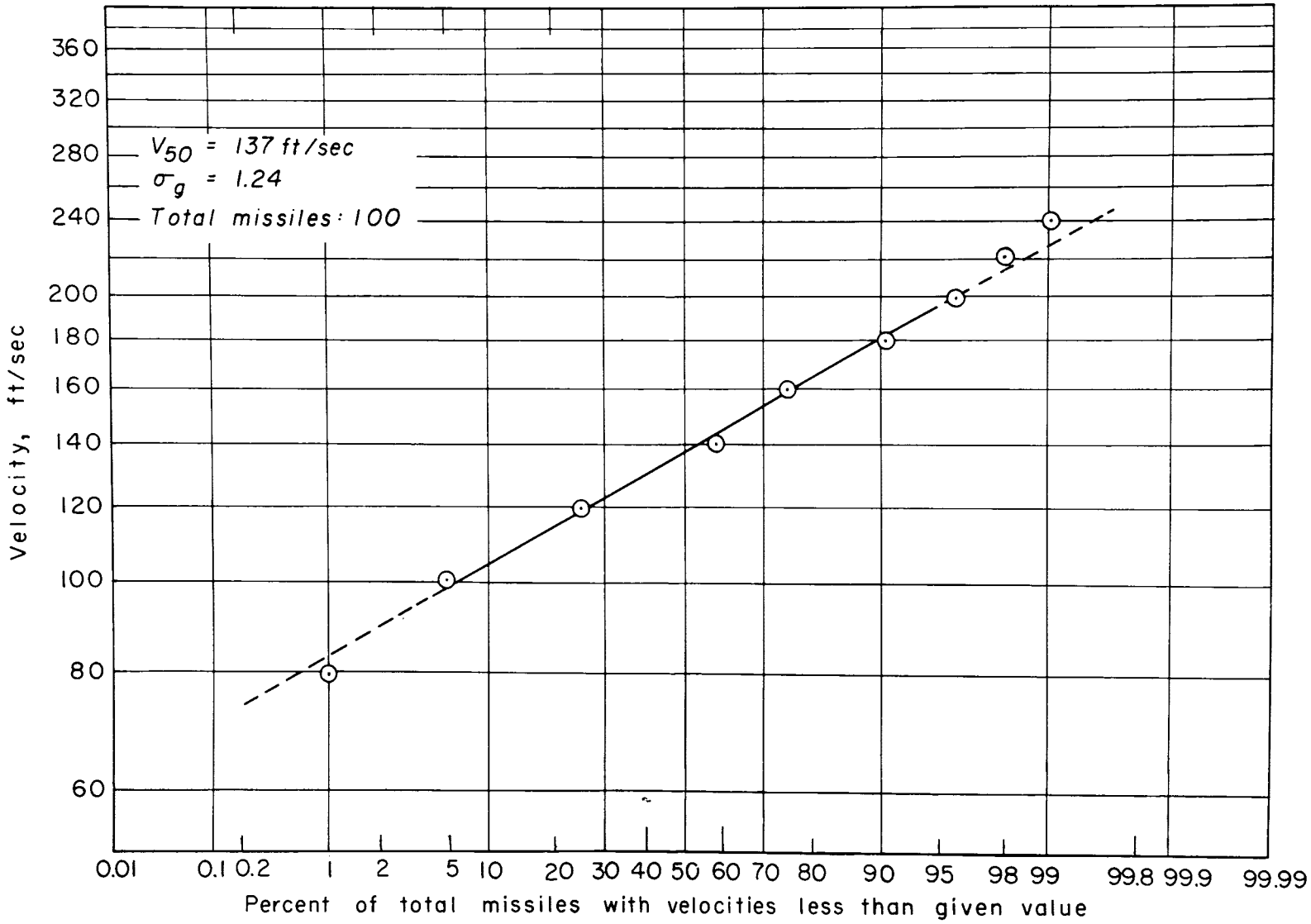

Fig. 5.10—Logarithmic velocity-frequency summation curve for missiles from trap 2H.

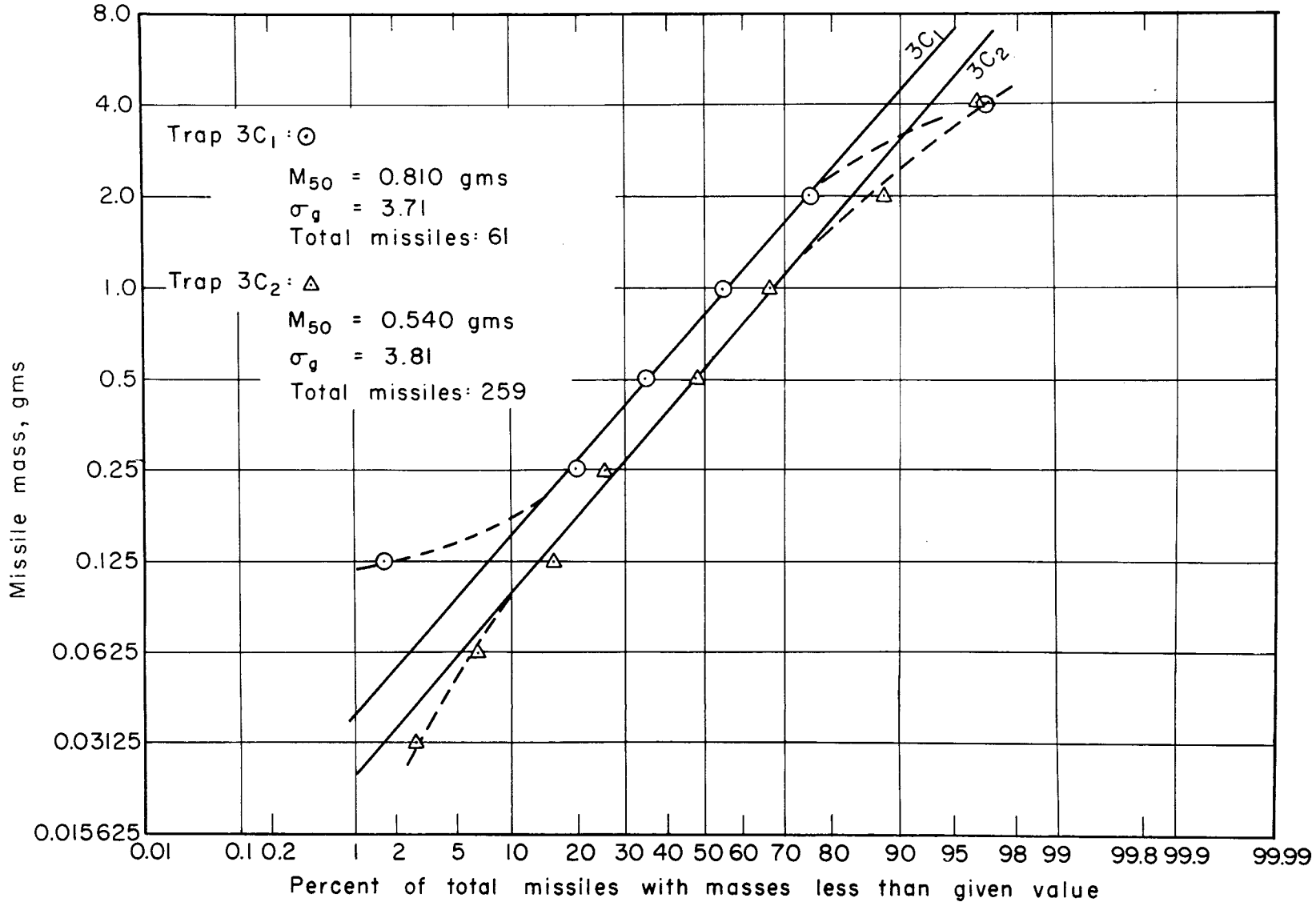

Fig. 5.11—Logarithmic mass-frequency summation curves for missiles from traps $3C_1$ and $3C_2$.

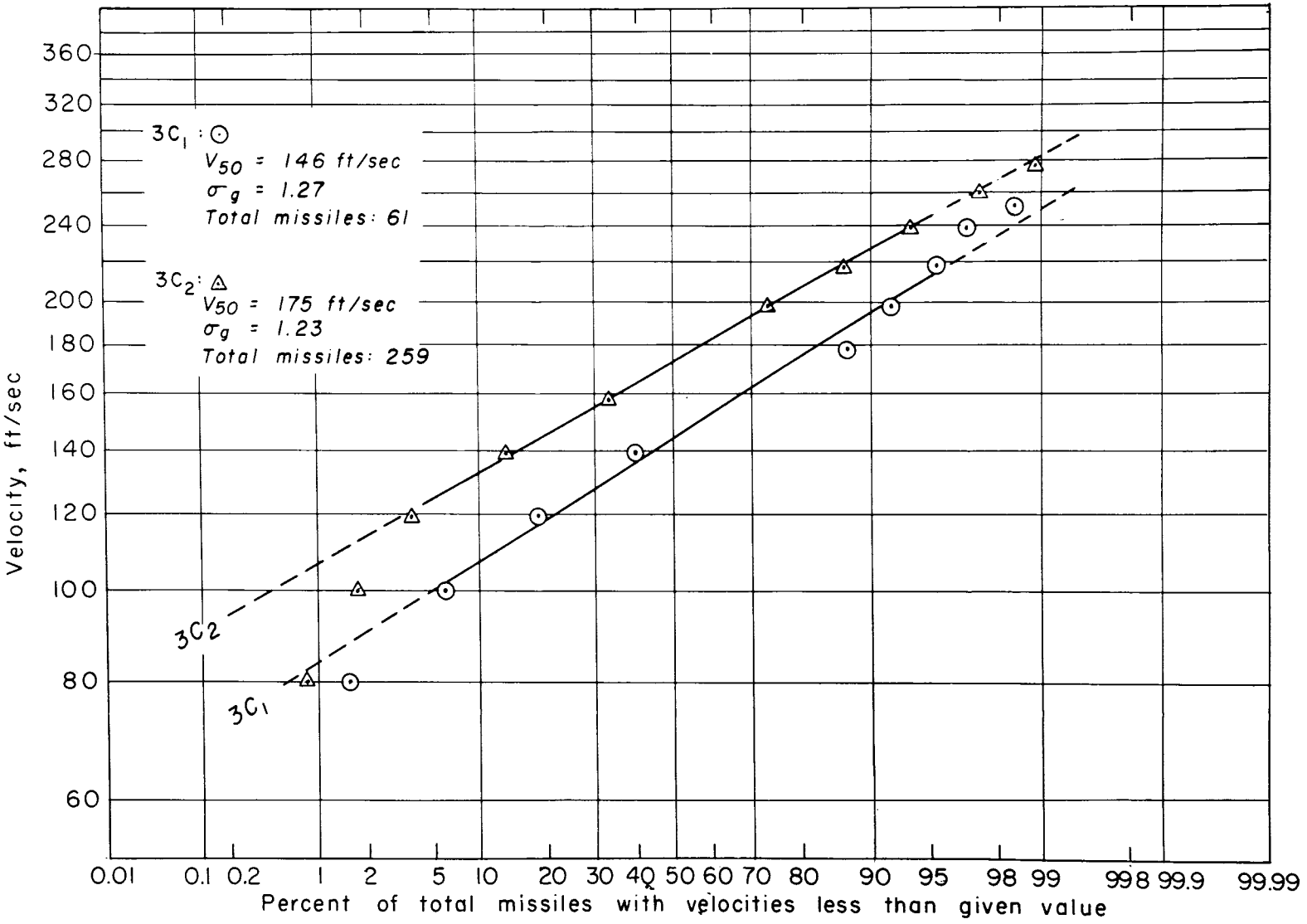

Fig. 5.12—Logarithmic velocity-frequency summation curves for missiles from traps $3C_1$ and $3C_2$.

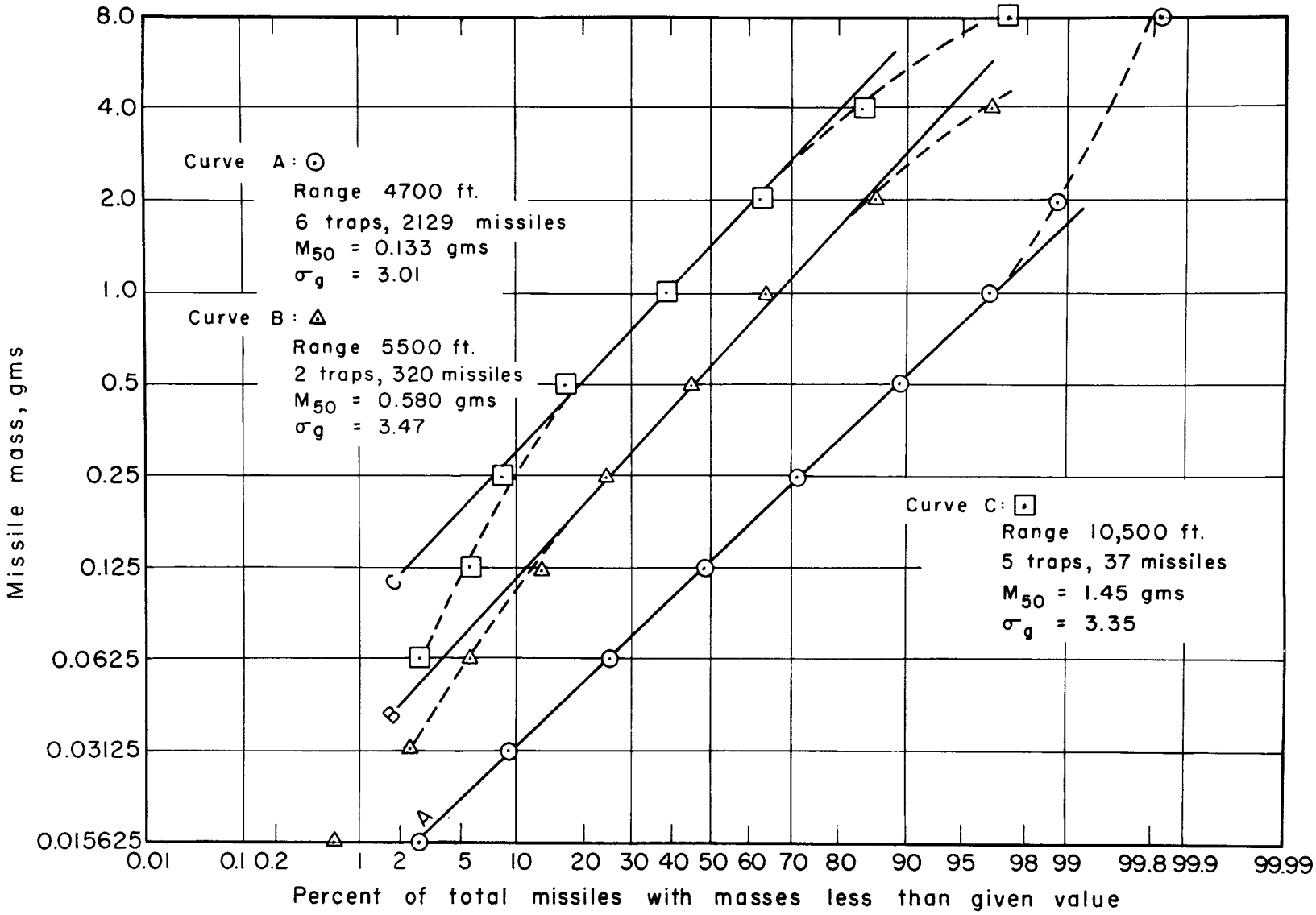

Fig. 5.13—Logarithmic mass-frequency summation curves for missiles from traps placed at different ranges from Ground Zero.

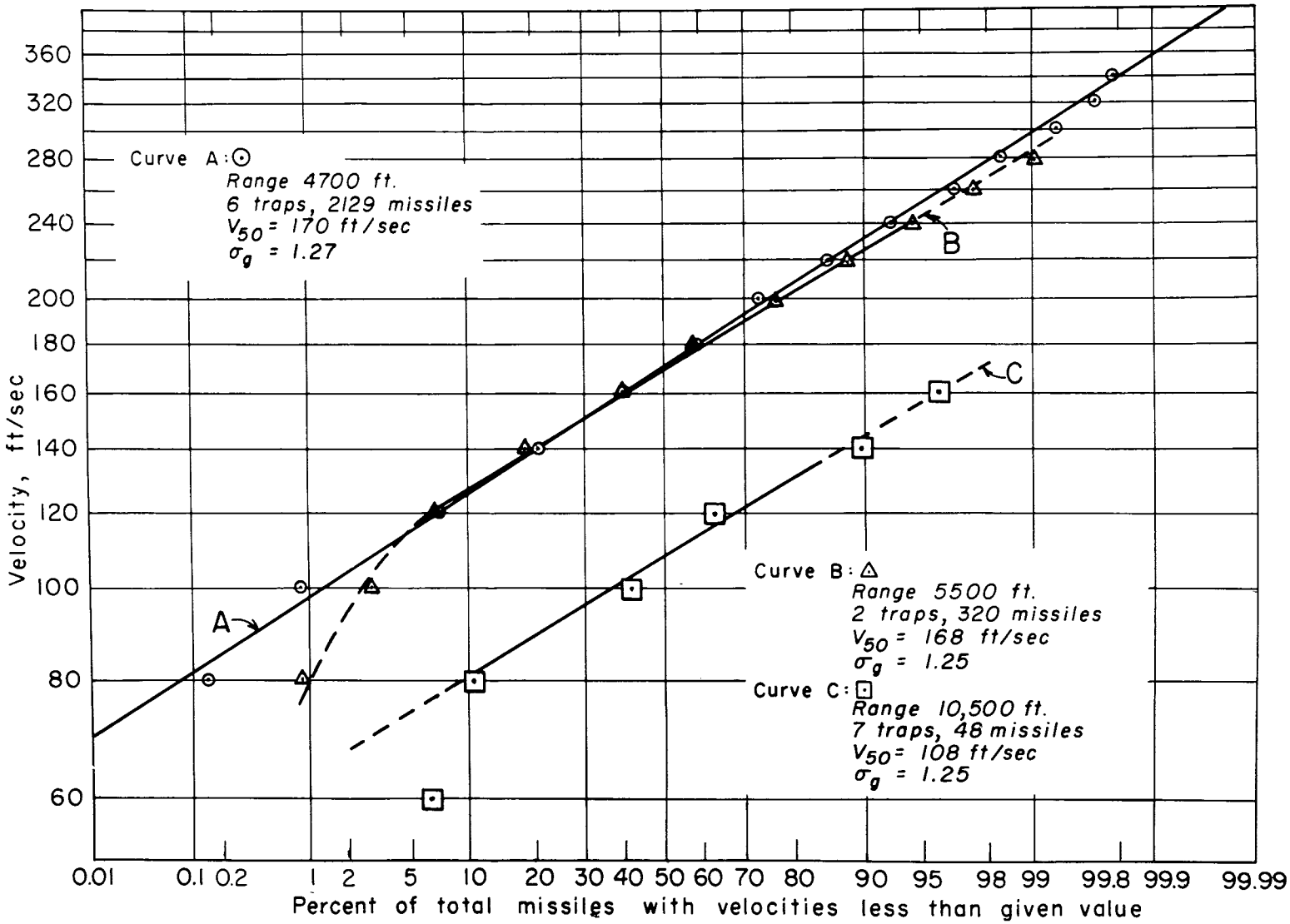

Fig. 5.14—Logarithmic velocity-frequency summation curves for missiles from traps placed at different ranges from Ground Zero.

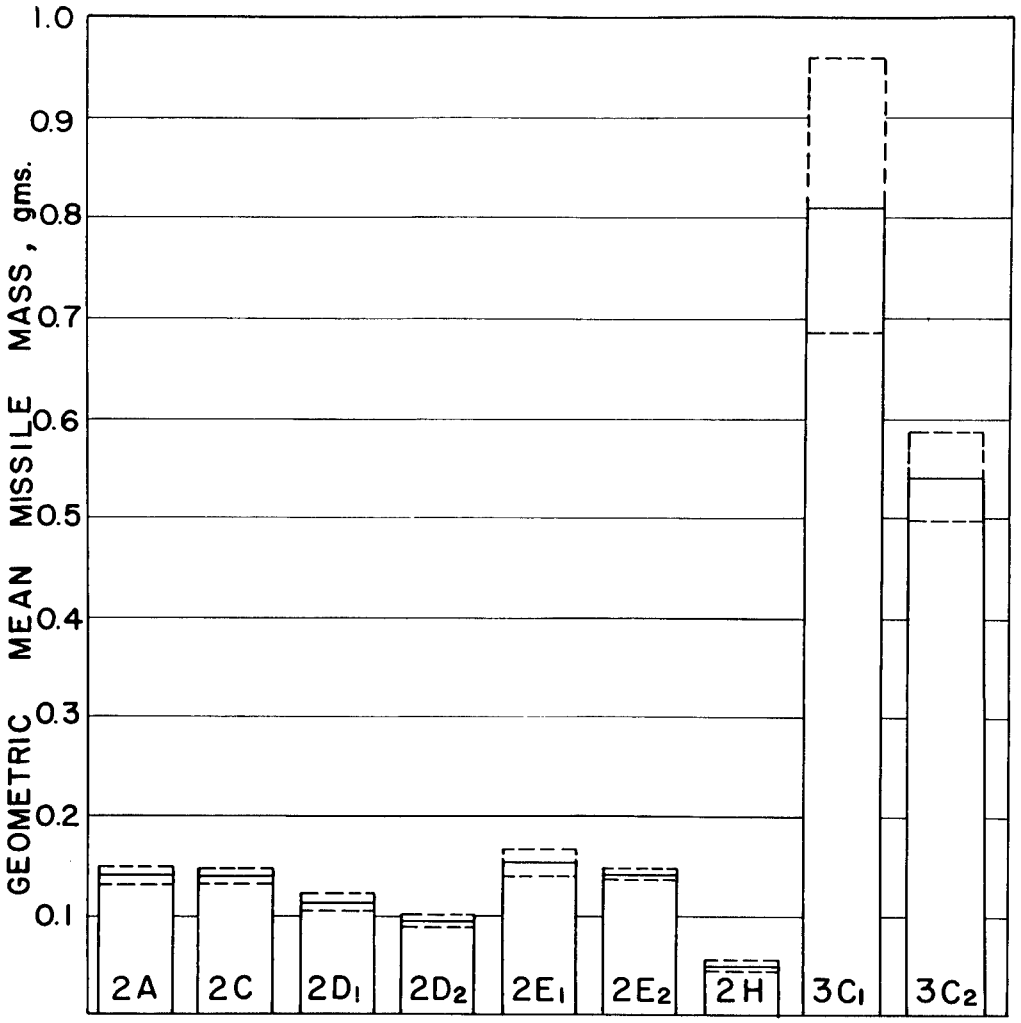

Fig. 5.15—Geometric mean masses for missiles from various traps. Trap 2H was in an open area 100 ft behind the rambler house at the 4700-ft range; other traps indicated were inside the houses behind windows facing Ground Zero—2A, 2C, $2D_1$, $2D_2$, $2E_1$, and $2E_2$ at the 4700-ft range and $3C_1$ and $3C_2$ at the 5500-ft range. Dashed lines represent the standard error of the mean.

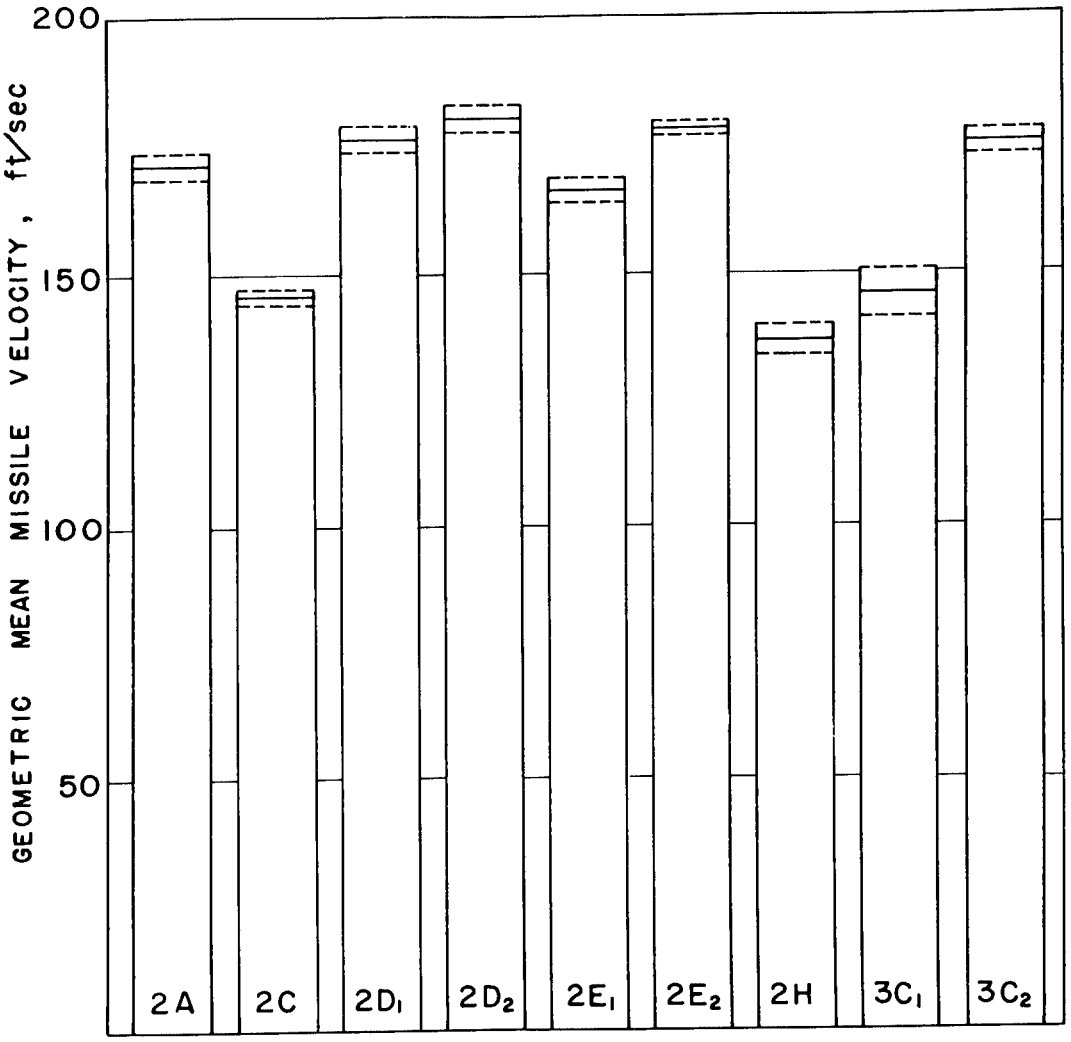

Fig. 5.16—Geometric mean velocities for missiles from various traps. Trap 2H was in an open area 100 ft behind the rambler house at the 4700-ft range; other traps indicated were inside the houses behind windows facing Ground Zero—2A, 2C, $2D_1$, $2D_2$, $2E_1$, and $2E_2$ at the 4700-ft range and $3C_1$ and $3C_2$ at the 5500-ft range. Dashed lines represent the standard error of the mean.

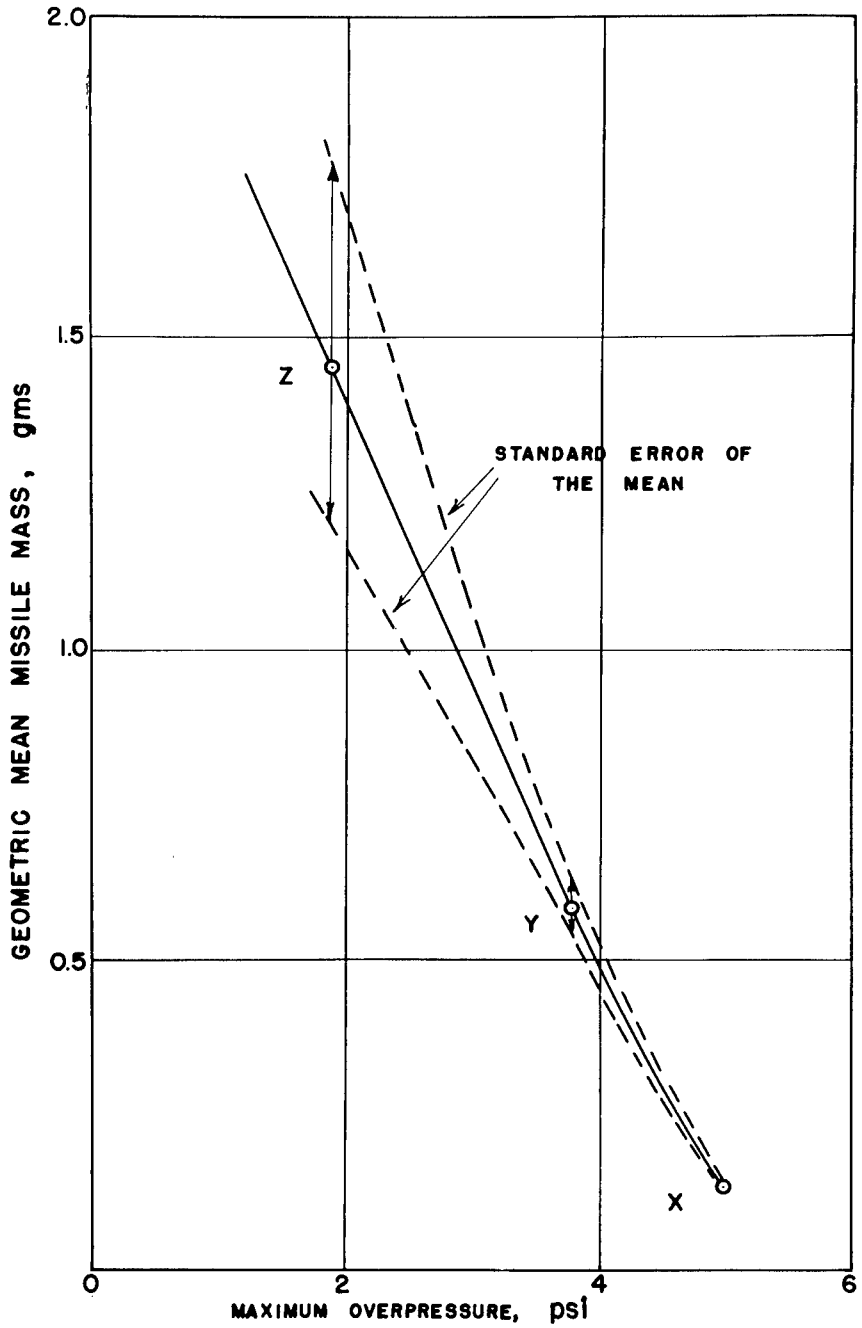

Fig. 5.17—Size of glass missiles from window panes as a function of maximum overpressure. Point X indicates data from traps at the 4700-ft range; point Y, at the 5500-ft range; and point Z, at the 10,500-ft range. Average thickness of window panes: X, 0.107 in.; Y, 0.118 in.; and Z, 0.104 in.

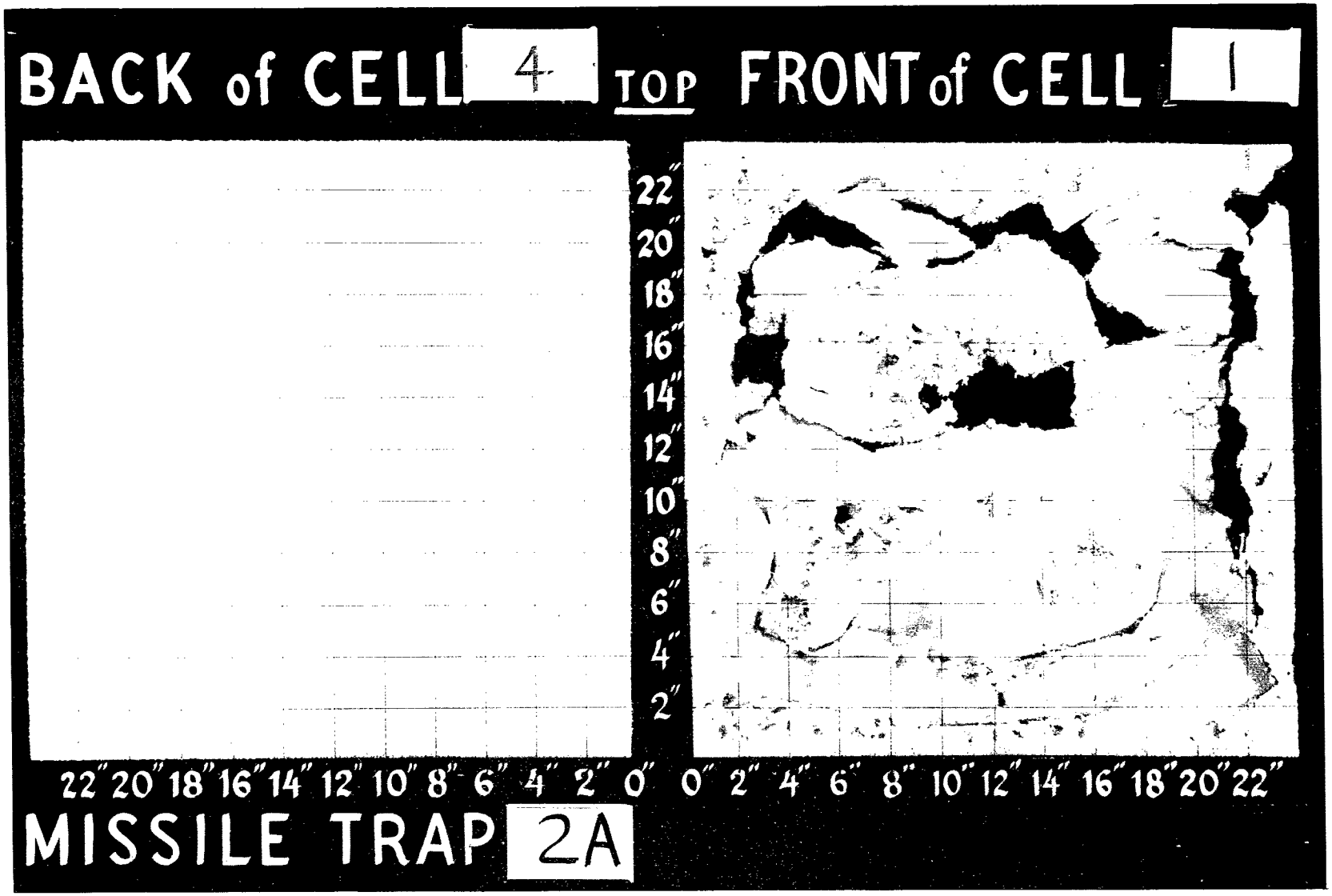

Fig. 5.18—Detail of front of cell 1 and back of cell 4, trap 2A.

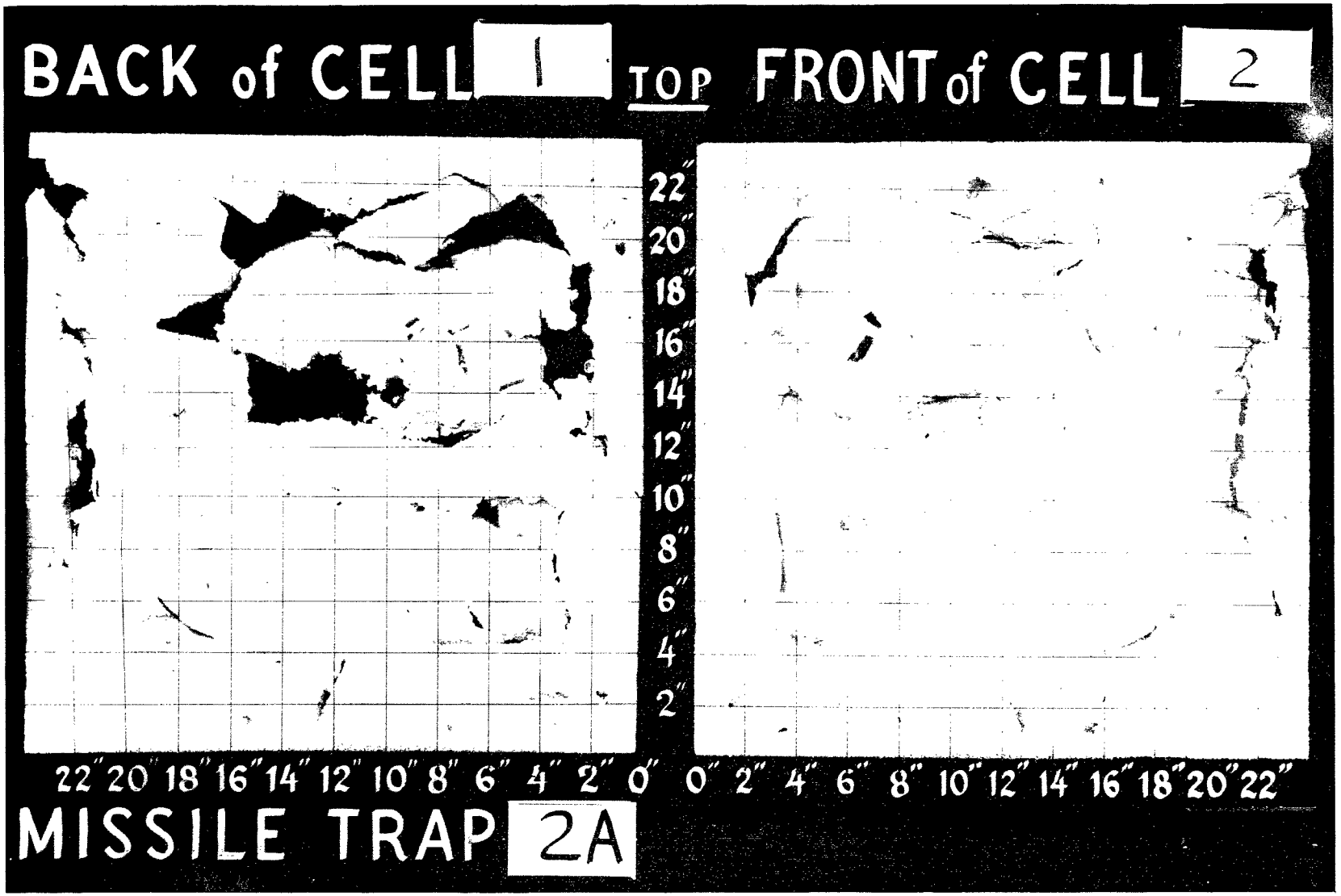

Fig. 5.19—Detail of front of cell 2 and back of cell 1, trap 2A.

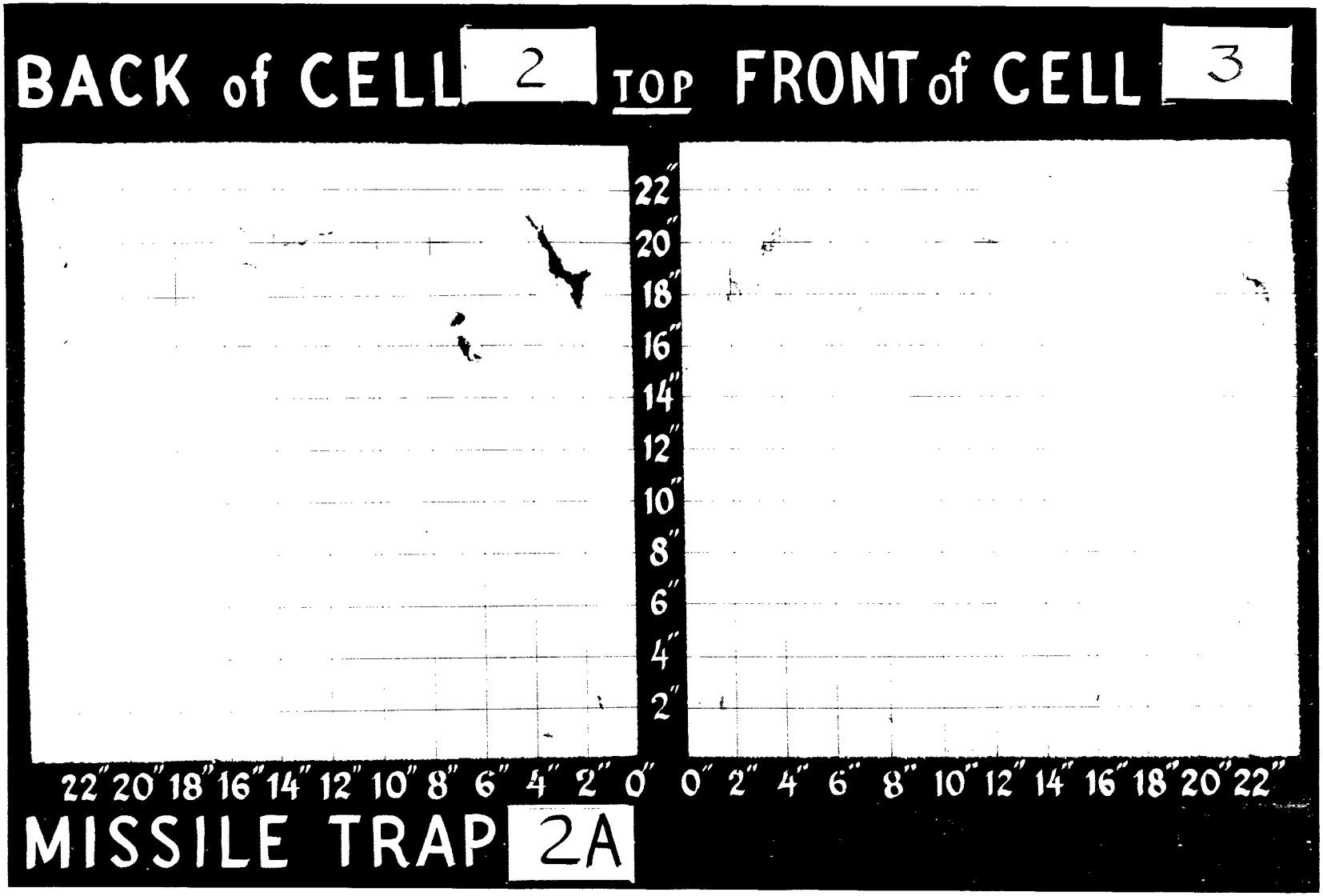

Fig. 5.20—Detail of front of cell 3 and back of cell 2, trap 2A.

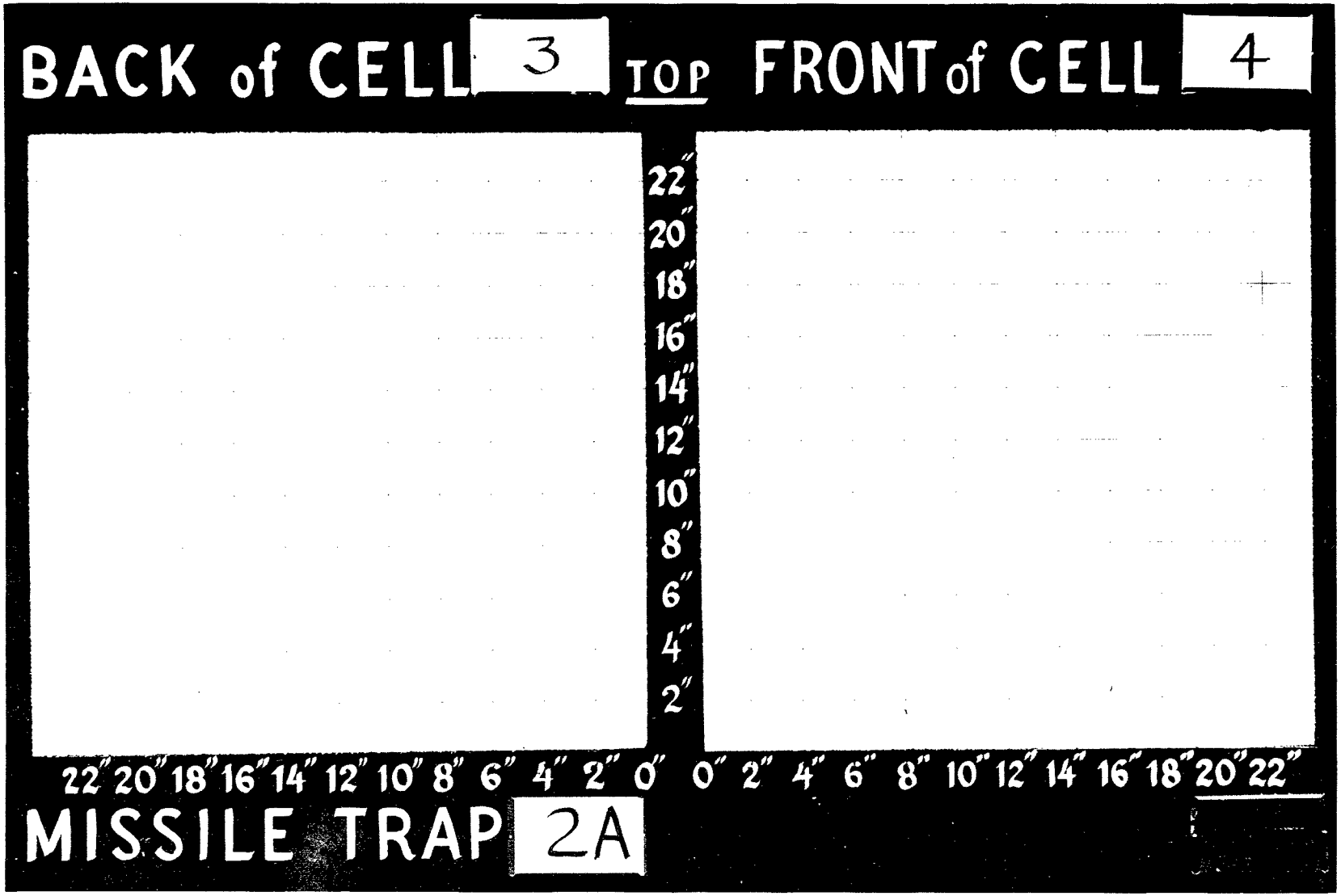

Fig. 5.21—Detail of front of cell 4 and back of cell 3, trap 2A.

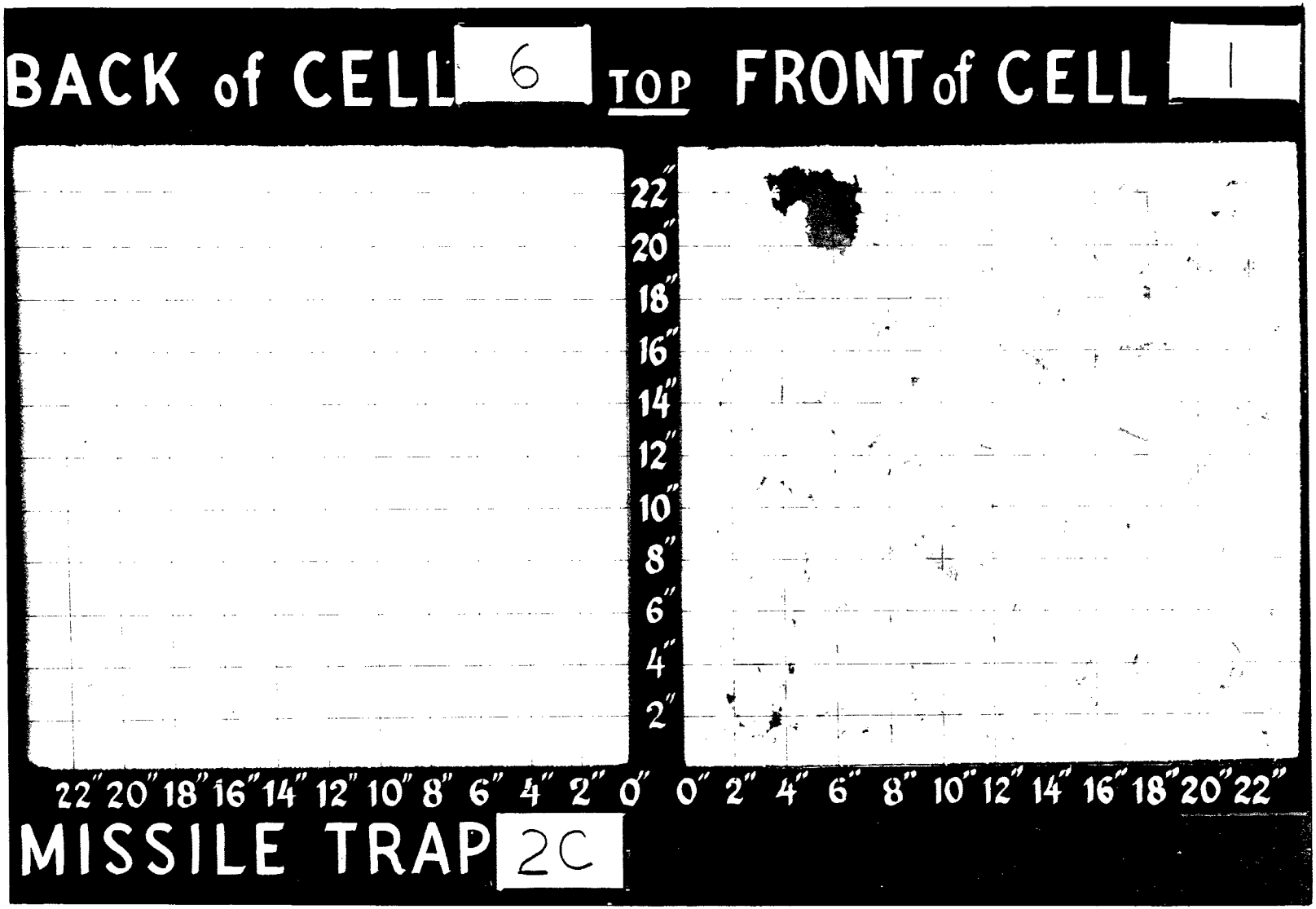

Fig. 5.22—Detail of front of cell 1 and back of cell 6, trap 2C.

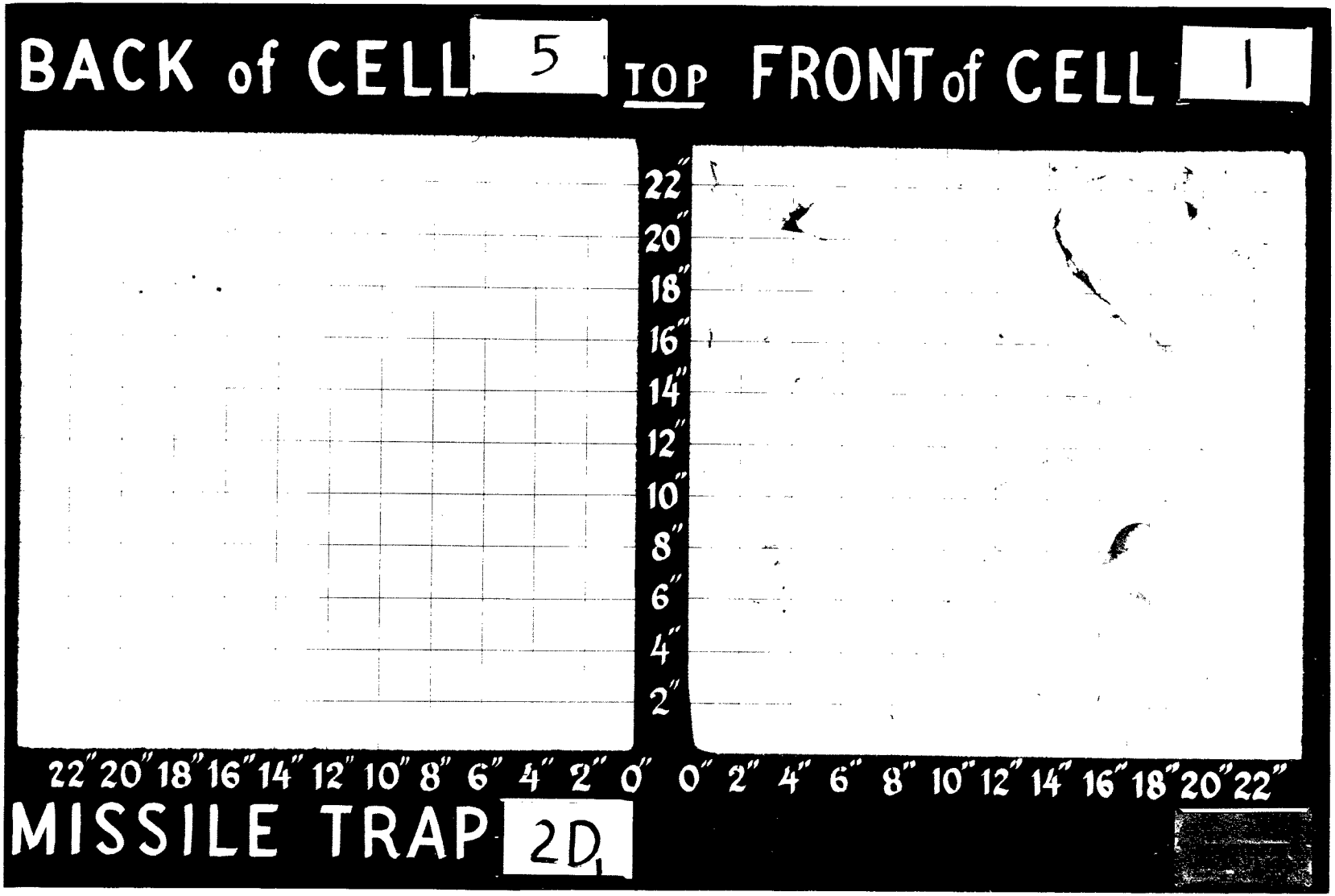

Fig. 5.23—Detail of front of cell 1 and back of cell 5, trap $2D_1$.

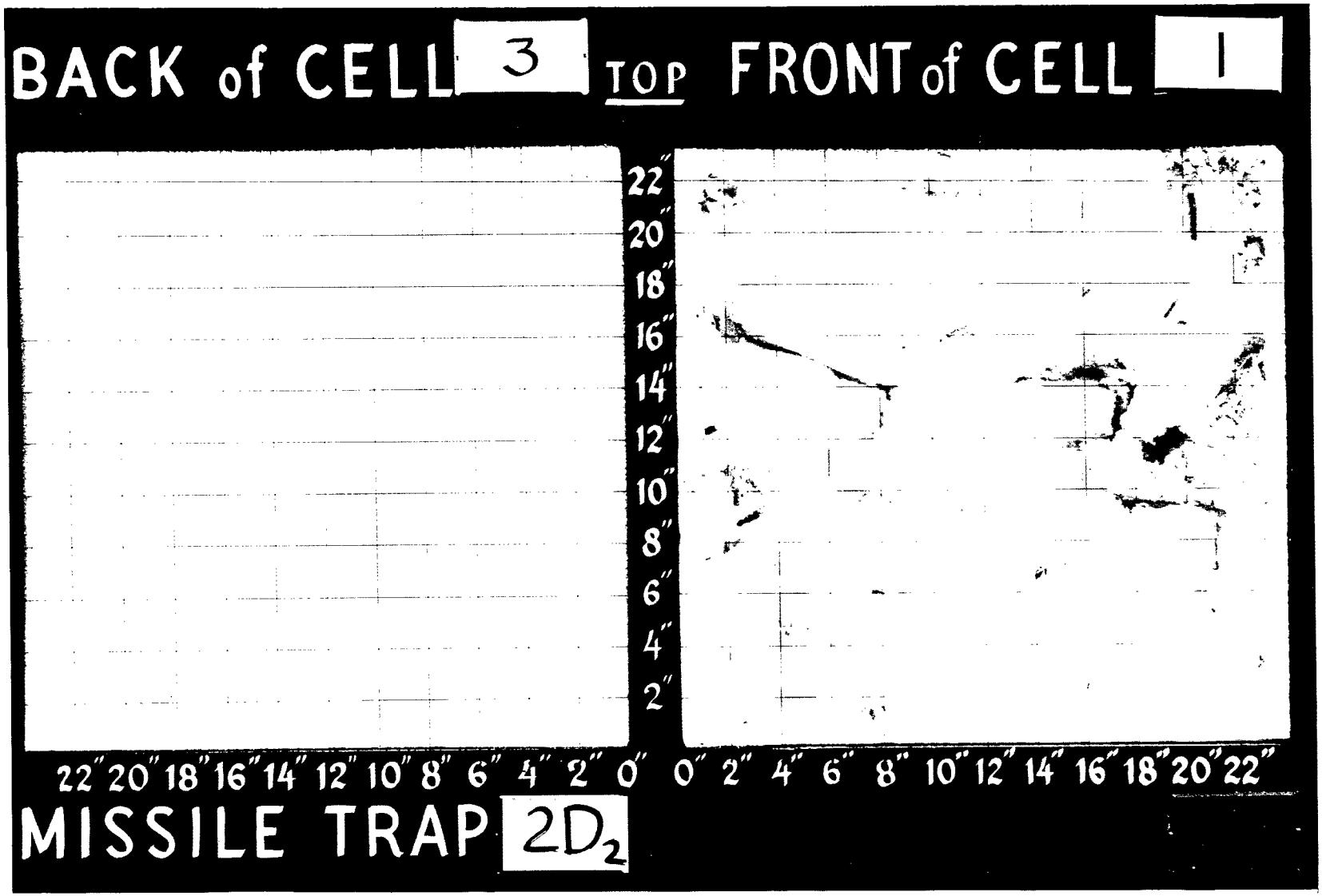

Fig. 5.24—Detail of front of cell 1 and back of cell 3, trap $2D_2$.

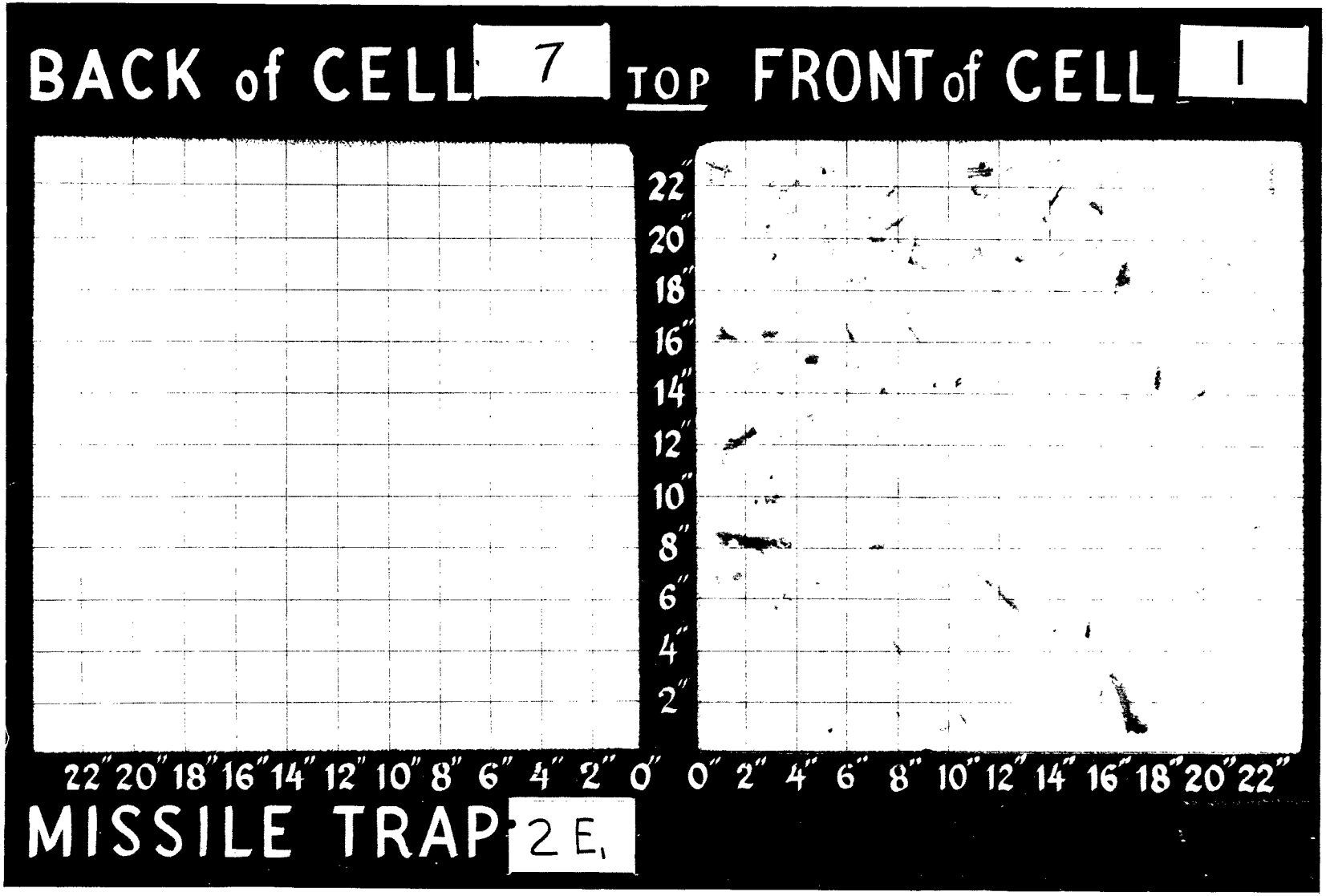

Fig. 5.25—Detail of front of cell 1 and back of cell 7, trap $2E_1$.

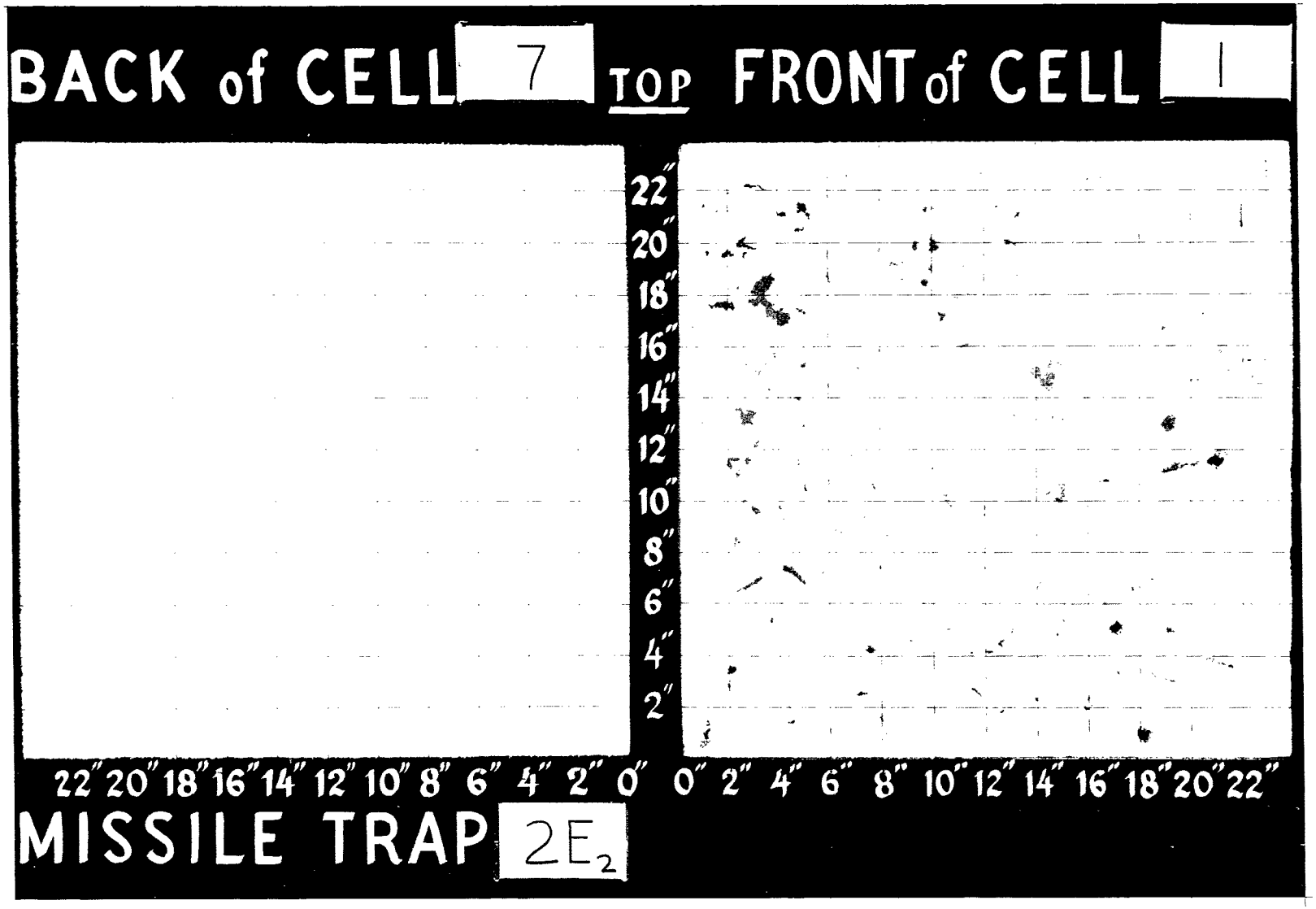

Fig. 5.26—Detail of front of cell 1 and back of cell 7, trap $2E_2$.

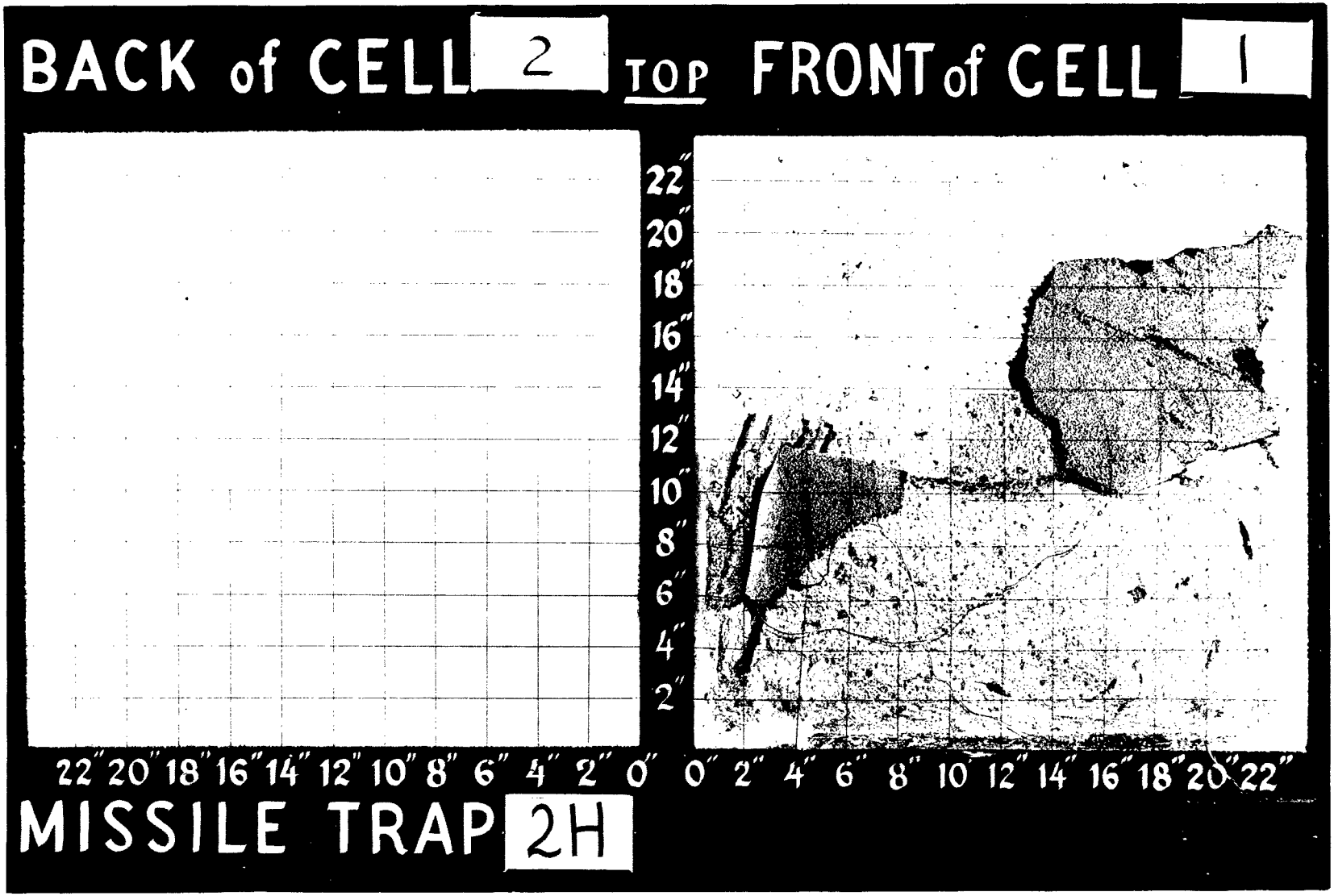

Fig. 5.27—Detail of front of cell 1 and back of cell 2, trap 2H.

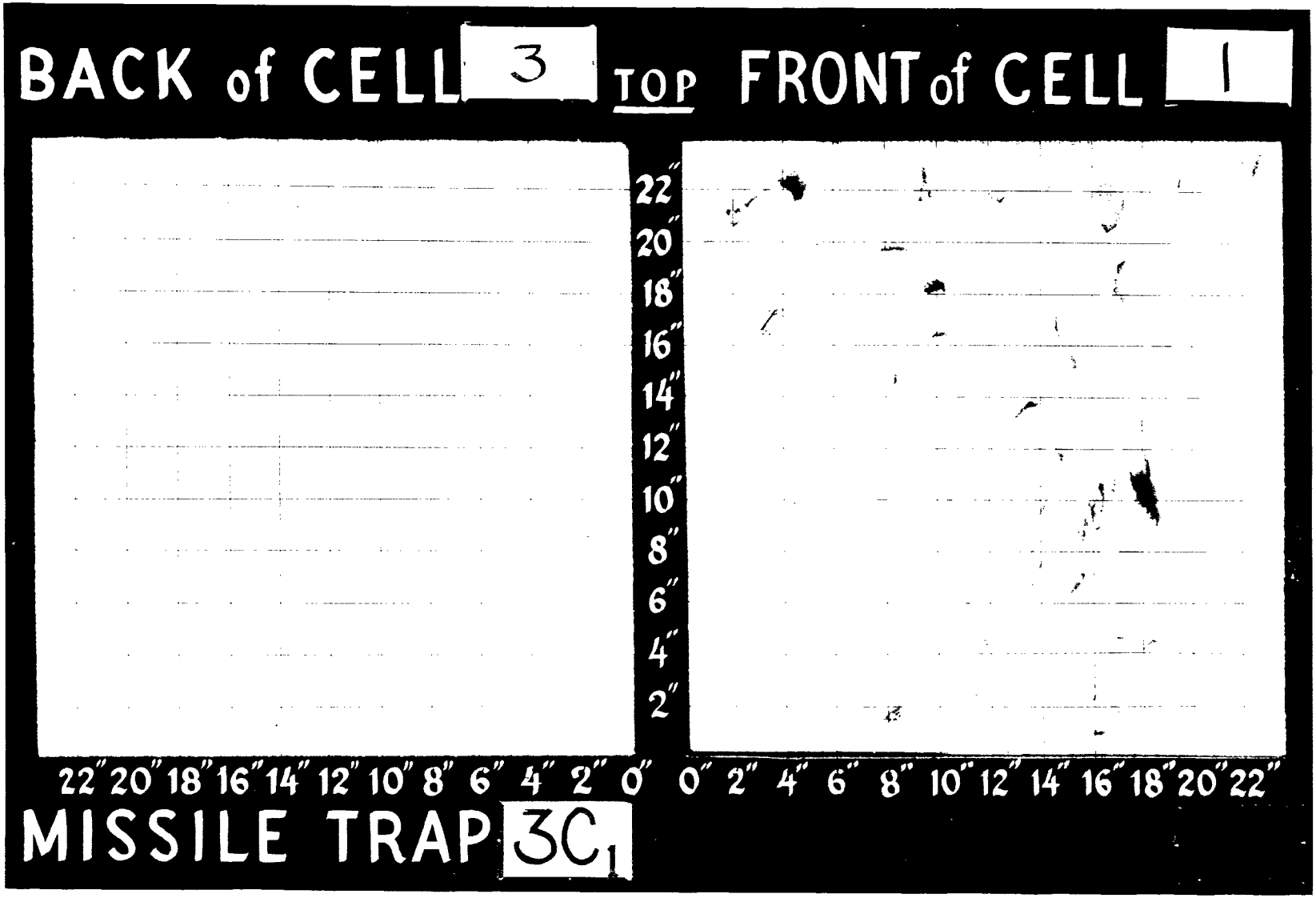

Fig. 5.28—Detail of front of cell 1 and back of cell 3, trap $3C_1$.

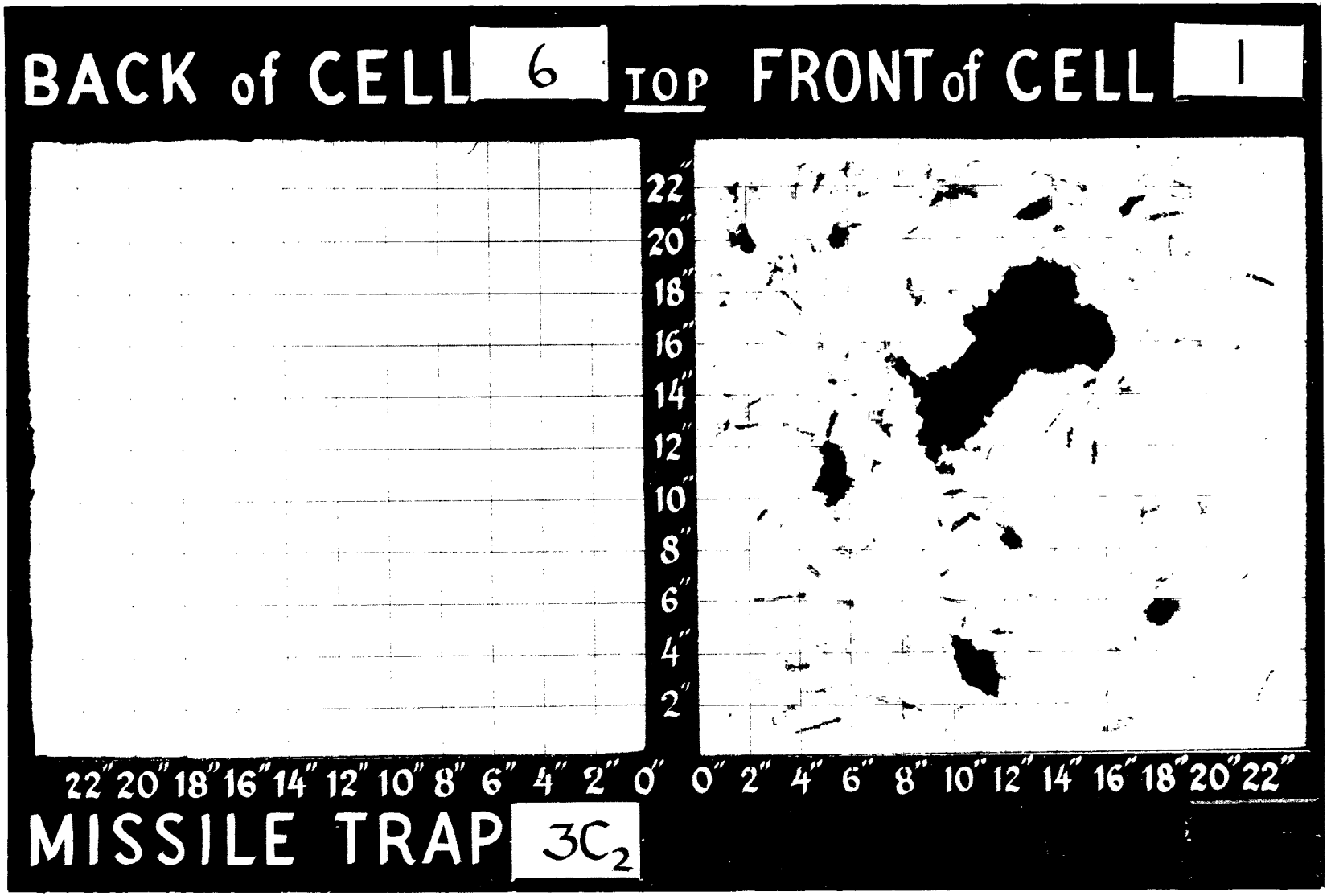

Fig. 5.29—Detail of front of cell 1 and back of cell 6, trap $3C_2$.

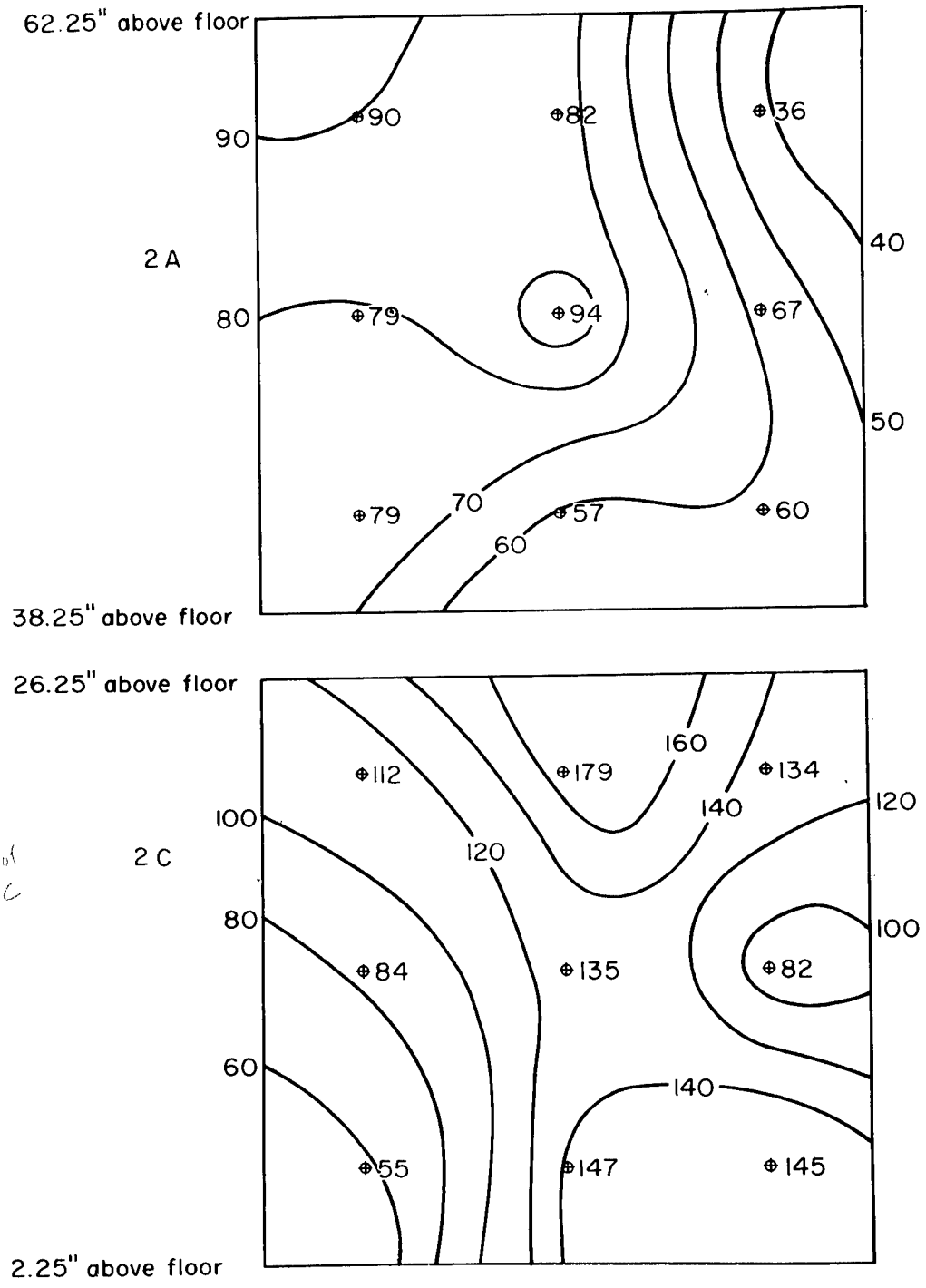

Fig. 5.30—Spatial distribution of missiles passing through the front surface of traps 2A and 2C. Numbers indicate missiles per square foot.

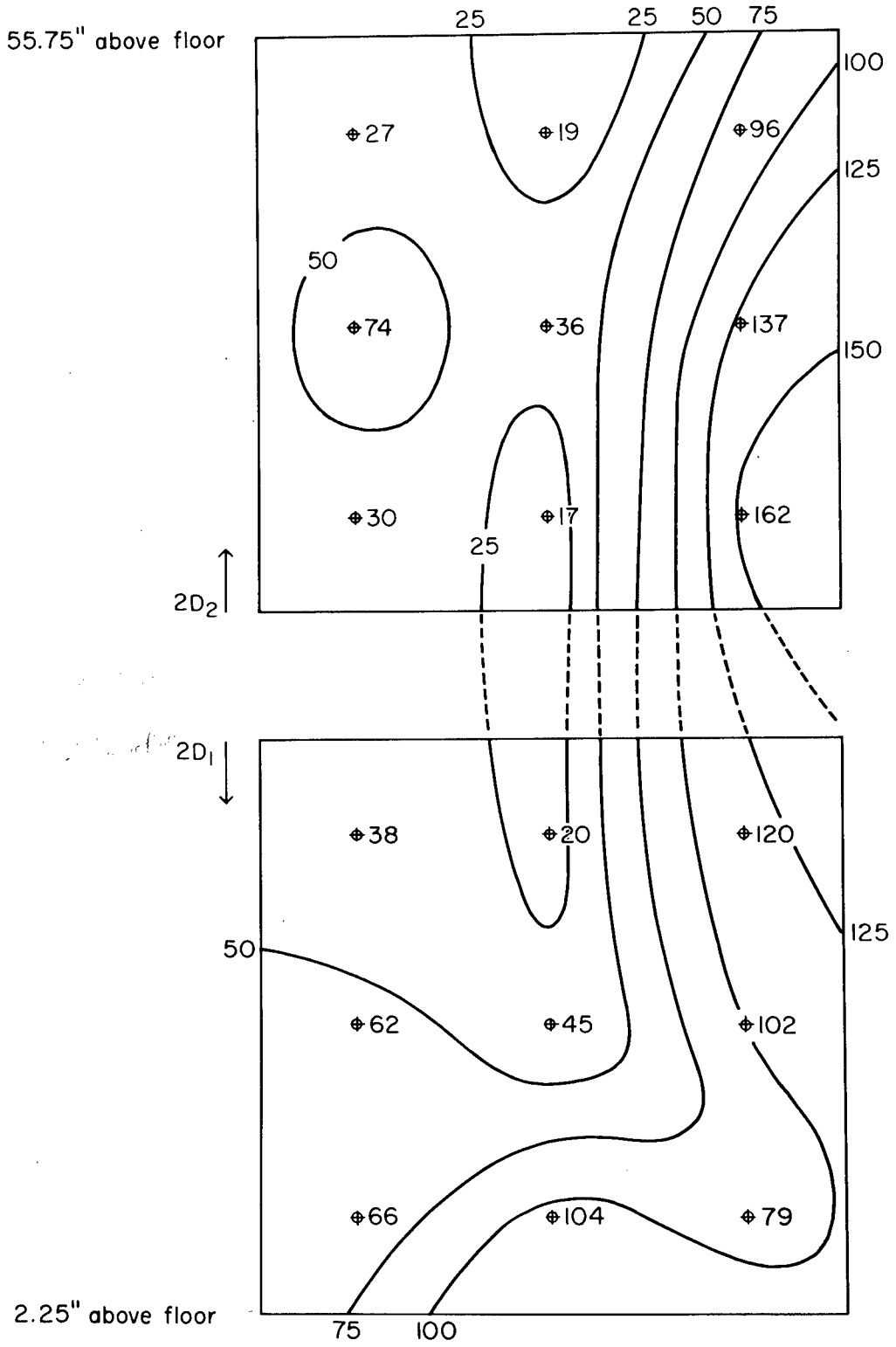

Fig. 5.31—Spatial distribution of missiles passing through the front surface of traps $2D_1$ and $2D_2$. Numbers indicate missiles per square foot.

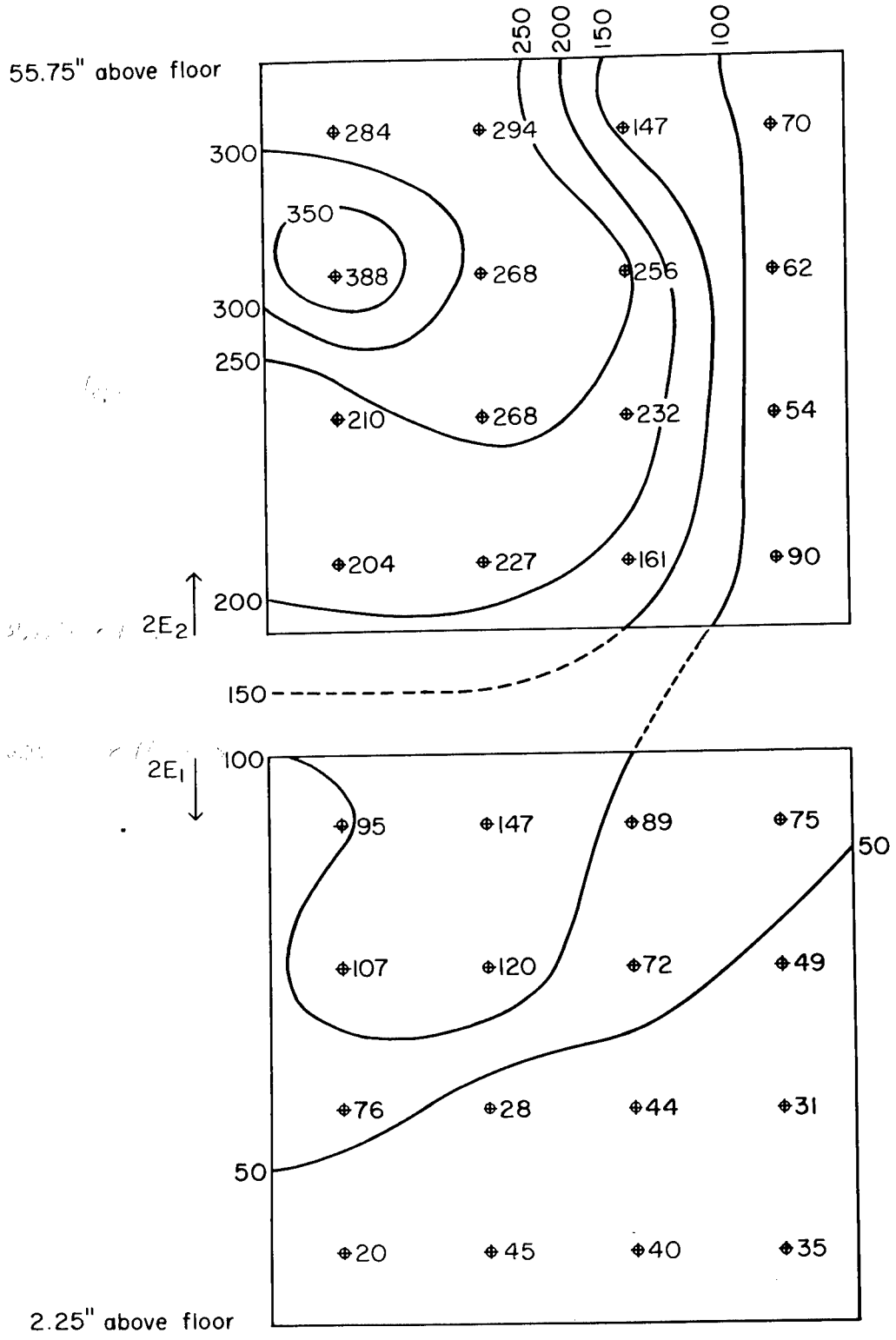

Fig. 5.32—Spatial distribution of missiles passing through the front surface of traps $2E_1$ and $2E_2$. Numbers indicate missiles per square foot.

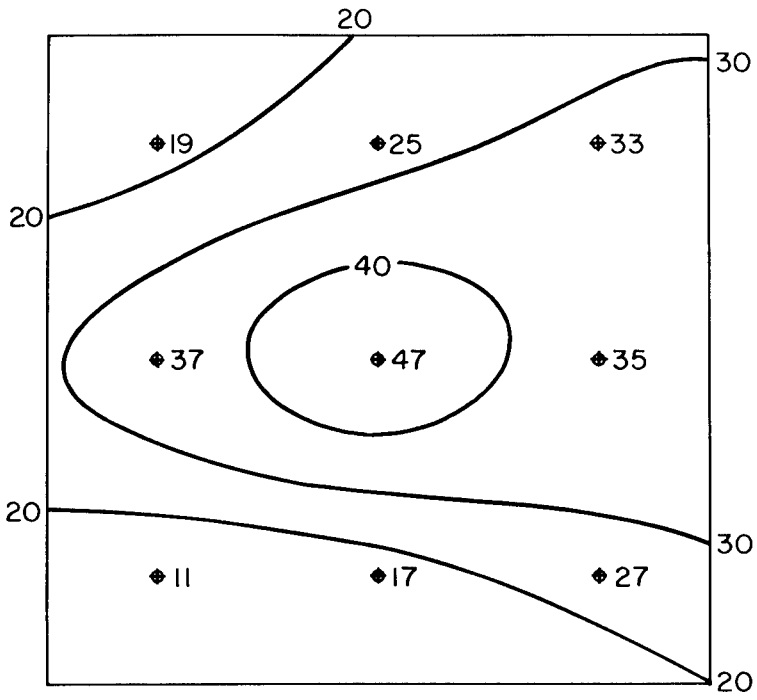

Fig. 5.33—Spatial distribution of missiles passing through the front surface of trap 2H. Numbers indicate missiles per square foot.

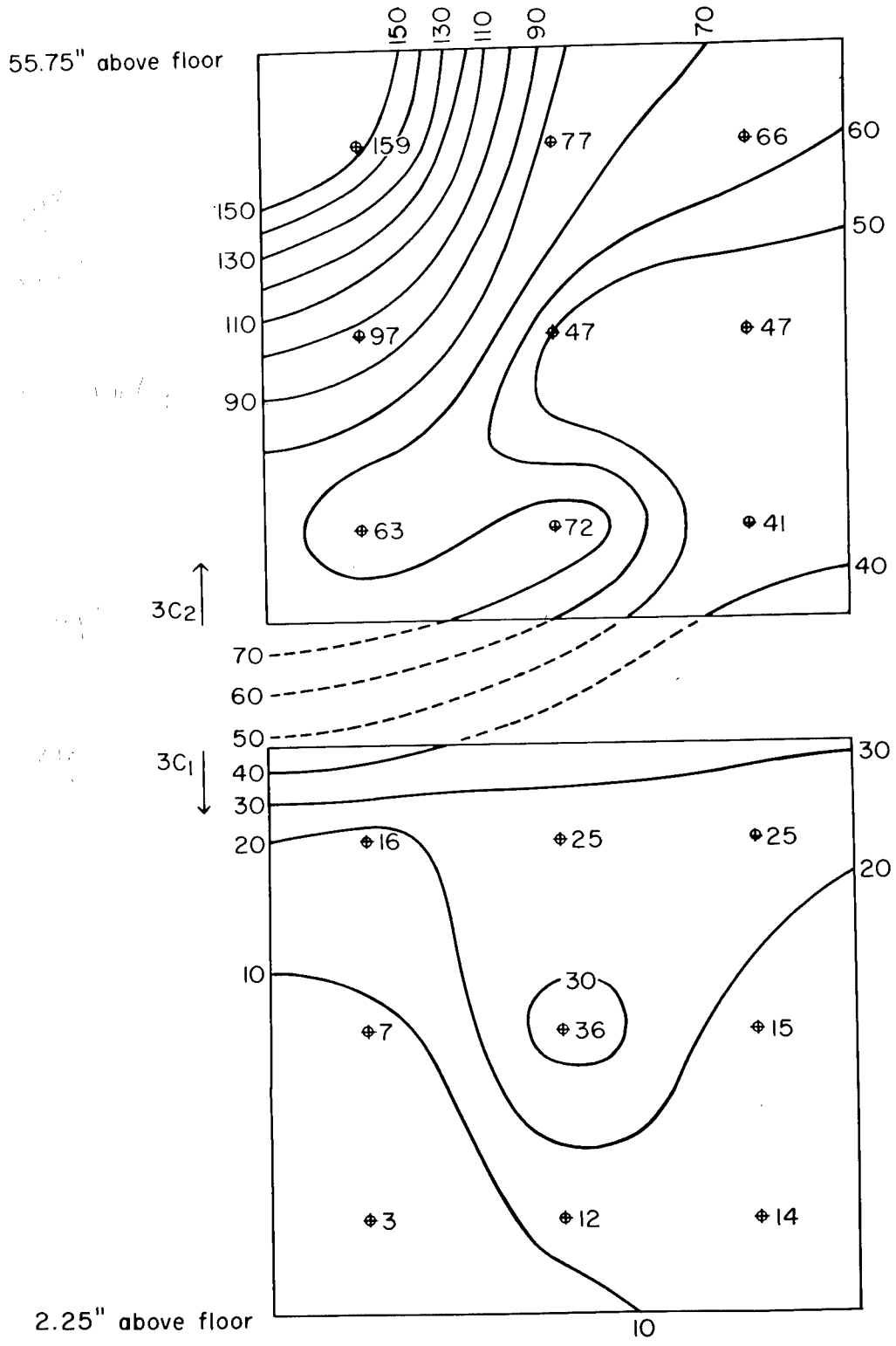

Fig. 5.34—Spatial distribution of missiles passing through the front surface of traps $3C_1$ and $3C_2$. Numbers indicate missiles per square foot.

CHAPTER 6

COMPUTATION OF STONE-MISSILE VELOCITIES FROM BLAST DATA

6.1 GENERAL

It was obvious that the value of a secondary missile program would be enhanced if it could be shown how missiles acquired the velocites which were measured. Since the blast parameters (wind speed and air density as a function of time) responsible for secondary missiles are difficult to delineate even under ideal conditions, it was decided to choose the simplest possible situation for the initial investigation. Thus it was decided to study stone missiles picked up by the wind in open areas rather than to attempt to explain the velocities of glass missiles originating in houses. As it will be seen, the stone-missile study did clarify the glass-missile problem to some extent.

6.2 COMPUTATION PROCEDURES

Newton's second law of motion can be written

$$F = m \frac{dv}{dt} \tag{6.1}$$

where F = force
m = mass
dv/dt = instantaneous time rate of change of velocity

The drag force acting on a missile moving in a wind field is

$$F = \frac{1}{2} \rho (u + v)^2 A C_d \tag{6.2}$$

where ρ = air density
u = wind velocity
v = missile velocity
A = presenting area of missile
C_d = drag coefficient of missile

Equations 6.1 and 6.2 were combined to eliminate F, and the resulting equation was solved for dv.

$$dv = \frac{\rho (u - v)^2 A C_d}{2m} dt \tag{6.3}$$

The mathematical solution of the differential equation, Eq. 6.3, would be impractical since it involves the four variables: missile velocity, wind velocity, air density, and time. However, an approximate solution was accomplished by integration in small steps of time, Δt. Thus dt was replaced by Δt; dv, by Δv; and instantaneous wind velocity u and air density ρ, by an average velocity $\bar{u}$ and density $\bar{\rho}$ corresponding to the time interval Δt.

Before proceeding further, it would be well to examine the time function Δt, which represents the small increment of time that a missile is exposed to wind of velocity $\bar{u}$ and air density $\bar{\rho}$. It is apparent that the time of exposure is longer if the missile is moving with the wind than it would be if the missile were at rest with respect to the ground. Thus it is necessary to evaluate Δt as a function of shock and missile velocities.

$$\Delta t = \Delta t_0 \frac{U}{U - v} \tag{6.4}$$

where Δt = actual time particle is exposed to wind of average velocity $\bar{u}$
Δt_0 = time required for wind of velocity $\bar{u}$ to pass a fixed point
U = shock velocity, or velocity at which wind of velocity $\bar{u}$ moves forward with respect to a fixed point

Using this new value of Δt and substituting Δv for dv, $\bar{u}$ for u, and $\bar{\rho}$ for ρ, Eq. 6.3 becomes

$$\Delta v = \frac{AC_d}{2m} \bar{\rho} (\bar{u} - v)^2 \, \Delta t_0 \frac{U}{U - v} \tag{6.5}$$

It has been pointed out that $\bar{\rho}$ and $\bar{u}$ are average values of air density and wind velocity for the time interval Δt_0. Correspondingly, v should be the average missile velocity for the same time period. An approximate average v could be determined by trial solution of Eq. 6.5 or by extrapolation after several values of Δv have been determined. In the present study, however, the missile velocity at the beginning of the time period was used for v. This approximation made the term $(\bar{u} - v)^2$ too high and the term $U/(U - v)$ too low.

The quantity U has been defined as the velocity at which a particular wind-velocity region moves away from the center of the detonation. At a given range from Ground Zero, this velocity would be greatest for the shock front and would gradually decrease in the region behind the shock front. However, the velocity U was assumed to be constant in the present study. Consequently, it is recognized that the values computed for $U/(U - v)$ were too low, but it is doubtful that this is of significance for the analytical approach used here.

6.3 AERODYNAMIC CONSTANTS FOR STONE MISSILES

Sighard F. Hoerner[1] assigns to spheres and cylinders the drag coefficients 0.47 and 1.2, respectively, in the range of Reynolds numbers applying to this study. Since the texture and shape of natural stones vary quite widely (see Fig. 6.1), it would be impossible to assign all stones a single drag coefficient. The critical factor in the present computations was not an accurate evaluation of the coefficient of drag, but rather a reasonable value for the product of the drag coefficient and the presenting area (Eq. 6.5). Therefore it was decided to use a value of 1.0 for the drag coefficient and to compute area in a manner similar to that used in the Styrofoam penetration studies.

Section 3.4 describes a method for determining the diameter of irregular missiles which is effective in the penetration of Styrofoam. It was found that the effective diameter is larger than the average diameter by 0.041 in. This correction is particularly significant for missiles of small average diameters.

It seemed reasonable to assume that the diameter effective in aerodynamic drag would also be larger than the average diameter by a constant amount. For lack of better information the missile diameters effective in aerodynamic drag were assumed to be the same as those in Styrofoam drag.

The missiles from trap 2H were used in this study since it was the only trap placed in an open area which caught a sizable number of stones. The upper graph in Fig. 6.2 is a plot of the

Fig. 6.1 — Typical glass-fragment missiles (top row) from window panes and stone (middle row) and stick (bottom row) missiles from open areas. Glass-fragment masses, in grams (left to right): 0.0074, 0.0148, 0.0301, 0.0613, 0.1254, 0.2403, 0.5000, 1.114, 2.623, 6.840. Stone masses, in grams: 0.0063, 0.0101, 0.0142, 0.1028, 0.1059, 0.4234, 0.6719, 4.516. Stick masses, in grams: 0.0068, 0.0307, 0.0324, 0.0974.

effective diameters of 86 stone missiles caught by this trap as a function of missile mass. The dashed curve, indicating maximum effective diameter values, was arbitrarily used to determine drag areas for 0.01-, 0.1-, and 1.0-g missiles used in this study.

6.4 RESULTS

Air density, overpressure, and wind velocity as a function of time were determined by methods devised by Vortman and Merritt.[2] These data are plotted in Fig. 6.3 for a maximum overpressure of 5 psi at a range of 4700 ft from Ground Zero. The chosen range of 4700 ft proved to be somewhat low since the results of the present computations indicate that the missiles caught by trap 2H originated at a range of about 4790 ft, approximately 10 ft in front of this trap which was placed 4800 ft from Ground Zero. See the lower portion of Fig. 6.2 and Fig. 6.5 which will be mentioned later.

The increments of time (Δt_0) used in the computations of missile velocity were 2 msec for the first 20 msec, 10 msec for the next 80 msec, and 20 msec thereafter. The average air density and wind velocity for each of these time periods were taken from the curves shown in Fig. 6.3. Also shown in Fig. 6.3 are the results of the series of computations for stone missiles weighing 0.01, 0.1, and 1.0 g. The change in missile velocity with time is maximum just after the arrival of the shock front and gradually decreases to zero as the wind and missile velocities reach the same value.

Figure 6.4 is a logarithmic plot of computed missile velocity data vs time of missile travel. It should be noted that the time of missile travel is slightly longer than the time plotted in Fig. 6.3. This apparent "elongation" in missile travel time is due to the fact that the missile is moving with the shock front.

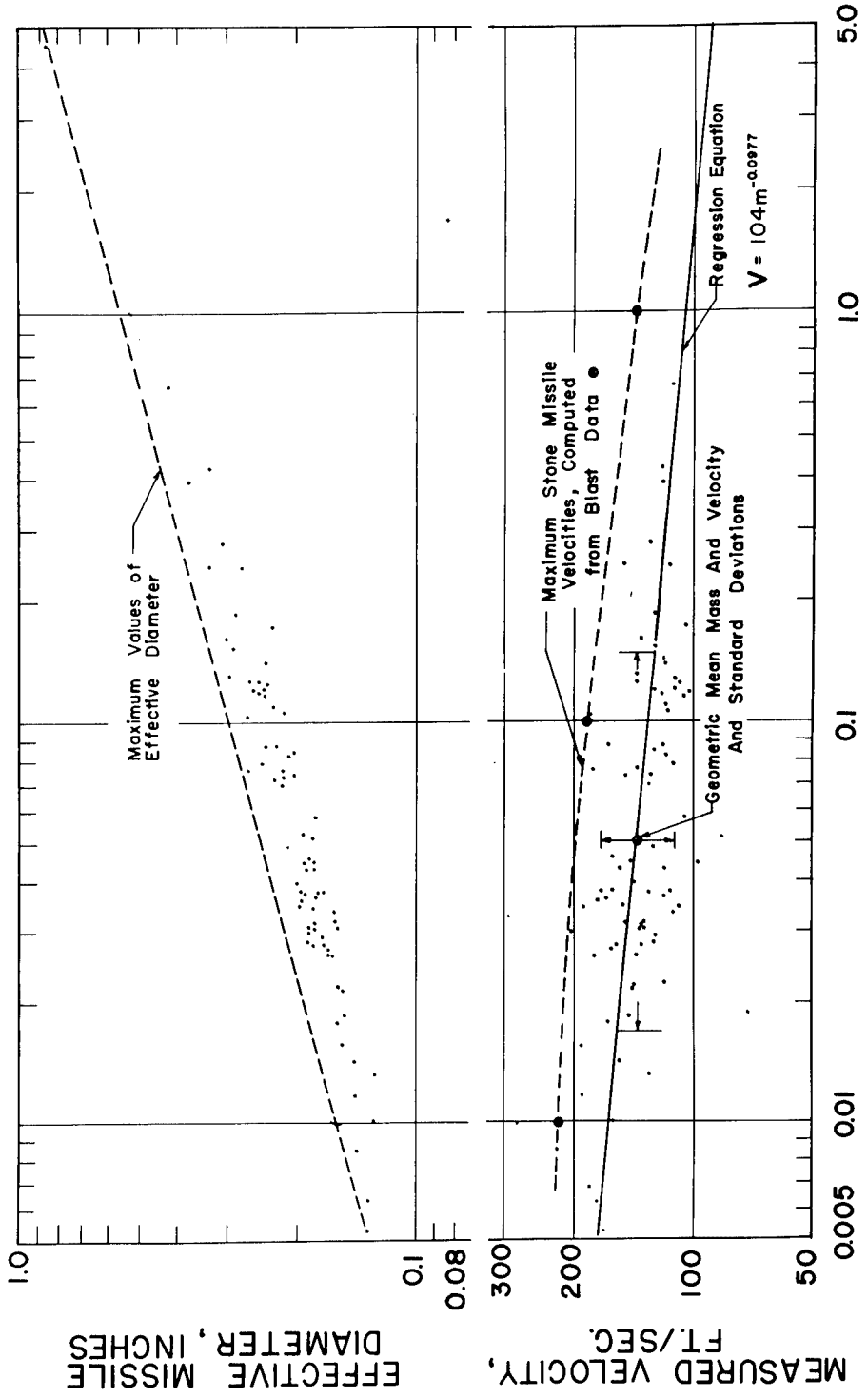

Fig. 6.2— Analysis of 86 stone missiles from trap 2H. Upper graph: effective diameter vs missile mass; effective diameter = average diameter + 0.041 in. (calibration data for Styrofoam). Lower graph: measured velocity as a function of missile mass.

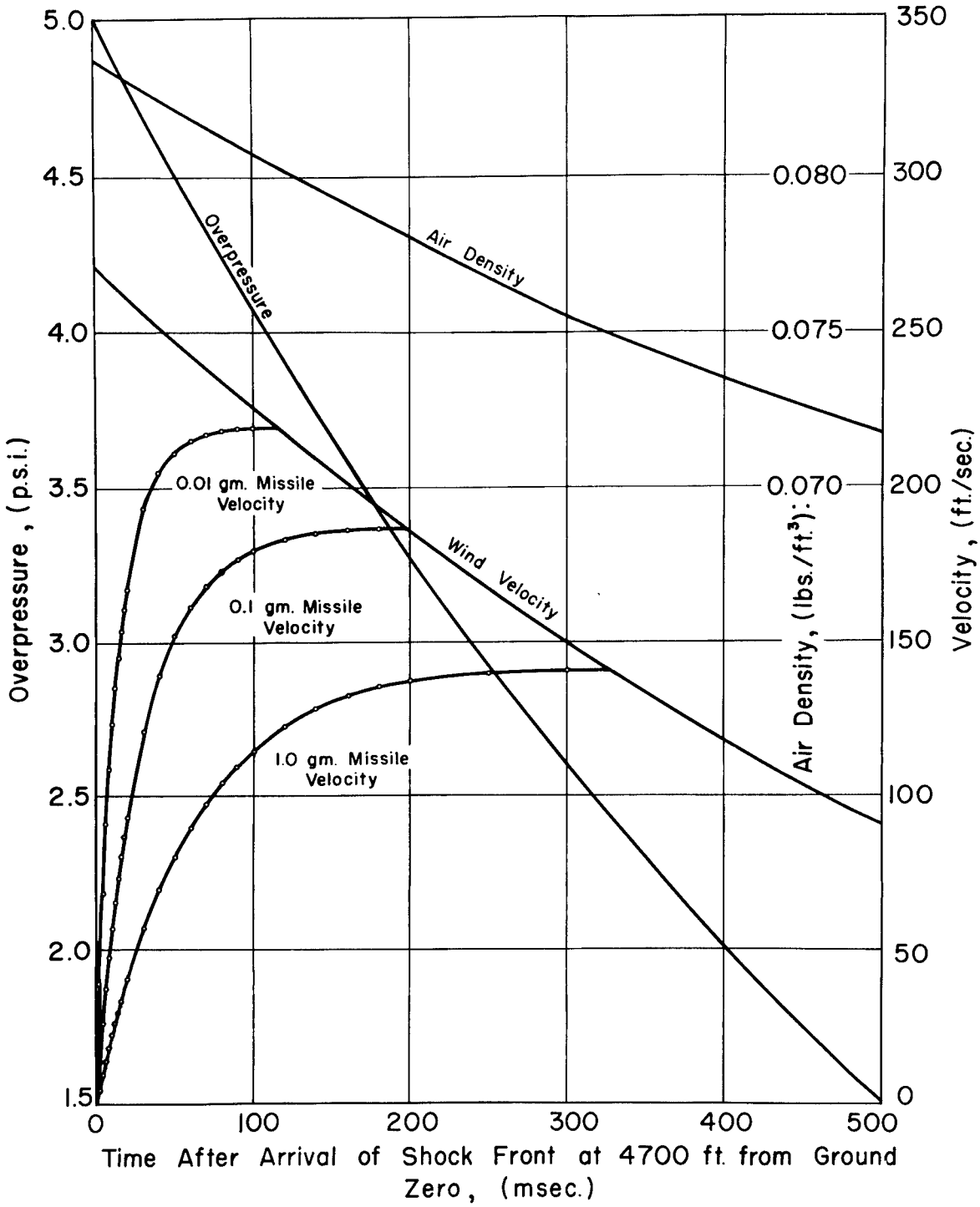

Fig. 6.3—Blast data used to estimate stone-missile velocities in open areas, 4700 ft from Ground Zero. Maximum overpressure: 5 psi.

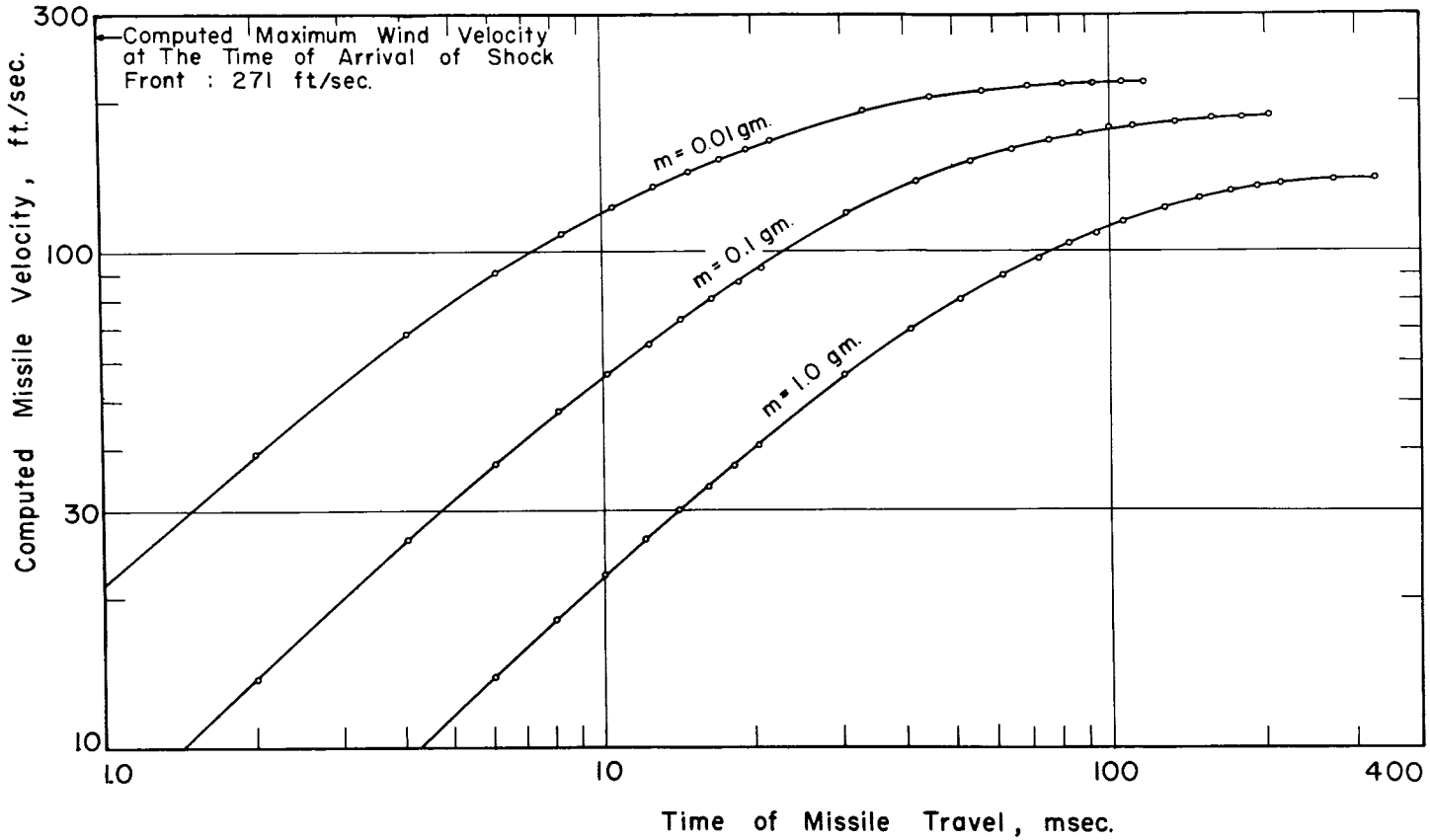

Fig. 6.4—Computed velocities as a function of time of travel for 0.01-, 0.1-, and 1.0-g stone missiles in open areas, 4700 ft from Ground Zero. Maximum overpressure: 5 psi.

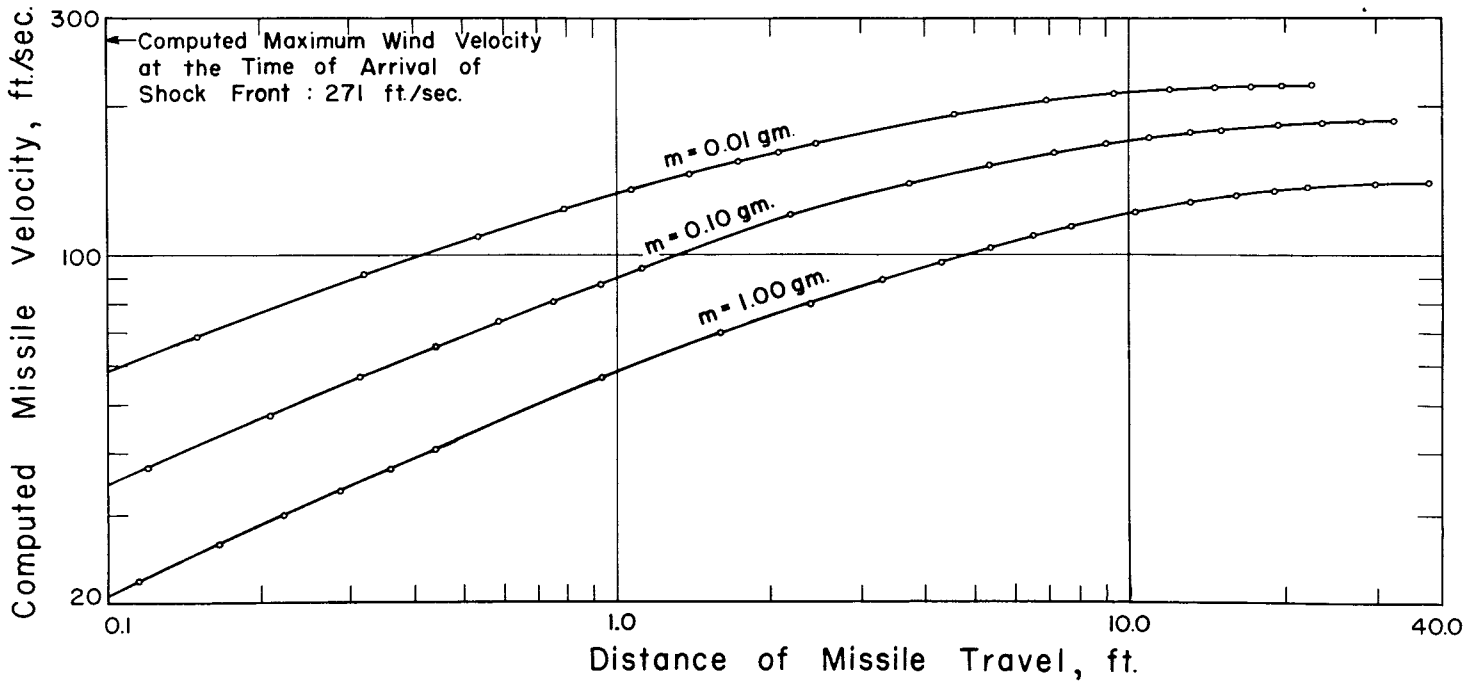

Fig. 6.5—Computed velocity as a function of distance of travel for 0.01-, 0.1-, and 1.0-g stone missiles in open areas, 4700 ft from Ground Zero. Maximum overpressure: 5 psi.

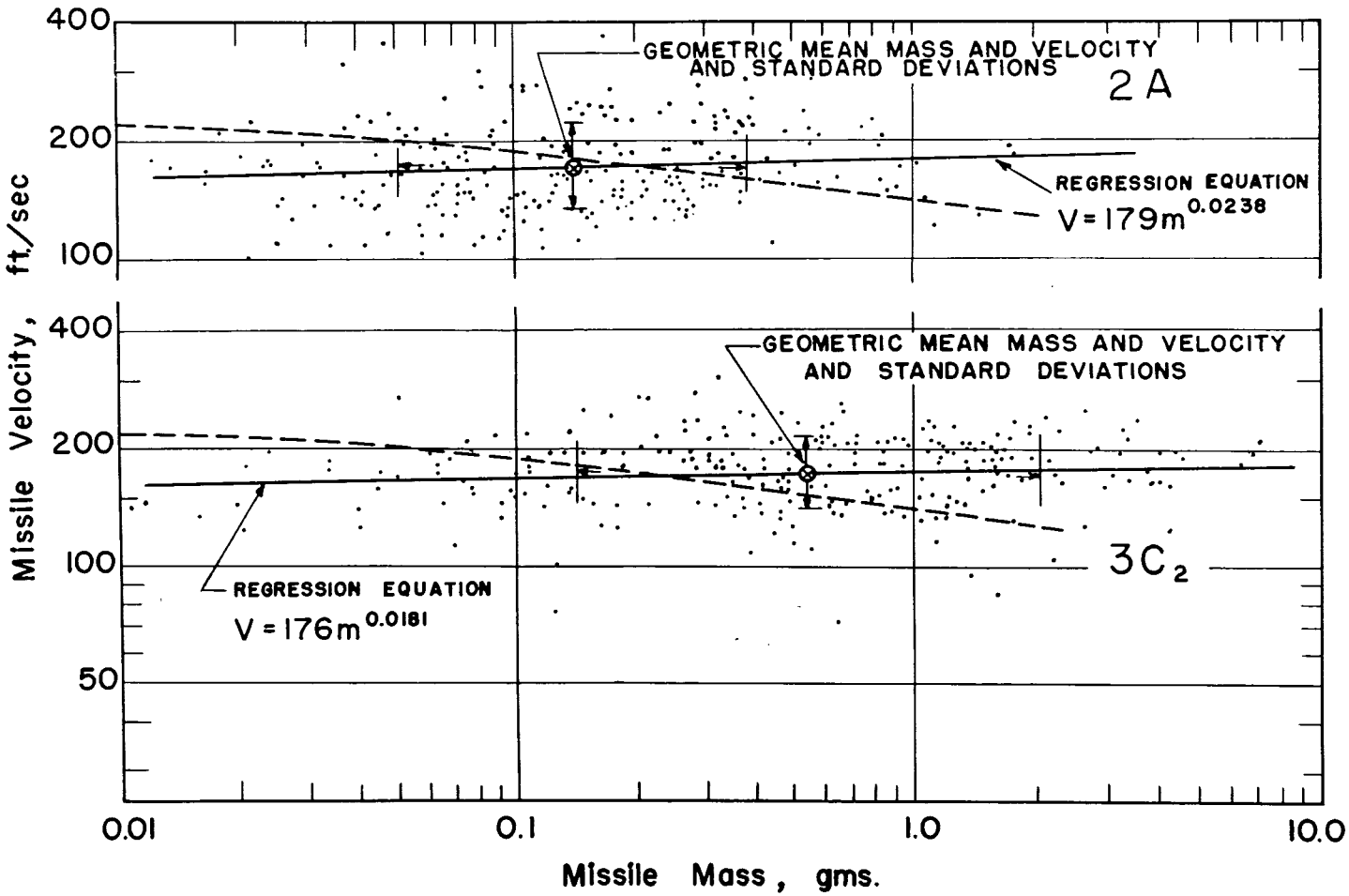

Fig. 6.6—Velocity as a function of mass for 254 glass missiles from trap 2A and 259 glass missiles from trap $3C_2$. Dashed curves: predicted maximum velocities for stones in open areas (see text).

Figure 6.5 is a logarithmic plot of computed missile velocity as a function of distance of missile travel. It is of interest to note that the 0.01-, 0.1-, and 1.0-g missiles obtain 50 per cent of their final velocities in the first 0.55, 1.1, and 1.6 ft of travel, respectively. Similarly, 90 per cent of the final velocities are acquired in the first 5.5, 9.5, and 12 ft of travel.

6.5 DISCUSSION

The lower graph shown in Fig. 6.2 is a plot of measured velocity vs mass for 86 stone missiles obtained from trap 2H, placed 100 ft behind the 4700-ft-range rambler house. The dashed curve connects the computed maximum velocity values for 0.01-, 0.1-, and 1.0-g missiles. In general, the measured and the computed maximum velocity values show good agreement.

An analysis was made using the data obtained from trap 2H to determine the dependence of velocity upon missile mass. The regression equation was found to be

$$V = 104m^{-0.0977} \tag{6.6}$$

and is plotted on the lower chart in Fig. 6.2. It is significant that the slope of this curve is about the same as that of the dashed curve indicating the computed maximum stone-missile velocities. The geometric mean mass and velocity and standard deviations in mass and velocity (Figs. 5.9 and 5.10) are plotted on the same graph. It is of interest to note that the variation in velocity as expressed by the regression curve from the lower to the higher missile masses is more than twice the standard deviation of the geometric mean velocity.

In order to compare the behavior of stone missiles in open areas to that of glass missiles originating in houses, the data for traps 2A and $3C_2$ were analyzed in a manner similar to that described above for trap 2H. Both traps were behind windows facing Ground Zero, 2A at the 4700-ft range (Fig. 4.2), and $3C_2$ at the 5500-ft range (Fig. 4.6). The velocity and mass data for each missile from these traps are plotted in Fig. 6.6, 2A data on the upper and $3C_2$ data on the lower chart. The dashed-line curves superimposed on these charts represent the computed maximum velocities for stones in open areas on the 5-psi line, 4700 ft from Ground Zero. The regression curves determined from the missile mass and velocity data have the following equations:

$$\text{Trap 2A:} \qquad V = 179m^{0.0238} \tag{6.7}$$

$$\text{Trap } 3C_2\text{:} \qquad V = 176m^{0.0181} \tag{6.8}$$

These equations are plotted in Fig. 6.6 as solid lines. The geometric mean masses and velocities and standard deviations (Figs. 5.3, 5.4, 5.11, and 5.12) are indicated on the same charts for each of these traps. The small positive slope in the regression curves indicates that the larger missiles were traveling slightly faster than the light ones. However, the total variation in velocity from the lightest to the heaviest missile is, in each case, less than one standard deviation of the geometric mean velocity.

Thus an analysis of the data shown in Figs. 6.2 and 6.6 indicates that at ranges of 4700 to 5500 ft (a) glass-fragment missiles travel faster than stone missiles and (b) large glass fragments travel slightly faster than small ones, whereas large stones travel significantly slower than small ones.

REFERENCES

1. Sighard F. Hoerner, "Aerodynamic Drag," 1st edition, p. 21 (published by the author), Midland Park, N. J., 1951.
2. L. J. Vortman and M. L. Merritt, Methods for Estimating Blast Loading on Simple Structures, Sandia Corporation, Albuquerque, N. Mex., September 1953.

CHAPTER 7

DISCUSSION

7.1 GLASS-FRAGMENT MISSILES IN HOUSES

7.1.1 Glass-fragment Mass Vs Overpressure

If a pane of glass is struck by a hard object, such as a hammer, it seems reasonable that the size of the resulting fragments would depend in some way upon the mass, velocity, and area of impact of the striking object. In the present study it was found that the size, or mass, of window-pane fragments was at least partially dependent upon the magnitude of the shock front measured in maximum overpressure. Figure 5.17 shows the relation between the geometric mean mass of glass fragments and the maximum overpressure of the shock front. The geometric mean mass was used here rather than average mass because the former is a more reliable measurement for purposes of comparison since it is changed very little by the presence of a few large masses. Maximum overpressure probably is not the only parameter determining the mass of glass fragments. Other factors which may be significant are (a) type and thickness of the glass, (b) dimensions of each pane, (c) method of mounting, (d) orientation with respect to the shock front, and (e) secondary breakage against walls, furniture, etc. The data collected in this study are not sufficient to evaluate systematically the effects of the factors listed above. For instance, the fragments analyzed were caught in traps and, therefore, free from secondary breakage. Further study of window-glass-fragment size as a function of some parameter or parameters of blast could possibly provide a tool which would be useful in estimating the magnitude of the blast under conditions where conventional methods for the measurement of blast parameters do not exist.

7.1.2 Glass-fragment Velocity

An examination of Eq. 6.5 indicates that the rate at which a particular missile gains velocity is dependent upon the ratio of presenting area to mass. It can be seen that this ratio is constant for flat glass fragments of the same thickness if the presenting area is the flat surface of the fragment. In actuality, this condition is satisfied until the fragment starts to tumble. If most of the missile's velocity is gained before tumbling sets in, it would be reasonable to expect the heavy missiles to have velocities as great as the light ones. In a given situation, then, the velocities of the glass fragments would be randomly distributed, the differences in values being determined chiefly by different periods of stability before tumbling. The results of the computation of stone velocities lend credence to this hypothesis since a very rapid gain in velocity is indicated in the first part of the missile's trajectory (see Figs. 6.3 to 6.5).

An examination of the velocity-frequency summation curves for traps 2A, 2C, $2D_1$, $2D_2$, $2E_1$, and $2E_2$ (Figs. 5.4, 5.6, and 5.8) reveals that from 1 to 4 per cent of the measured missile velocities were above the maximum wind velocity of 271 ft/sec calculated for conditions in the open. These high velocities can possibly be explained by an intensification of the shock front

upon reflection against both the window and the walls of the house. If the window yields but the wall does not, then the momentary high reflected-pressure region acting against the walls would be partially relieved by air flow through the window. The reflected-pressure phenomenon lasts for a comparatively short time; an action of longer duration would be a funneling of winds through the window following the shock front. This effect would persist until the pressure inside the house was the same as that outside. The shock front reaches the rear of the house before pressure equilibrium can be reached: evidence of this can be found in the fact that rear windows facing away from the blast break inward, not outward.

In addition to the wind which follows the arrival of the pressure front, one other factor may be of significance in imparting velocity to window glass. At the instant of arrival of the shock front at the window, there exists a static pressure gradient across the glass. In the process of breaking, some velocity would be imparted to the glass fragments. After breakage the static pressure gradient across the glass would very quickly disappear, and after this the magnitude of the wind would govern the velocity-time history of the glass fragment.

Upon consideration of the foregoing arguments one could postulate that for the same blast conditions (a) fragments from window panes would have higher velocities than stones originating from the ground in open areas, (b) the effect of mass on velocity would be small for glass fragments, (c) fragments originating from a window facing Ground Zero in the center of a house would have higher velocities than those originating from a similar window facing Ground Zero near the corner of the house, (d) the velocity of glass fragments for a particular house would depend to some extent upon the ratio of house size to window area, and (e) the very rapid failure of the walls or roof of a house would influence the velocity of glass missiles originating from windows.

7.2 AERODYNAMIC DRAG STUDIES USING THE TRAP METHOD FOR DETERMINING VELOCITY

The present study has demonstrated that velocity data can be obtained for a large number of missiles using relatively simple instrumentation. The standard error of estimate for glass-fragment velocity determinations was found to be 10.5 per cent. The principal source of this error was variation in the area of impact. However, even if the accuracy of the velocity for an individual missile is somewhat uncertain, statistical accuracy is achieved by obtaining data for a large number of missiles.

Styrofoam 22 was used successfully as the missile absorbing agent in regions where the overpressure was as high as 5 psi. According to the manufacturer's specifications, it could probably be used in overpressure regions up to 10 psi. This pressure range could be extended by use of similar absorbing materials having higher compressive strength. An undesirable property of Styrofoam is its low melting point—175 to 200°F. However, adequate protection against thermal radiation was afforded by the use of a thin layer of aluminum foil.

It has been pointed out that glass missiles traveling less than about 50 ft/sec are not embedded in Styrofoam. Although these low-velocity missiles may be biologically significant, their importance relative to the high-velocity missiles would be small.

A theoretical method for the computation of secondary missile velocities is discussed in Chap. 6. This technique could be refined by field tests using missile traps and artificial missiles of regular shapes whose presenting areas and drag coefficients were accurately known. These missiles would be placed at measured distances from the traps. Blast parameters, determined by conventional methods, along with known missile aerodynamic constants could be used to compute missile velocity as a function of time and distance of travel. The missile's measured terminal velocity determined from the trap would check the accuracy of the technique. Such a method could then be employed to compute velocities for missiles with other aerodynamic constants and under different blast conditions.

CHAPTER 8

SUMMARY

8.1 BACKGROUND

Evidence was cited that significant biological damage on the perimeter of large-scale explosions has been caused by secondary missiles.[1–3] Nevertheless, little analytical attention in the past has been given to those physical effects of a detonation which are responsible for and govern the behavior of debris which may assume dangerous velocities. The purpose of the present study was to determine the ballistic properties of low-velocity missiles which are produced in various types of houses following an actual nuclear explosion. Also, some attention was given to missile production in the vicinity of houses and in small home type shelters.

8.2 OBJECTIVES

The specific objectives of this investigation concerned the empirical and theoretical evaluation of the following parameters for secondary missiles in and around various structures at different distances from Ground Zero:

1. Composition.
2. Shapes.
3. Masses.
4. Velocities.
5. Trajectories.
6. Spatial density.

8.3 INSTRUMENTATION

A missile trap was described which used Styrofoam 22 as an absorbing agent for missiles striking it. Laboratory tests showed that the depth to which a particular missile penetrated the Styrofoam depended upon its mass, impact area, and impact velocity. Thus a calibration equation was derived (Eq. 3.5) by means of which could be determined the velocity at impact of missiles whose average diameter was less than 1 in. A method for determining the velocity of large missiles was also described.

A special calibration was made for missiles consisting of fragmented window glass. A method was developed to determine the impact velocities of glass fragments using only the missile mass and the depth of penetration in Styrofoam. Figure 3.4 shows the results of this study and also another study (to be presented in a separate report) which determined the probability of penetration of glass fragments into the abdomen of a dog as a function of missile mass and depth of penetration in Styrofoam.

The air gun used in the calibration studies was described, as well as the electronic method used to determine impact velocities.

8.4 MISSILE-TRAP INSTALLATIONS AND THE GROSS EFFECTS OF THE DETONATION

A total of 27 missile traps were used in the open shot of Operation Teapot (see Table 4.1). A detailed description of the location of these traps is presented by means of an area map and floor plans of the houses where traps were located (Figs. 4.1 to 4.8). Twenty of the traps were placed in houses at ranges of 4700, 5500, and 10,500 ft from Ground Zero. Six traps were placed in open areas behind houses at ranges of 4700 and 10,500 ft. One trap was placed in a basement exit type shelter at a range of 1470 ft.

Photographs were used to depict representative missile-trap installations before and after the detonation (Figs. 4.9 to 4.29). The only significant blast damage suffered by the traps was a compression of the Styrofoam in the trap at a range of 1470 ft (see Fig. 4.9).

8.5 RESULTS (ANALYSIS OF DATA)

Data were obtained for a total of 2611 missiles, 95 per cent of which were glass fragments. The results obtained for a typical trap (2A) and for all traps catching less than 100 missiles were presented in Tables 5.1 and 5.2.

Missile mass and velocity data for those traps catching as many as 100 missiles were analyzed statistically. Logarithmic mass-frequency and velocity-frequency summation curves were presented for these traps in Figs. 5.3 to 5.14, inclusive. Geometric mean masses and velocities and standard geometric deviations in mass and velocity were determined from the curves mentioned above. These data, along with other statistical parameters, were listed for each trap in Table 5.3.

Pictures of individual Styrofoam cells (1 in. by 24 in. by 24 in.) were shown in Figs. 5.18 to 5.29. The spatial distribution of missiles striking various traps was shown in Figs. 5.30 to 5.34. It was found that spatial missile density was modified by various circumstances such as a venetian blind striking the trap.

8.6 COMPUTATION OF STONE-MISSILE VELOCITIES FROM BLAST DATA

A theoretical method for the computation of missile velocities from blast data was proposed for objects located in open areas. The blast parameters used in the computations were wind velocity and air density as a function of time and shock velocity. The drag coefficient was assumed to be 1.0, and the presenting area was computed in a manner similar to that used in the Styrofoam penetration studies.

Predicted velocites as a function of time after arrival of the shock front were computed for 0.01-, 0.1-, and 1.0-g missiles and were found to be 220, 187, and 141 ft/sec, respectively. The predicted data for missile velocity as a function of time after the arrival of the shock front, missile velocity as a function of the time of missile travel, and missile velocity as a function of the distance of missile travel were presented graphically in Figs. 6.3, 6.4, and 6.5, respectively.

Using empirical data obtained for the stone missiles caught in trap 2H at 5 psi to test the adequacy of the theoretical approach, a satisfactory "fit" was demonstrated as shown in the lower portion of Fig. 6.2. The correspondence between the predicted and measured data indicated that the theoretical approach was promising, although further experience with a variety of missiles at different ranges may either confirm or modify the analytical methods employed in this study.

REFERENCES

1. George Armistead, Jr., The Ship Explosions at Texas City, Texas, on April 16 and 17, 1947, and Their Results, Engineering Consultants Report to John G. Simonds and Company, Inc., Oil Insurance Underwriters, New York City; Washington, D. C., 1 June 1947.
2. Virginia Blocker and T. G. Blocker, The Texas City Disaster — A Survey of 3000 Casualties, Am. J. Surg., 78: 756-771 (1949).
3. Los Alamos Scientific Laboratory, "The Effects of Atomic Weapons," U. S. Government Printing Office, Washington, September 1950.